# Extended methods

## Biological samples

Peripheral blood mononuclear cells (PBMCs) used in this study were collected from children aged between 10 and 16 years old as part of the longitudinal study Asthma in the Life of Families Today (ALOFT, recruited from November 2010 to July 2018, Wayne State University Institutional Review Board approval #0412110B3F) ( Resztak et al. (2021)), which was established to explore the effects of family environments on childhood asthma. The 96 samples included in the current study were randomly selected from a pool of 136 samples passing the following criteria: donor's age 10-16 years old, donor's race self-reported as Black, availability of at least 3.5 million cryopreserved PBMCs, and to ensure a 50:50 ratio between female and male participants. For each participant multiple samples were collected longitudinally, but we included in this study only the earliest sample passing the filtering criteria. PBMCs collected into two BD Vacutainer™Glass Mononuclear Cell Preparation Tubes (Becton Dickinson and Co., East Rutherford, NJ) were extracted using a previously-published Ficoll centrifugation protocol ( Weckle et al. (2015)), cryopreserved in freezing media (70% RPMI, 20% CS-FBS, 10% DMSO; $3-8\times10^6$ cells/ml) and stored in liquid nitrogen until the day of the experiment.

## Cell culture and single-cell preparation

Cells were processed in batches of 16. For each batch, PBMCs were removed from liquid nitrogen storage and quickly thawed in 37°C water bath before diluting with 6 ml of warm starvation media (90% RPMI 1640, 10% CS-FBS, 0.1% Gentamycin) and counting using Trypan blue staining on Countess II (Life Technologies Corporation, Bothell, WA). Cells were subsequently centrifuged at 400×g for 10 minutes and resuspended in culture medium at $2\times10^6$ cells/ml. 500 $\mu$l of cell suspension was plated in each of 5 wells of a 96-well round-bottom cell culture plate for each sample. Cells were incubated in starvation media overnight (approx. 16 hours) at 37°C and 5% $CO_2$. The following morning each of the five wells for each individuals were treated with either: 1 $\mu$g/ml LPS ( Barreiro et al. (2010)) + 1 $\mu$M dexamethasone ( Moyerbrailean et al. (2016)), 1 $\mu$g/ml LPS + vehicle control alone, 2.5 $\mu$g/ml PHA ( Moyerbrailean et al. (2016)) + 1 $\mu$M dexamethasone, 2.5 $\mu$g/ml PHA + vehicle control alone, or vehicle control alone (control). Note that the vehicle control used was 1$\mu$l of ethanol in 10 ml of media, so that the effect of the vehicle control was negligible. After six hours, cells were pooled across individuals for a total of five treatment-specific pools. The pools were centrifuged at 300 rcf for 5 min at 4°C, washed with 5 ml ice-cold PBS + 1% BSA and centrifuged again. Each pool was resuspended in 2 ml ice-cold PBS + 1% BSA and filtered through a 40 $\mu$m Flow-Mi™strainer (SP Scienceware, Warminster, PA). Cell concentration was determined using Trypan blue staining on Countess II, and adjusted to $0.7\times10^6$ cells/ml to $1.2\times10^6$ cells/ml. Each pool was loaded onto a separate channel of 10x Genomics®Chromium machine (10x Genomics, Pleasanton, CA), according to the manufacturer's protocol, with batches 4, 5 and 6 loaded on two separate Chromium Chips for a total of 2 wells per treatment pool. Batches 1-4 and one chip of batch 5 were processed using v2 chemistry, and the other chip of batch 5 and batch 6 were processed using v3 chemistry. Library preparation was done according to the manufacturer's protocol.

## Sequencing

Sequencing of the single-cell libraries was performed in the Luca/Pique-Regi lab using the Illumina NextSeq 500 and 75 cycles High Output Kit with 58 cycles for R2, 26 for R1, and 8 for I1.

## Genotype data

All individuals in this study were genotyped from low-coverage (∼0.4X) whole-genome sequencing and imputed to 37.5 M variants using the 1000 Genomes database by Gencove (New York, NY). These data were used for all genetic analyses and to calculate PCs of genotypes to be used as covariates in downstream statistical analyses. Genotype PCA was run on all biallelic autosomal SNPs with cohort MAF$<=0.1$ using library SNPRelate ( Zheng et al. (2012)) in R 4.0 ( R Core Team (2020)).

## single-cell RNA-seq raw data processing (Alignment and demultiplexing)

The raw FASTQ files were mapped to the GRCh38.p12 human reference genome using the `kb` tool (a wrapper of `kallisto` and `bustools`) with the argument of workflow setting to be `lamanno` ( Melsted et al. (2021)). Two procedures were performed in the `kb` tool. First, we used `kallisto` to pseudo align reads to the reference genome and quantify abundances of transcripts ( Bray et al. (2016)). Second, we transformed the `kallisto` outputs into BUS (Barcode, UMI, Set) single cell format using `bustools` ( Melsted et al. (2019)). A total of 45 pooled libraries were generated in our experiment. Among 45 libraries and 6 batches, 3 experiments (LPS+DEX, PHA and PHA+DEX) in batch 2 and 3 experiments (LPS+DEX, PHA and PHA+DEX) in batch 3, were excluded because of failure of the 10x Genomics instrument resulting in broken emulsions, for a total of 39 libraries remaining for all subsequent analyses. We removed debris-contaminated droplets using the `DIEM R` package ( Alvarez et al. (2020)). With this procedure, we obtained a count matrix of 301,637 cells with 116,734 genes features (including spliced and unspliced) across 39 library pools. The aligned counts matrix were transformed into a `Seurat` object for the subsequent functional analysis. To demultiplex the 16 individuals pooled together for each batch, we used the `popscle` pipeline (`dsc-pileup` followed by `demuxlet`) with the default parameters ( Kang et al. (2018)). Two input files are required to provide for dsc-pileup, a BAM file and VCF file. The BAM files were generated by running `cellranger` (v2.1.1) `count` function aligned to the GRCh37 human reference genome (downloaded from 10x Genomics, 3.0.0). The VCF file obtained from DNA genotype data (see above) was filtered to remove any SNP that was not covered by scRNA-seq reads. The resulting VCF contained 935,634 SNPs after removing SNPs with MAF less than 0.05. After assigning the identity to each cell, we removed mismatching barcodes between individual identity and batch. A total of 292,394 cells with 116,734 genes (including spliced and unspliced) were entered into the downstream analysis. For 96 Individuals, we had both control and LPS conditions, while the other three conditions (LPS+DEX, PHA, PHA+DEX) were assayed for 64 individuals because of instrument channel failure in batches 2 and 3 for those experimental conditions. This clean dataset had a median of 7,994 cells (Figure S48), a median of 4,251 UMI counts, and 1,810 genes measured on average in each cell across 39 experiments (Figure S49). In terms of spliced reads, we detected a median of 2,705 UMIs and 892 genes for each cell across all 39 experiments (Figure S50).

## Clustering, UMAP and cell type annotation

`Seurat`(V3) was employed for preprocessing, clustering, and visualizing the scRNA-seq data ( Stuart et al. (2019)). We performed log-normalization on all the data using `NormalizeData` with default parameters and selected 2,000 highly variable genes using `FindVariableFeatures` with variance-stabilizing transformation (`vst`) followed by standardization of these highly variable genes for downstream analysis using `ScaleData`. Linear dimensionality reduction was carried out by `RunPCA` on scaled data with 100 principal components (PCs). We ran `RunHarmony` with chemistry as covariates to correct chemistry effects (V2 and V3), which is scalable to a large number of cells and robust Korsunsky et al. (2019). The Harmony-adjusted PCs were then used to construct a Shared Nearest Neighbor (SNN) graph using `FindNeighbors` (dims=1:50) and cell clustering was subsequently implemented by running `FindClusters` with the resolution set to 0.15. Finally, Uniform Manifold Approximation and Projection (UMAP) was applied to visualize the clustering results using the top 50 Harmony-adjusted PCs. Cells from different chemistries, batches, and treatments shared similar clustering patterns (Figure S51, Figure S52, Figure S53).

We identified 13 clusters and then annotated cell clusters based on the following canonical immune cell type marker genes (Figure S2 and S55), B cells (*MS4A1* or *CD79A*), Monocytes (*CD14* or *MS4A7*), natural killer (NK) cells (*GNLY* or *NKG7*) and T cells (*CD3D* or *CD8A*). Clusters 0, 4, 5, and 7-12 were annotated as T cells with 183,289 cells, clusters 3 and 6 were annotated as monocytes (30,393), cluster 1 was defined as NK cells (47,824) and cluster 2 as B cells (30,888). We also explored to break the T cell group into the two major sub-clusters (Cluster 0) which is CD4-like T cell and Cluster 4 (CD8-like cytotoxic T cell); yet we only found a limited number of differences for Cluster 4 in the genes responding to the treatments (Figure S55). This is likely

because we would need to profile a larger number of cells to explore in depth differences in these subtypes of T lymphocytes.

## Aggregation of single-cell-level data for differential gene expression and genetic analyses

We generated pseudo-bulk RNA-seq data by summing the spliced counts from `kallisto` for each gene and each sample across all cells belonging to each of the four cell types (B cell, Monocyte, NK cell and T cell), separately. This generated a data matrix of 42,554 genes from autosomes (rows) and 1,536 combinations of cell type+treatment+individual (columns). The number of cells in each combination displayed a similar distribution between treatments for most cell types (Figure S54 and Table S2, S24). B cells have the smallest number of cells for each combination while T cells have the most number of cells for each combination (Figure S54), which is consistent with the cell type compositions in PBMCs. Next, we focused on protein coding genes and filtered out genes with less than 20 reads across cells and removed combinations with less than 20 cells. This last filtering step resulted in a data matrix of 15,770 protein coding genes (rows) and 1,419 combinations (columns), which were used for all subsequent differential expression and genetic analyses.

## Differential gene expression analysis

We carried out differential gene expression analysis for each of the five batches separately using `R DESeq2` package ( Love et al. (2014)) and then combined the results across five batches using meta-analysis. For each batch, we estimated gene expression effects of the treatments using four contrasts: (1) LPS, LPS vs CTRL; (2) LPS+DEX, LPS+DEX vs LPS; (3) PHA, PHA vs CTRL; (4) PHA+DEX, PHA+DEX vs PHA. We found that compared to adding a batch covariate in DESeq2, our approach of dividing the analysis by batch produced more robust results in our data , likely because the overdispersion parameter of DESeq2 was estimated for each batch separately. In the meta-analysis procedure, we first extracted the summary statistics, including estimated effects ($\beta_i$) and standard error ($s_i$). Based on the fixed-effects model of meta-analysis, the weighted average effects are calculated by $\hat{\beta} = \frac{\sum 1/s_i^2 \beta_i}{\sum 1/s_i^2}$ and its estimated variance can be expressed by $\hat{\nu} = (\sum 1/s_i^2)^{-1}$. We then constructed the test statistics $z = \frac{\hat{\beta}}{\sqrt{\hat{\nu}}}$ which follows a normal distribution under the null hypothesis. To correct for multiple hypothesis testing, we used the `qvalue` function in `R` 4.0 to estimate false discovery rate (FDR) from a list of $p$-values from the above $z$ test statistics for each condition, separately. Differentially expressed genes (DEG) were defined as those with FDR less than 0.1 and absolute estimated $\log_2$ fold change larger than 0.5. We carried out Gene Ontology (GO) enrichment analysis [i.e., Biological process (BP), molecular function (MF), and cellular component (CC)], for these DEGs identified across conditions using `R ClusterProfiler` package (V3.16.1) ( Yu et al. (2012)).

## Estimation of gene expression mean and dispersion

Using the single-cell data generated from Fluidigm experiment Sarkar et.al proposed a zero-inflated negative binomial (ZINB) distribution to estimate gene expression variance ( Sarkar et al. (2019)). Some literature demonstrated that it is not necessary to consider the zero inflation term in the model for droplet-based single-cell RNA data ( Svensson (2020)). Based on the computational framework that was established by Sarkar et.al, we adapted a negative binomial (NB) distribution to model the count data for each gene $j$, using two main parameters for the mean($\mu_j$) and dispersion($\phi_j$) in our scRNA data. Then, we derived the variance of gene expression by $\hat{\mu_j}^2 \hat{\phi_j}$. The details on NB model are described as follows,

$$r_{jk} \sim Poisson(.; R_k \lambda_{jk}) \tag{2}$$

$$\lambda_{jk} \sim Gamma(.; \mu, \phi) \tag{3}$$

Where $r_{jk}$ is the number of molecules for $k$ cell, $j$ gene;$R_k$ is a size factor of each cell, equal to total reads in each cell divided by median reads across cells, to account for difference in cellular sequencing depth; $\lambda_{jk}$ is a latent variable, representing gene abundance and further is assumed to be Gamma distribution with mean value $\mu$,

variance $\mu^2\phi$. By integrating the latent variable $\lambda_{jk}$, we derived density function for each observation as follows,

$$\begin{aligned}\Pr(r_{jk}) &= \int_0^\infty \frac{(R_k\lambda_{jk})^{r_{jk}}\exp^{-(R_k\lambda_{jk})}}{\Gamma(r_{jk}+1)}\frac{(\mu_j^{-1}\phi_j^{-1})^{\phi_j^{-1}}}{\Gamma(\phi_j^{-1})}\lambda_{jk}^{(\phi_j^{-1}-1)}\exp^{-(\mu_j^{-1}\phi_j^{-1})\lambda_{jk}}\,d(\lambda_{jk}) \\ &= \frac{\Gamma(r_{jk}+\phi_j^{-1})}{\Gamma(r_{jk}+1)\Gamma(\phi_j^{-1})}(\frac{R_k}{R_k+\mu_j^{-1}\phi_j^{-1}})^{r_{jk}}(\frac{\mu_j^{-1}\phi_j^{-1}}{R_k+\mu_j^{-1}\phi_j^{-1}})^{\phi_j^{-1}}\end{aligned} \tag{4}$$

Then, we estimated parameters of $\mu_j$ and $\phi_j$ by minimizing the negative log likelihood using the `optim` function in `R` 4.0 using the "L-BFGS-B" algorithm. Two filters were applied prior to estimation of gene expression parameters (mean and dispersion): (1) removing genes with less than 20 reads across cells (with a total of 30,972 autosomal genes remaining for the analysis); (2) removing the combinations (cell type+treatment+individual) with less than 20 cells (with a total of 1,419 combinations across all our data). To guarantee robust parameter estimation, we focused on genes with more than 15 reads that are expressed across at least 15 cells for each cell type/treatment combination.

Similar to what reported in previous studies ( Eling et al. (2019b,a); Fan et al. (2016); Fair et al. (2020)), we observed that both gene variance or dispersion linearly depended on mean parameters (Figure S11A,B). To further correct the dependence between dispersion and mean, we defined a residual dispersion, capturing the departure from the global trend. The residual dispersion was calculated by removing the part of dispersion that could be predicted by the overall trend of gene mean across genes in each cell type separately. This adjusted dispersion was uncorrelated with the gene mean value (Figure S11C) across genes.

The well established method (regression BASiCS model) were proposed to perform-differential test for gene expression variability, which can correct the mean confounder by fitting a global linear trend of mean and dispersion across genes in a bayesian hierarchical framework ( Eling et al. (2018)). In analogy to the BASiCS model, we quantified gene expression variability that was not confounded by mean expression by the two discrete stages (1) Use a negative binomial model to obtain the estimation of the parameters mean and dispersion similar to Sakar et al. approach; (2) Fit a linear model between mean and dispersion across genes to remove the part of dispersion that can be predicted by mean expression. We always used the adjusted values unless otherwise stated.

## Calculation of pathway specific score

We calculated the score of a specific GO term or pathway using the transcriptional matrices (mean and dispersion) patterns of genes involved in that term/pathway across all the conditions as follows: (1) extracted the subset of differentially expressed genes in at least one condition belonging to a specific GO term or pathway; (2) scaled mean-centered gene matrices values (mean and dispersion) for each gene across individuals for each cell type and batch separately; (3) subtracted gene expression values of individuals in the CTRL condition to calculate relative expression changes; and, (4) calculated the average values as a specific pathway score across genes for each individual.

## Differential gene variability analysis

We focused on 15,770 protein-coding genes for differential gene variability analysis. To account for the noise from the batch, we implemented the same strategy for differential gene expression analysis for differential gene variability and differential gene mean analyses via fitting models by batch separately and we meta-analyzed the summary statistics. We first took the $\log_2$ transformation of residual dispersion and mean, then fitted models using linear regression where treatments were considered for each batch, separately. To obtain more robust estimation of the gene expression parameters for statistical inference, we only focused on genes that had at least 3 individuals in the treatment and 3 individuals in the control condition that was being contrasted. The differentially variable genes (DVG) and differential mean genes (DEG) were defined as those with FDR less than 0.1 and absolute value of $\log_2$ fold change greater than 0.5. We also used `ClusterProfiler` in `R` to carry out GO enrichment analysis for these identified DVGs.

## DLDA response pseudotime method

We developed a new pseudotime method based on diagonal linear discriminant analysis (DLDA) to characterize the degree to which single cells respond to immune treatments. A key difference compared to previous methods ( Qiu et al. (2017); Haghverdi et al. (2016)) is that DLDA is supervised and estimates a straight line trajectory between two endpoints which should be particularly suitable for a short time treatment. Basically, the trajectory is a one dimensional line connecting the two centroids of a treatment and control conditions for each cell type. In DLDA only a subset of genes that are highly differentially express between the two conditions are used based on the following formula ( Pique-Regi et al. (2005)):

$$g(x)_A = \sum_{i=1}^{p} \left( \frac{\hat{\mu}_A(x_i) - \hat{\mu}_B(x_i)}{\hat{\sigma}_i} \right) \left( \frac{x_i - \hat{\mu}(x_i)}{\hat{\sigma}_i} \right) \gamma_i \tag{5}$$

Where the subscripts of A and B represent the two conditions considered in each contrast, respectively; $\hat{\mu}_i$ denoting mean gene expression of the $i_{th}$ gene for A, B or across groups and $\hat{\sigma}_i$ meaning standard deviation of the $i_{th}$ gene across conditions. In this application of DLDA we only used the DEGs that were differentially expressed in the corresponding condition (10%FDR by DESeq2) by introducing an indicator variable ($\gamma_i$, assigning to 1 if the $i_{th}$ gene is a significant DEG in the contrast of A versus B or 0 otherwise. This is equivalent to denoising by hard thresholding instead of the soft thresholding that a method like nearest shrunken centroids would use. Note that the left term of the summation is a weight that is exactly a standardized effect size, and the right term evaluates for a given gene how far it is from the midpoint between all the cells. By ignoring the off-diagonal terms and only considering genes that are differentially expressed, DLDA achieves a more robust classification performance when the number of samples available for training is relatively limited. While this approach assumes the shortest Euclidean distance alignment between the centroids of the treated and untreated cells, it should be a reasonable assumption for short time-periods (here 6 hours), compared to learning a complex curved one-dimensional manifold in a high dimensional space. This assumption provides a more robust and stable trajectory followed by the cells from the control to the treated state when we iteratively repeat the procedure resampling the data, compared to more complex nonlinear trajectory methods.

Four kinds of DLDA axes were calculated by the following contrasts for each cell type separately, (1) DLDA axis of LPS was estimated in the CTRL and LPS conditions to infer the response pseudotime to LPS; (2) DLDA axis of LPS+DEX was computed in the LPS and LPS+DEX conditions to calibrate the response pseudotime to DEX; (3) DLDA axis of PHA was estimated in the CTRL and PHA conditions to characterize the response pseudotime to PHA stimuli ; and, (4) DLDA axis of PHA+DEX was estimated in the PHA and PHA+DEX conditions to characterize the response pseudotime to DEX. To achieve this, we excluded the data from batches 2 and 3, resulting in 264,545 cells. Next, to correct chemistry effects, we performed standard log-normalization for each subset (split by chemistry) followed by integrating datasets together using Seurat (V3) for each cell type, separately. After the DLDA representing the trajectory pseudotime is calculated for each cell type and treatment, we use a sliding window approach (10% cells in each window, sliding along the defined pseudotime with a step of 0.1% cells), we analyzed gene expression dynamic changes along the response pseudotime within each treatment for each cell type separately and identified different dynamic patterns of gene expression using the *k*-means algorithm

## Validation of the accuracy of DLDA in response pseudotime

We performed resampling analysis to demonstrate the robustness and stability of the DLDA compared to two existing methods: Monocle 3 ( Qiu et al. (2017)) and SCANPY ( Wolf et al. (2018)). For the simplification of the analysis, we focused on the T -cells treated with PHA+DEX or PHA that were measured using 10x Genomics chemistry V3, including 29,157 cells and 6,571 DEGs. To validate the effectiveness of the novel approach (DLDA), we randomly re-sampled half the dataset for 50 replications. In each replication, we applied our novel approach DLDA and the two other methods to compute response pseudotime. We do not have the underlying

ground truth on how the cells should be exactly ordered according to response pseudotime; yet, we can still assess how expression for each of the responding genes correlates with the estimated pseudotime in each iteration across all cells. Ideally, the cells would be sorted similarly in each iteration, and the correlation of the gene expression with the pseudotime would stay constant. For each iteration, we calculated the Pearson correlation of the pseudotime and each gene expression in cells. Two indexes were employed to assess the performance of the three methods, (1) variance of correlation coefficients for each gene across replications; (2). Jaccard index of the top 20 highly correlated genes between 1,225 pairwise replications.

## Data normalization for genetic analyses

For downstream genetic analyses, we first removed all lowly-expressed genes, defined as having less than 0.1 CPM in more than 20% of the samples in each condition, separately. We quantile-normalized the count data using the voom function in the `limma` v3.44.3 package ( Ritchie et al. (2015)) in `R` 4.0 and regressed out the following confounding factors: experimental batch, sex, age, and top three principal components of genotypes in each cell type-treatment combination, separately.

For gene expression variability, for each gene-treatment-cell type combination, we discarded data from batches represented by less than 3 individuals. We considered genes with gene expression variability measures available for at least 20% of remaining individuals in each treatment-cell type combination. We quantile-normalized the data using the `voom` function in the `limma` v3.44.3 package ( Ritchie et al. (2015)) in `R` 4.0. We regressed out the following confounding factors on the subset of genes with no missing data across all individuals in each condition: experimental batch, sex, age, and top three principal components of genotypes processing each cell type-condition combination and performed PCA on variability residuals to use as covariates in variability-eQTL mapping. Mean gene expression estimates were processed using the same pipeline as gene expression variability data.

## *cis*-eQTL mapping

We used `FastQTL` v2.076 ( Ongen et al. (2016)) to perform eQTL mapping on gene expression residuals calculated for each cell type and condition as outlined above. For each gene, we tested all genetic variants within 50 kb of the transcription start site (TSS) and with cohort minor allele frequency (MAF)$> 0.1$. We optimized the number of gene expression PCs in the model to maximize the number of eGenes across all conditions combined. The model that yielded the largest number of eGenes included 4 gene expression PCs. eQTL discovery for mean and variability data was performed similarly, except we modelled quantile-normalized data and regressed out the effects of experimental batch, sex, age, and top three principal components of genotypes and PCs of residuals in the `FastQTL` model. The model that yielded the largest number of significant genes at 10% FDR included 5 PCs of residuals for variability and 7 PCs of residuals for mean data.

## Multivariate adaptive shrinkage

To improve power of eQTL discovery by taking advantage of parallel measures of genetic effects across many cell types and conditions, we employed the multivariate adaptive shrinkage (mash) method using the `mashr` package v.0.2.40 in `R` v4.0 ( Urbut et al. (2019)). As input, we provided the genetic effect size estimates from `FastQTL` analysis in each cell type-treatment combination, and their corresponding standard errors calculated as absolute effect size estimates divided by its $z$-score. We kept the gene-variant pairs with estimates across all cell types and conditions and eliminated the two genes causing a singular matrix. We fitted mash across all 20 cell type-condition combinations on a random subset of 200,000 gene-SNP pairs providing both canonical and data-driven covariance matrices (the latter estimated using mashr in-built `cov_ed` function on strong eQTLs from full data set, defined as those with ashr local false sign rate (LFSR)$< 0.05$).The LFSR refers to the probability that we incorrectly inferred the sign of genetic effects size ($\beta_j$), $LFSR_j = \min\{\Pr(\beta_j \geq 0|D), \Pr(\beta_j \leq 0|D)\}$ ( Stephens (2017)). We considered gene-variant pairs with posterior LFSR$< 0.1$ to be eQTLs. To analyze sharing of genetic effects across all conditions, we considered the direction of genetic effect across all conditions. Genetic effects are shared across conditions if they have the same sign and are significant in at least one of the conditions

considered. To analyze treatment- or cell type–specificity, we focused on pairwise comparisons of genetic effect sizes. An eQTL is specific to a condition if it is significant at LFSR$< 0.1$ in either condition and either the direction of effect differs or the difference in the magnitude of the genetic effects is at least two-fold. A gene is considered shared/specific if at least one eQTL for that gene is shared/specific across the given set of conditions. To discover response eQTLs (reQTLs) we considered the pair-wise union of significant eQTLs in each of the 16 treatment-control combinations. We defined reQTLs as genetic variants whose effect size on gene expression differed by at least two-fold between treatment and control conditions. Mash analyses on mean and variability estimates were conducted following this pipeline.

## DLDA-eQTL mapping

For mapping dynamic eQTLs that have genetic effects on gene expression interacting with pseudotime, we first equally divided cells in one immune treatment into three tertiles of the corresponding DLDA pseudotime. The three tertiles denoted 1, 2 and 3, represent early, middle and latter response pseudotime, respectively. Then, we mapped eQTLs interacting with these representative tertiles as dynamic eQTLs across cell types in the corresponding immune treatments as follows:(1) eQTLs interacting with LPS pseudotime were identified in cells treated with LPS; (2) eQTLs interacting with LPS+DEX pseudotime were identified in cells treated with LPS+DEX; (3) eQTLs interacting with PHA pseudotime were identified in cells treated with PHA; and (4) eQTLs interacting with PHA+DEX pseudotime were identified in cells treated with PHA+DEX. To do this, we summed gene expression data in each of the three DLDA bins for individuals with at least two bins containing at least 5 cells for each treatment. We considered genes with $>$0.1 CPM for at least 20% of remaining individuals in each treatment-cell type combination. We quantile-normalized the data followed by regressing out the following confounding factors: experimental batch, sex, age, and top three principal components of genotypes processing each cell type-condition combination separately. To identify genetic variants interacting with each DLDA, we fitted a linear model using the `lm` function in `R` 4.0 that included both the genotype dosage and the DLDA bin (numerically encoded as 1-3), as well as their interaction: $\texttt{Expression} \sim \texttt{dosage + DLDA\_bin + dosage} \times \texttt{DLDA\_bin}$ in each condition separately. Using the same cis-regions to the above analysis, we perform the interaction analysis for all genetic variants within 50 kb of the transcription start site (TSS) in the genes. We then applied Storey's q-value method on the p-values for the interaction term using a stratified FDR approach on significant and non-significant eGenes (from the `FastQTL` analysis, Figure S45).

# Extended results

## Comparison between genetic effects on gene expression mean and variability

To compare eQTLs and vQTLs, we considered the genetic effects on mean and variability estimated from the same model (Figure S34B, Table S20, Table S8, Table S21, and Table S22). We identified three distinct patterns (Figure 6F, Figure S40): genetic variants affecting gene expression levels only (7,155-11,314 gene-SNP pairs), genetic variants affecting gene expression variability only (1,709-2,128 gene-SNP pairs), and genetic variants affecting both gene expression levels and variability (669-1,207 gene-SNP pairs). Genetic effects in this last category were negatively correlated with opposite signs for eQTLs and vQTLs (Pearson correlation $-0.25$ - $-0.8$, p-value$< 0.05$).

For example, rs2071464 is an eQTL for the *PSMB9* gene in B cells stimulated with LPS+DEX, but we found no genetic effect of this variant on gene expression variability (Figure 6G, Figure S41). The *PSMB9* located in the MHC class II region encodes a member of the proteasome B-type family, which is a 20S core beta subunit of the proteasome. Several studies indicated the proteasome plays a critical role in cardiovascular diseases ( Sandri Robbins (2014); Wang Hill (2015)), inflammatory response and autoimmune diseases ( Karin Delhase (2000)). The subunit of proteasome encoded by *PSMB9* was found to be involved in the process of infectious diseases ( Silva et al. (2013)), autoimmune diseases ( Khuder et al. (2015)) and oncology ( Wang et al. (2014)). Previous TWAS study revealed that expression of *PSMB9* has also been implicated in a number of autoimmune disorders including asthma ( Zhang et al. (2020)). We found the C allele at the genomic position rs1197452483 to increase the gene expression variability of *RPS18* gene in monocytes treated with PHA+DEX, without any effect on mean gene expression levels (Figure 6H, Figure S42). This gene encodes a ribosomal protein that is a component of the 40S subunit, and its expression has been implicated in rheumatoid arthritis, multiple sclerosis, and psoriasis ( Zhang et al. (2020)). *In vitro* silencing of this gene leads to decreased rate of viral infection ( Tai et al. (2009); Sivan et al. (2013)). Genetic polymorphism at rs400063 confers effects on both gene expression mean and variability of the *RNASET2* gene in the T cells treated with PHA+DEX, but in opposite directions (Figure 6I, Figure S43). RNASET2 plays a crucial role in innate immune response by recognizing and degrading RNAs from microbial pathogens that are sensed by *TLR8* ( Greulich et al. (2019)). Expression of *RNASET2* has been implicated in Crohn's disease, inflammatory bowel disease, and rheumatoid arthritis ( Zhang et al. (2020)) via TWAS. eQTLs were likely to be also vQTLs (OR=10.45, p-value$< 2.2 \times 10^{-16}$); however, for the majority of vQTLs, we did not detect significant genetic effects on gene expression levels. vGenes were significantly enriched for genes with differential mean expression for six of the 16 conditions considered (LPS, LPS+DEX and PHA in B cells and T cells, Fisher's exact test p-value$< 0.05$, Table S9). vGenes were also enriched for genes with differential variability for seven contrasts (LPS and PHA in B cells and T cells; LPS and PHA+DEX in NK cells; and PHA+DEX in Monocytes; Fisher's exact test p-value $< 0.05$).

## Supplementary Figures

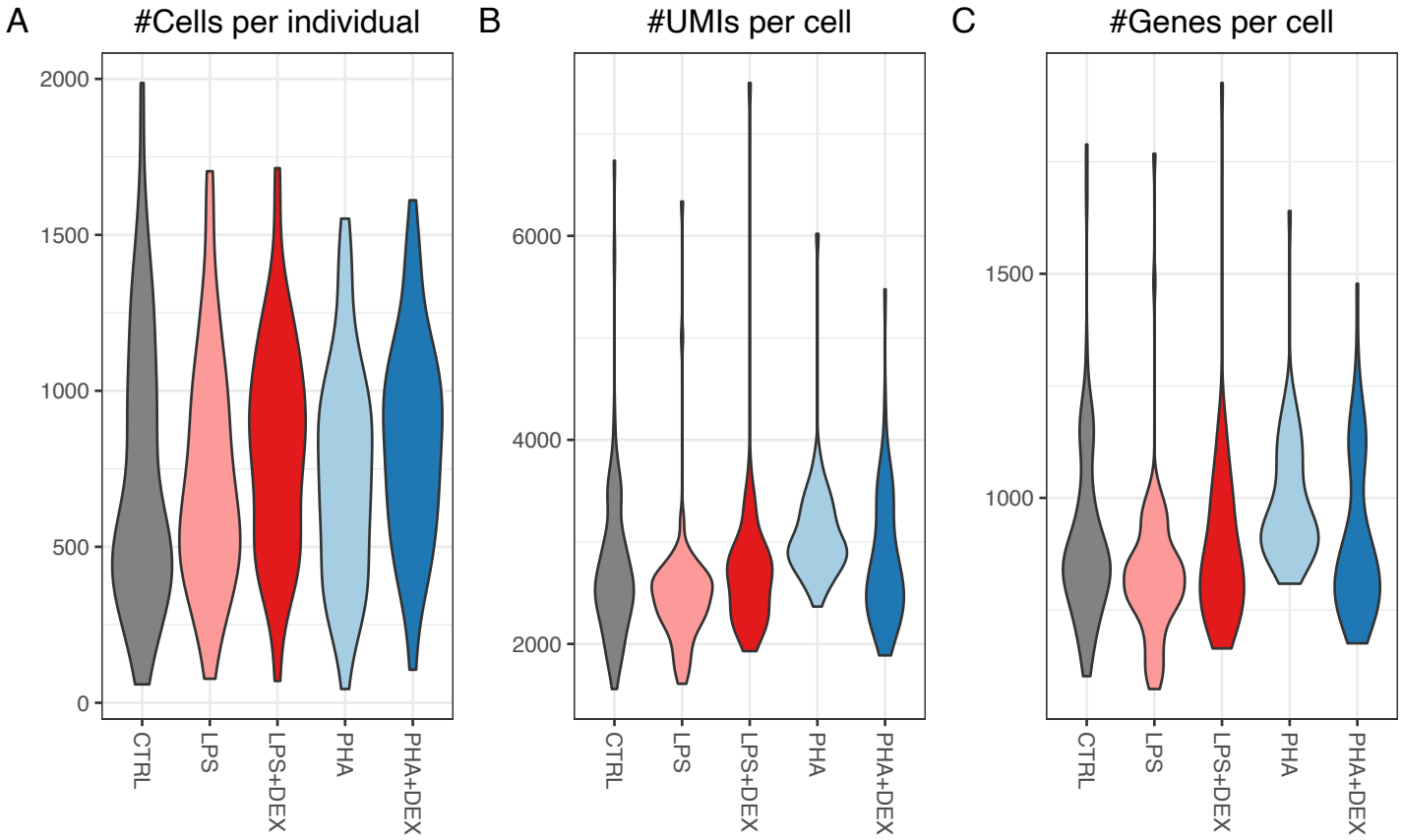


Figure S1: **Violin plots of summary statistics per individual across five conditions (A)** number of measured cells per individual for each treatment. **(B)** average UMIs per cell from one individual for each treatment. **(C)** average number of detected genes per cell from one individual for each treatment.

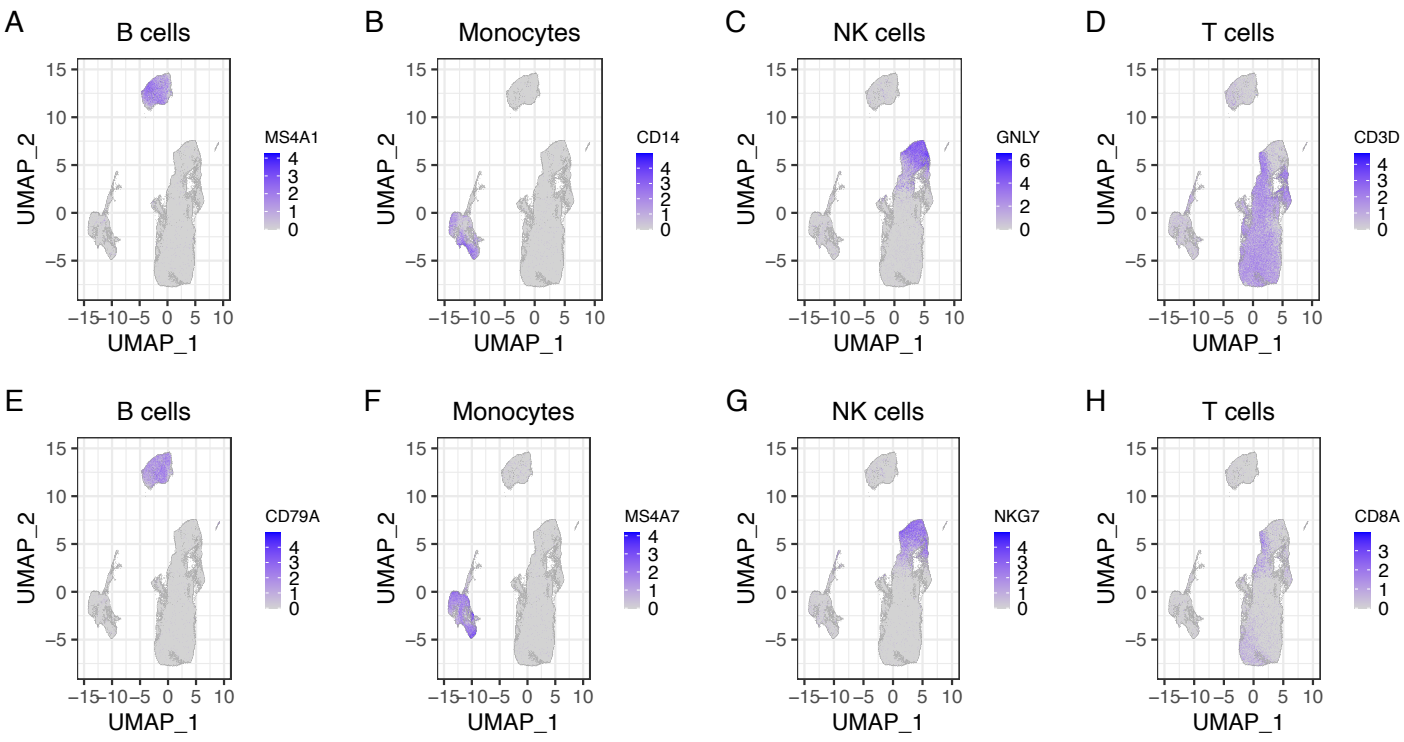


Figure S2: **Canonical immune cell type–specific markers expressed on UMAP: (A and E)** represent B cell-specific gene expressions (*MS4A1* and *CD79A*) on UMAP; **(B and F)** represent Monocyte-specific gene expressions (*MS4A7* and *CD14*) on UMAP; **(C and G)** represent NK cell-specific gene expressions (*GNLY* and *NKG7*) on UMAP; **(D and H)** represent T cell specific gene expressions (*CD3D* and *CD8A*) on UMAP.

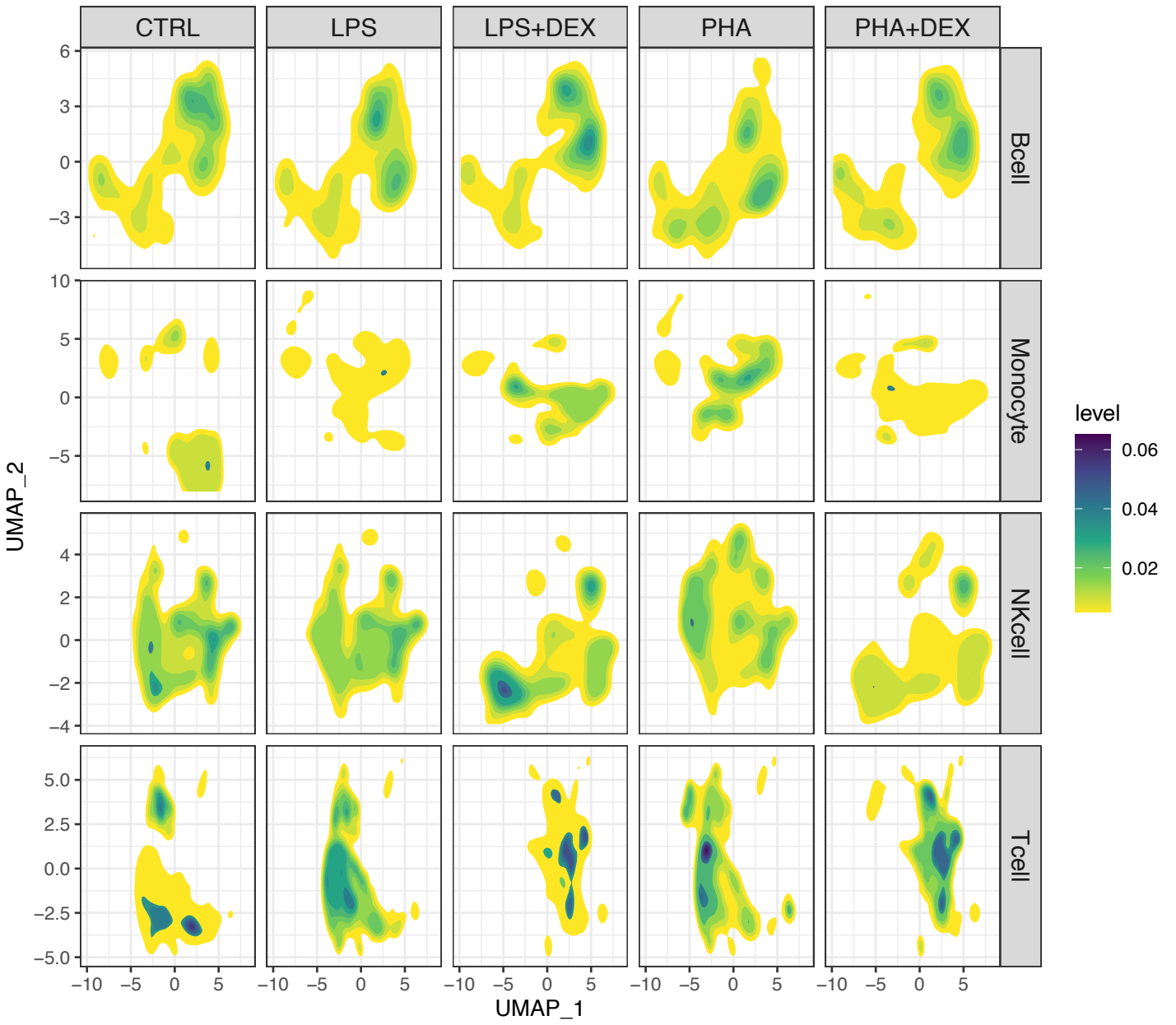


Figure S3: **Density distribution of cells on UMAP for cell types and treatment separately**. Blue color indicates high density of cells while yellow color indicates lower density.

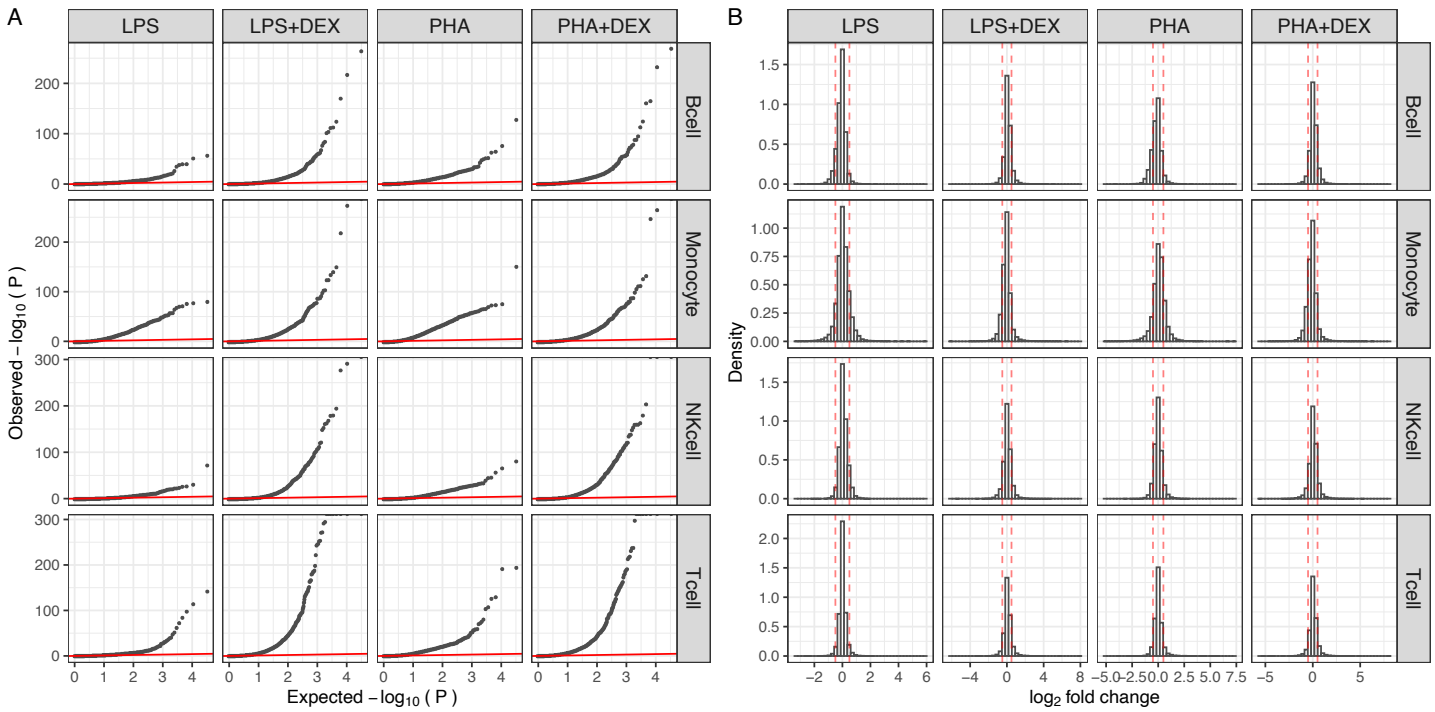


Figure S4: **Overview of results of differential expression analysis:** **(A)** Q-Q plots for 4 contrasts (LPS, LPS+DEX, PHA and PHA+DEX) across cell types, **(B)** Histograms of $\log_2$ fold changes of gene expression, red dashed lines denoting the —$log_2$FoldChange— being 0.5, the cutoff value that is used for defining differentially expressed genes (DEGs).

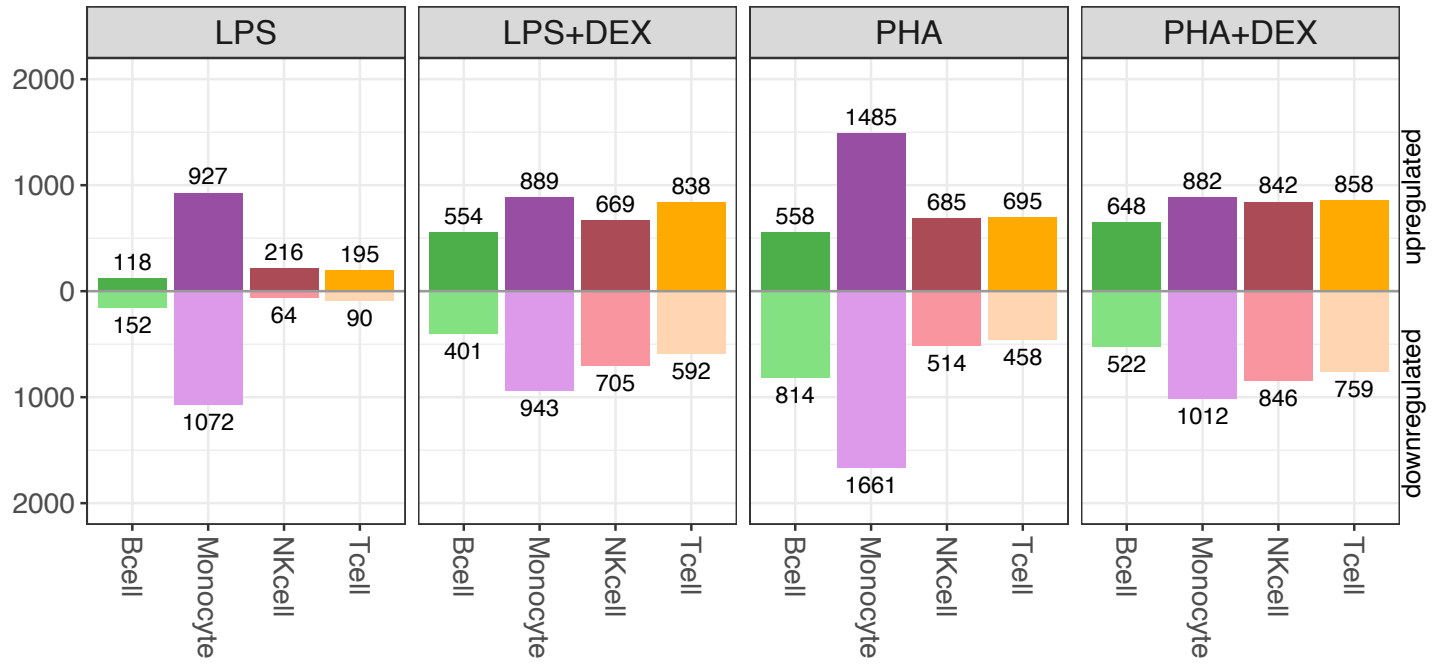


Figure S5: **Number of DEGs across contrasts and cell types;** B cells (green), Monocytes (purple), NK cells (maroon) and T cells (orange), below axis representing down-regulated genes and above axis representing up-regulated genes (FDR<10% and —LFC—>0.5%).

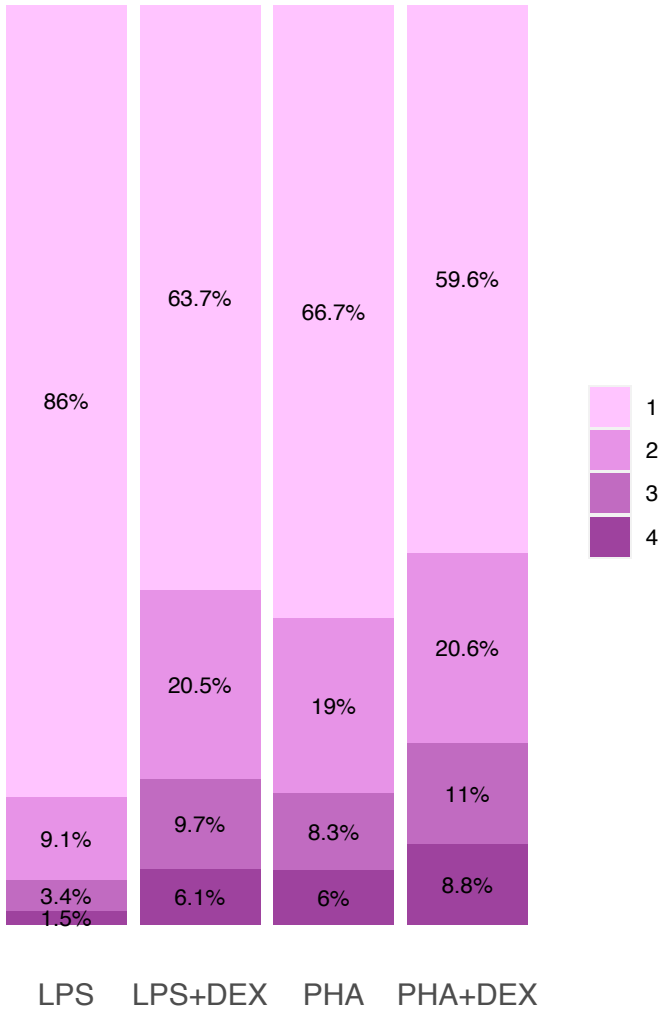


Figure S6: **Cell type sharing of DEGs in four contrast conditions, 1=DEGs detected in only a single cell type and 4=DEGs detected across all the four cell types.**

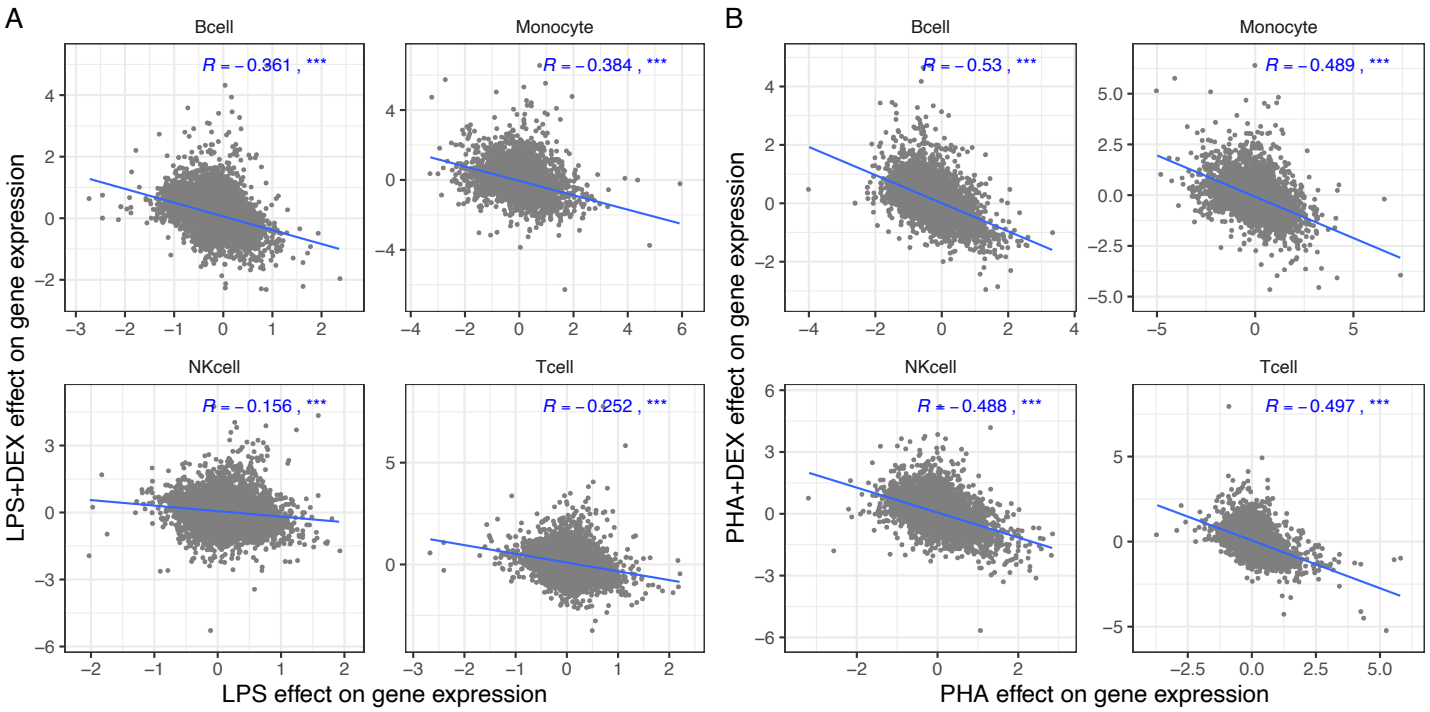


Figure S7: **Dexamethasone (DEX) reverses effects of activation by immune stimuli on gene expression:**. **(A)** Scatterplots of LPS effect on gene expression (x axis) against DEX effect on gene expression (y axis). **(B)** Scatterplots of PHA effect on gene expression (x axis) against DEX effect on gene expression (y axis). Blue lines represent the linear trend between the effects of immune stimuli and DEX treatments on gene expression. *R* represents the correlation coefficients of the effects of two types of immune treatments on gene expression, *denoting $p < 0.05$, ** denoting $p < 0.01$ and *** denoting $p < 0.001$.

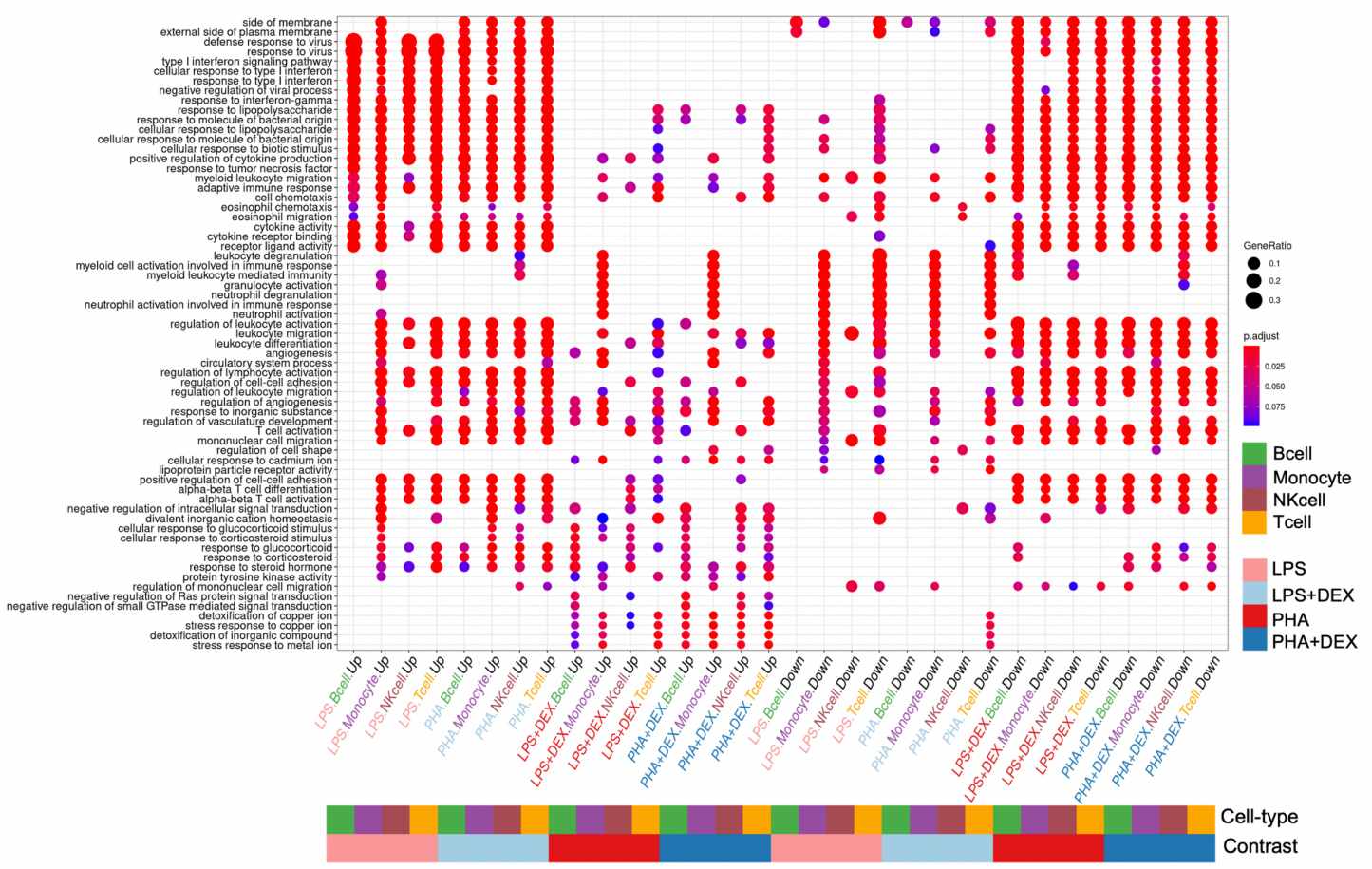


Figure S8: **Visualization of Gene Ontology (GO) enrichment analysis:** The dotplots show the union of the top 5 GO terms for each condition (down-regulated and up-regulated separately) across 16 conditions (4 contrasts $\times$ 4 cell types).

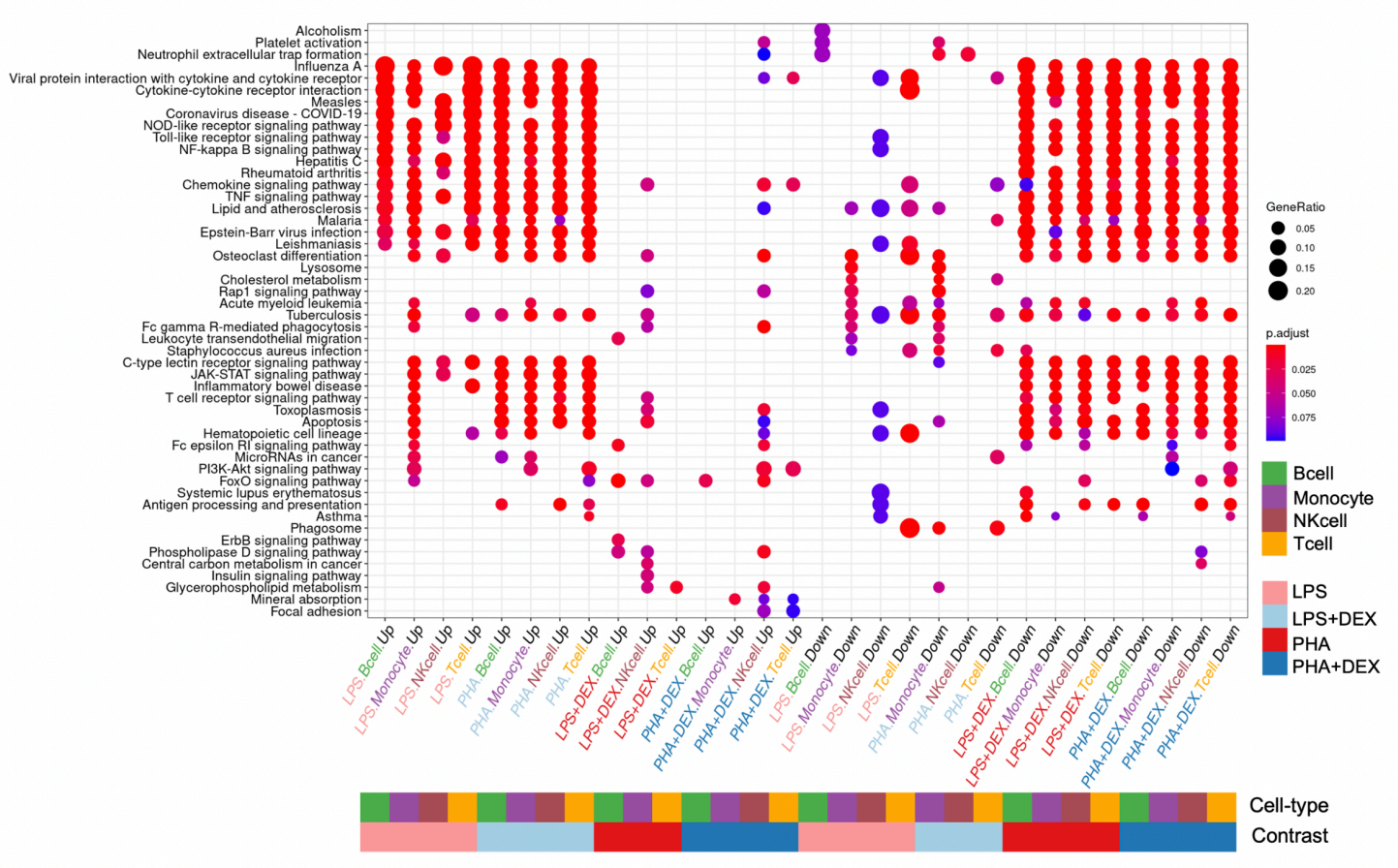


Figure S9: **Visualization of Kyoto Encyclopedia of Genes and Genomes (KEGG) enrichment analysis:** The dotplots show the union of the top 5 KEGG terms for each condition(down-regulated and up-regulated separately) across 16 conditions (4 contrasts $\times$ 4 cell types).

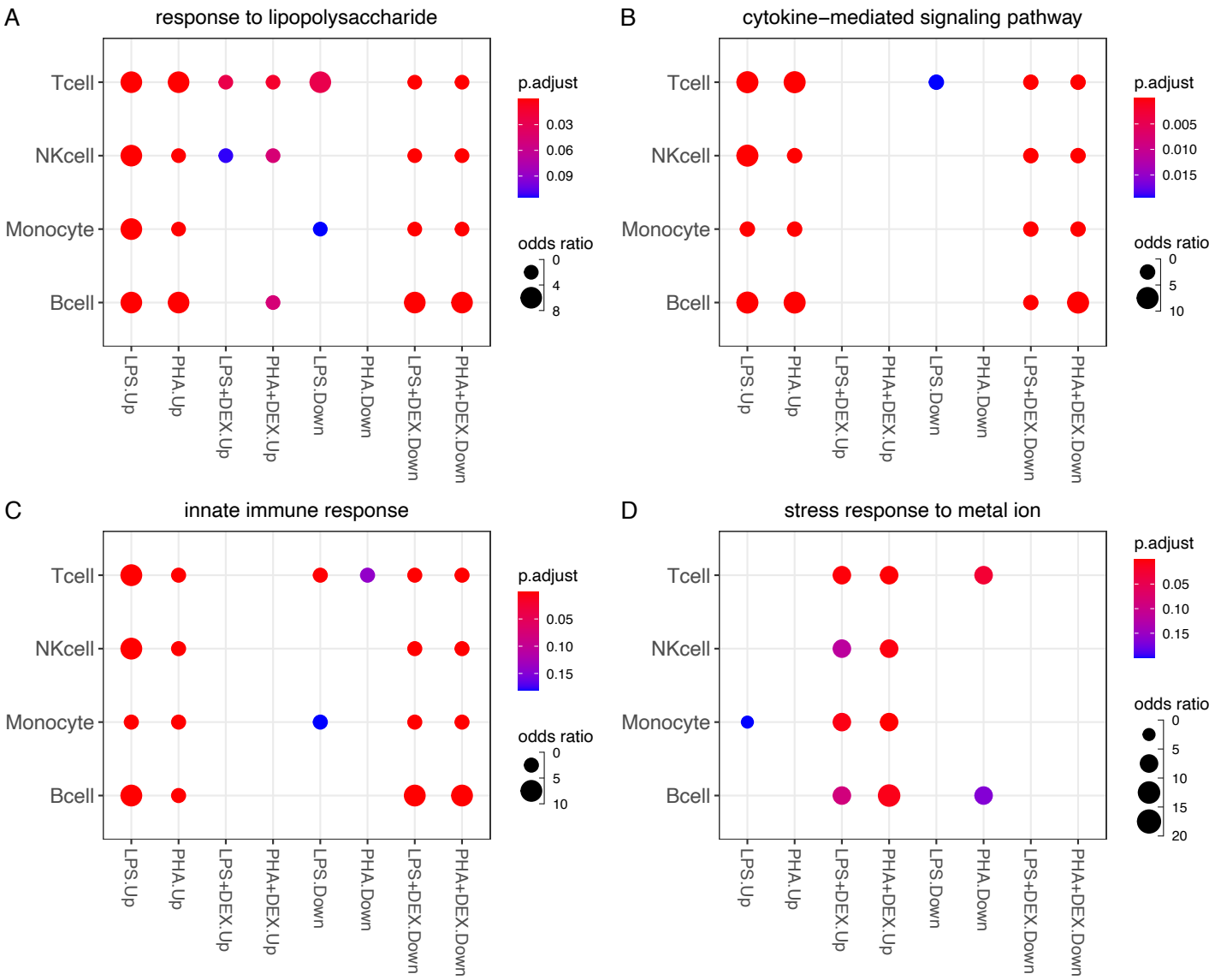


Figure S10: **Examples of the enriched pathways for DEGs: (A-D)**represents the enrichment results of the four example pathways across cell types and conditions,, response to lipopolysaccharide, cytokine-mediated signaling pathway, innate immune response and cellular response to glucocorticoid stimulus, respectively.

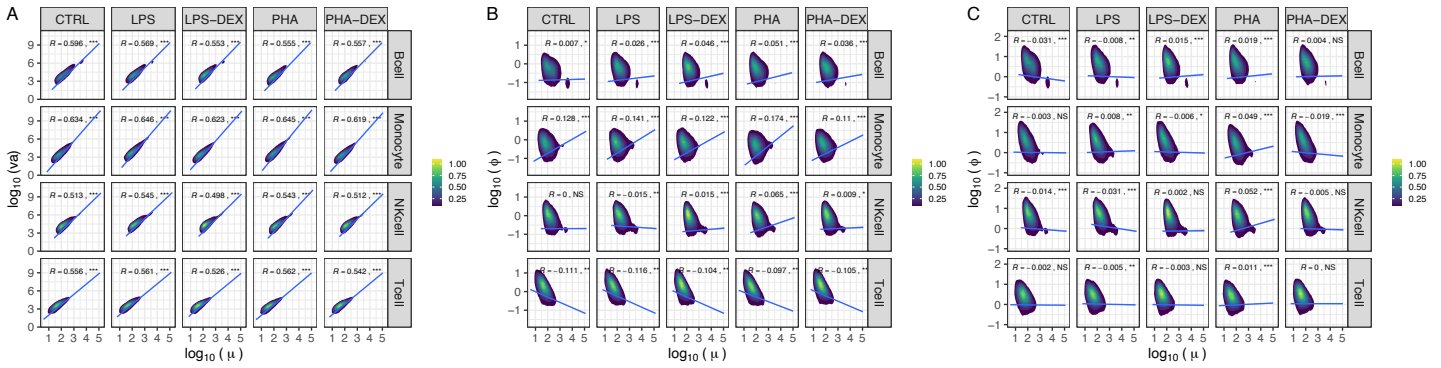


Figure S11: **Both variance and dispersion of gene expression strongly depend on mean gene expression while mean-corrected dispersion is relatively independent on mean expression value: (A)** Scatter plots of $\log_{10}$ mean gene expression (x axis) against $\log_{10}$ variance of gene expression. **(B)** Scatter plots of $\log_{10}$ mean gene expression (x axis) against $\log_{10}$ dispersion of gene expression. **(C)** Scatter plots of $\log_{10}$ mean gene expression (x axis) against $\log_{10}$ mean-corrected dispersion of gene expression, eventually used for measuring gene expression variability.

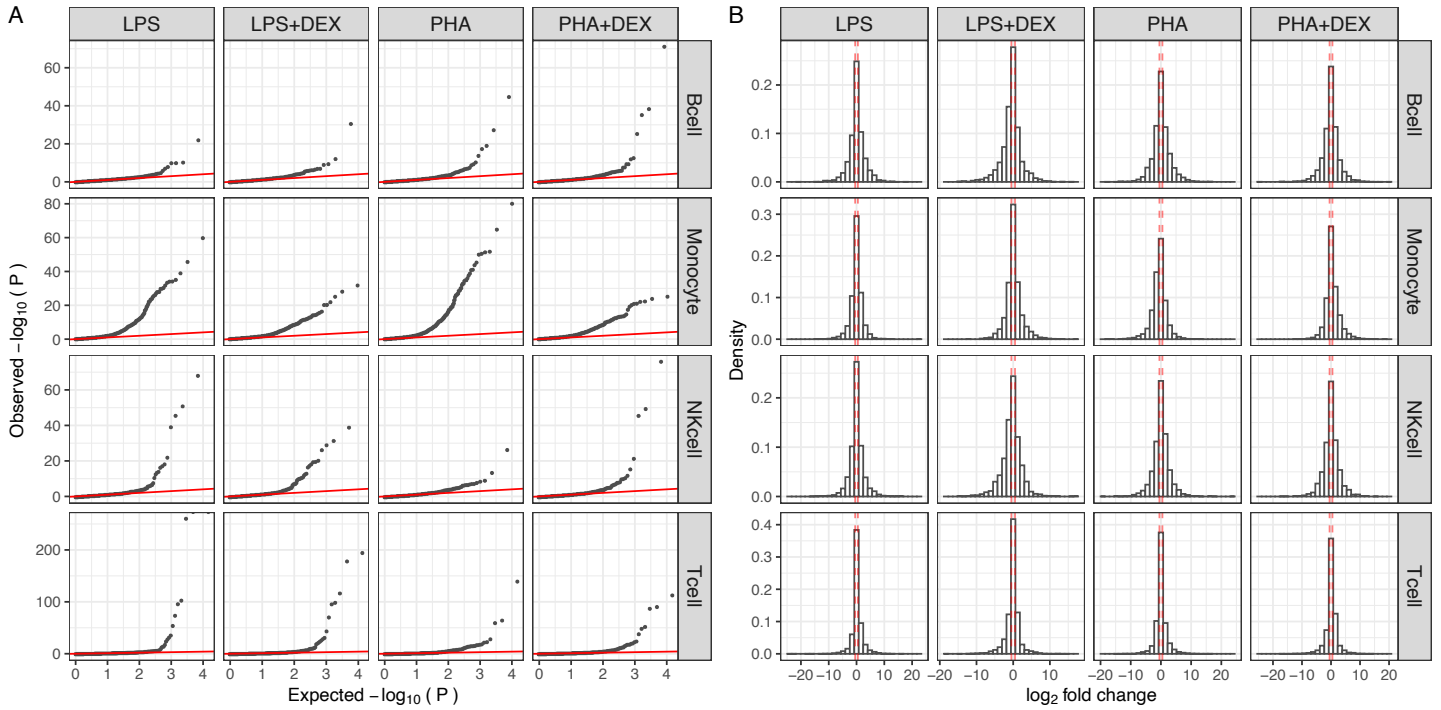


Figure S12: **Overview of results of differential gene variability analysis: (A)** Q-Q plots for 4 contrasts (LPS, LPS+DEX, PHA and PHA+DEX) across 4 cell types. **(B)** Histograms of $\log_2$ fold changes of gene variability, red dashed lines denoting the —$\log_2$FoldChange— being 0.5, the cutoff value that is used for defining differentially variable genes (DVGs)

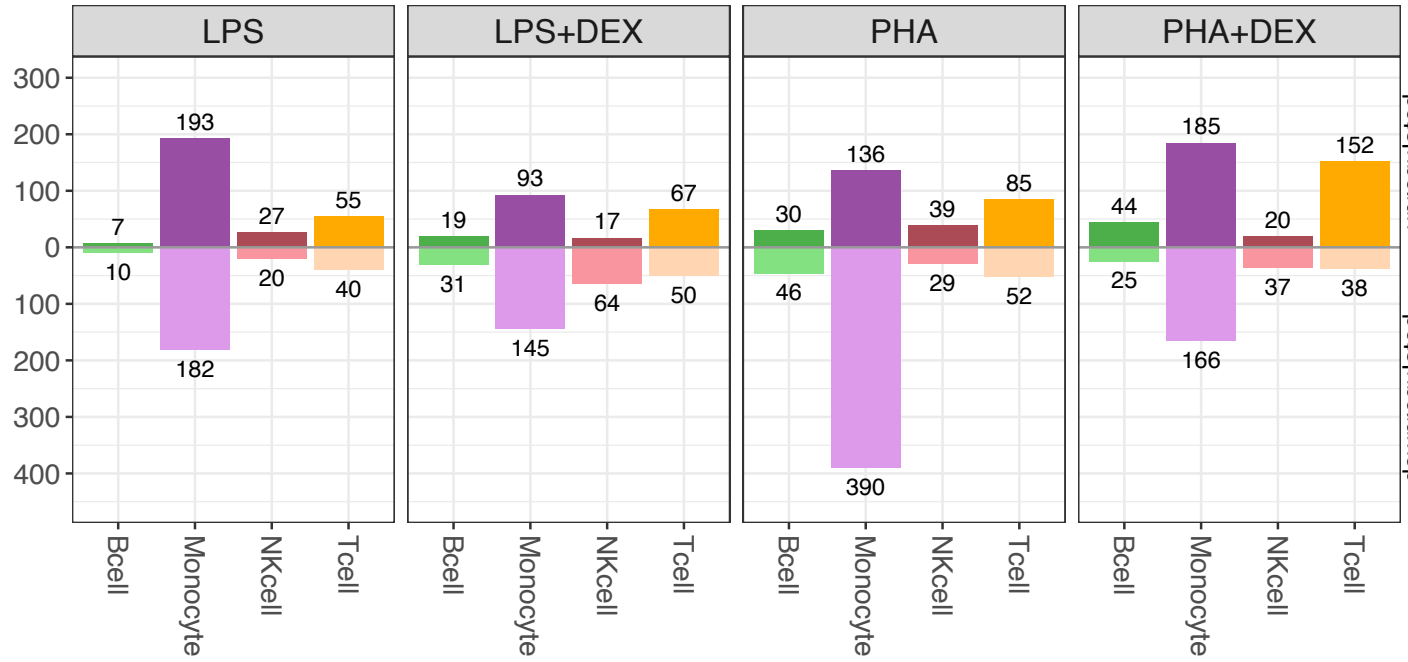


Figure S13: **Number of DVGs across contrasts and cell types:** B cells (green), Monocytes (purple), NK cells (maroon) and T cells (orange), below axis representing genes with decreased variability and above axis representing genes with increased variability (FDR<10% and —LFC—>0.5%)

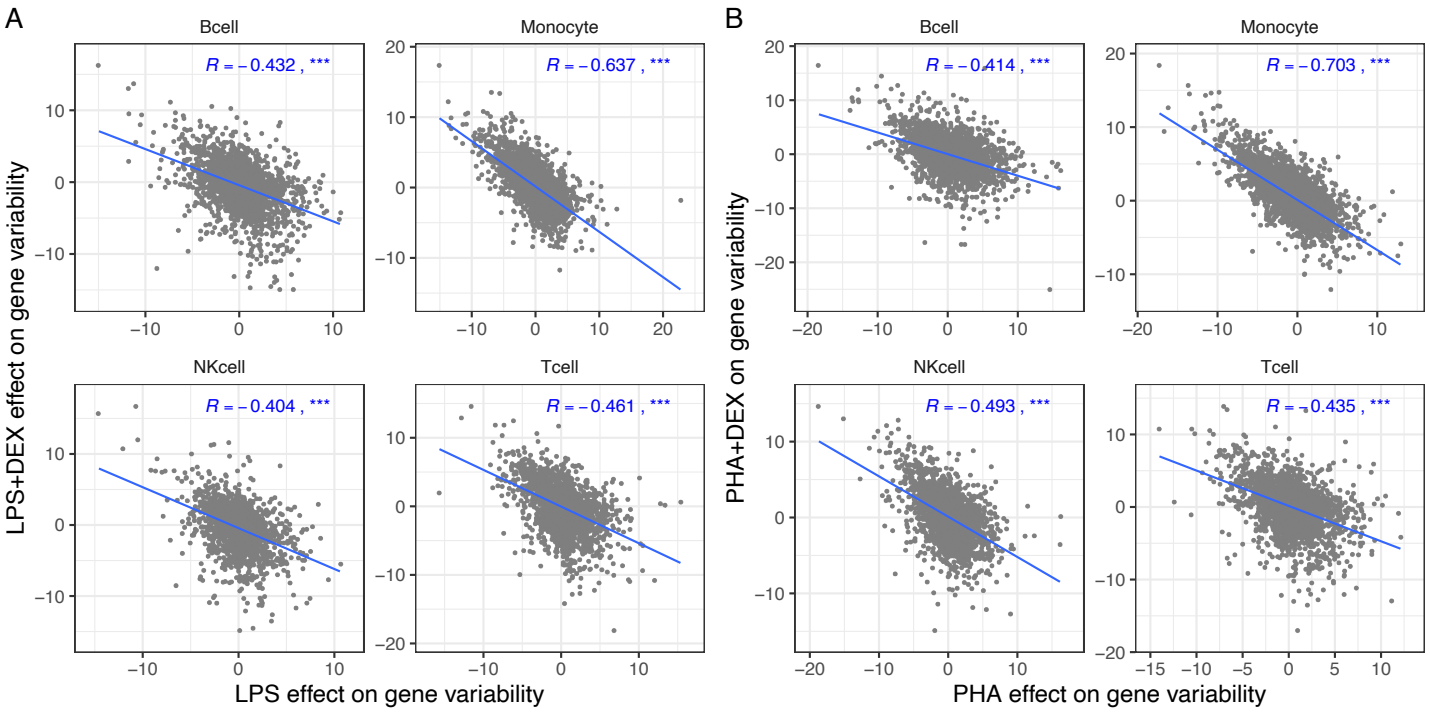


Figure S14: **Dexamethasone (DEX) reverses effect of activation by immune stimuli on gene variability A** Scatterplots of LPS effect on gene variability (x axis) against DEX effect on gene variability (y axis). **B** Scatterplots of PHA effect on gene variability (x axis) against DEX effect on gene variability (y axis). Blue lines represent the linear trend between the effects of immune stimuli and DEX treatments on gene expression. *R* represents the correlation coefficients of the effects of two types of immune treatments on gene expression, *denoting $p \leq 0.05$, ** denoting $p \leq 0.01$ and *** denoting $p \leq 0.001$.

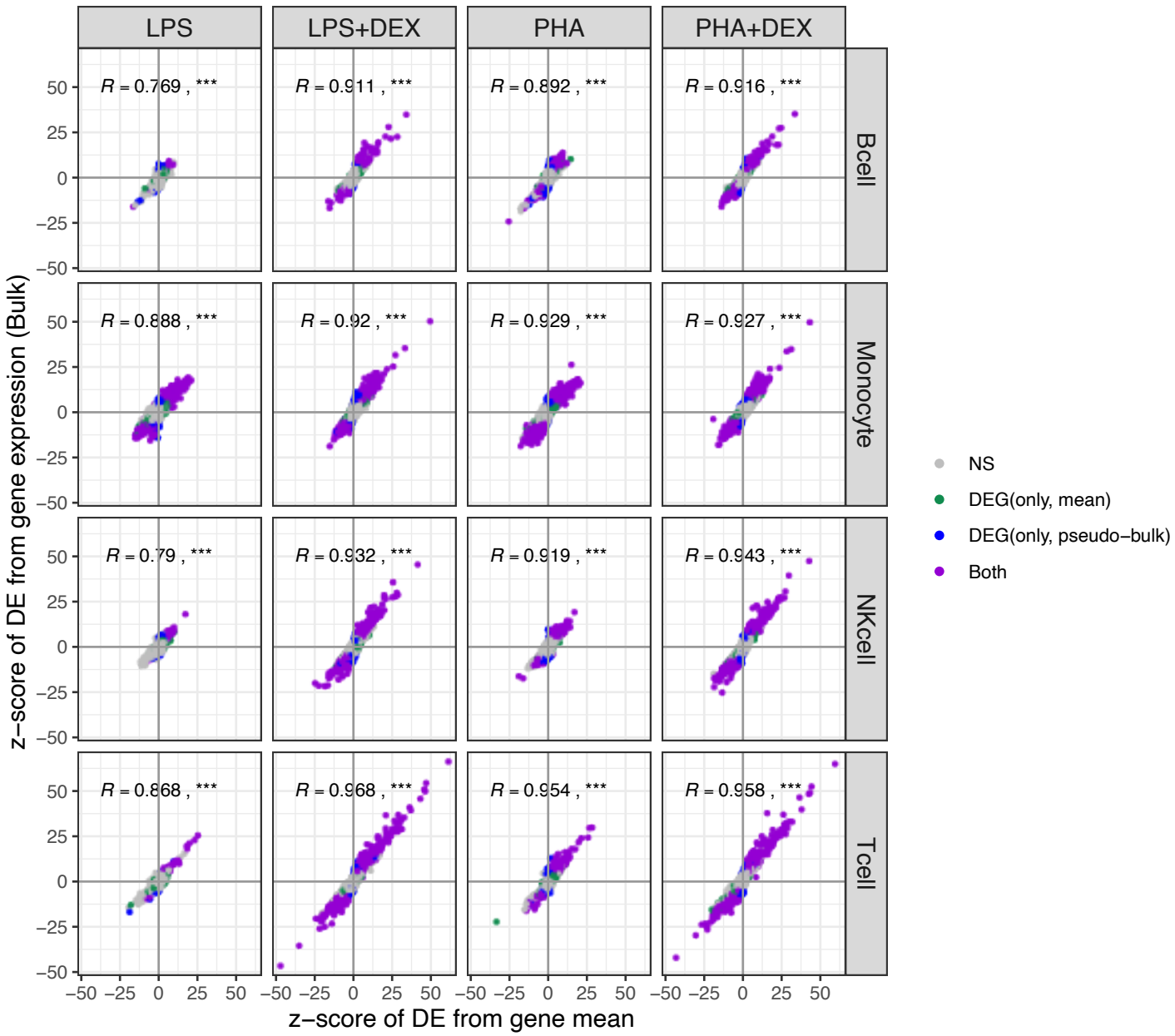


Figure S15: **The scatter plots of the z score of treatment effects on gene mean (x axis) from Negative bionomial distribution against the z score of treatment effects on gene expression (y axis) from bulk data:** Color represents significant treatment effects on gene mean only (green), bulk-derived DEGs only (blue), both (purple) and neither (gray). The *R* represents the correlation coefficients of the treatment effects on gene mean expression and gene bulk expression , $p \geq 0.05$ (NS), $p < 0.05$ (*), $p < 0.01$ (**) and $p < 0.001$(***).

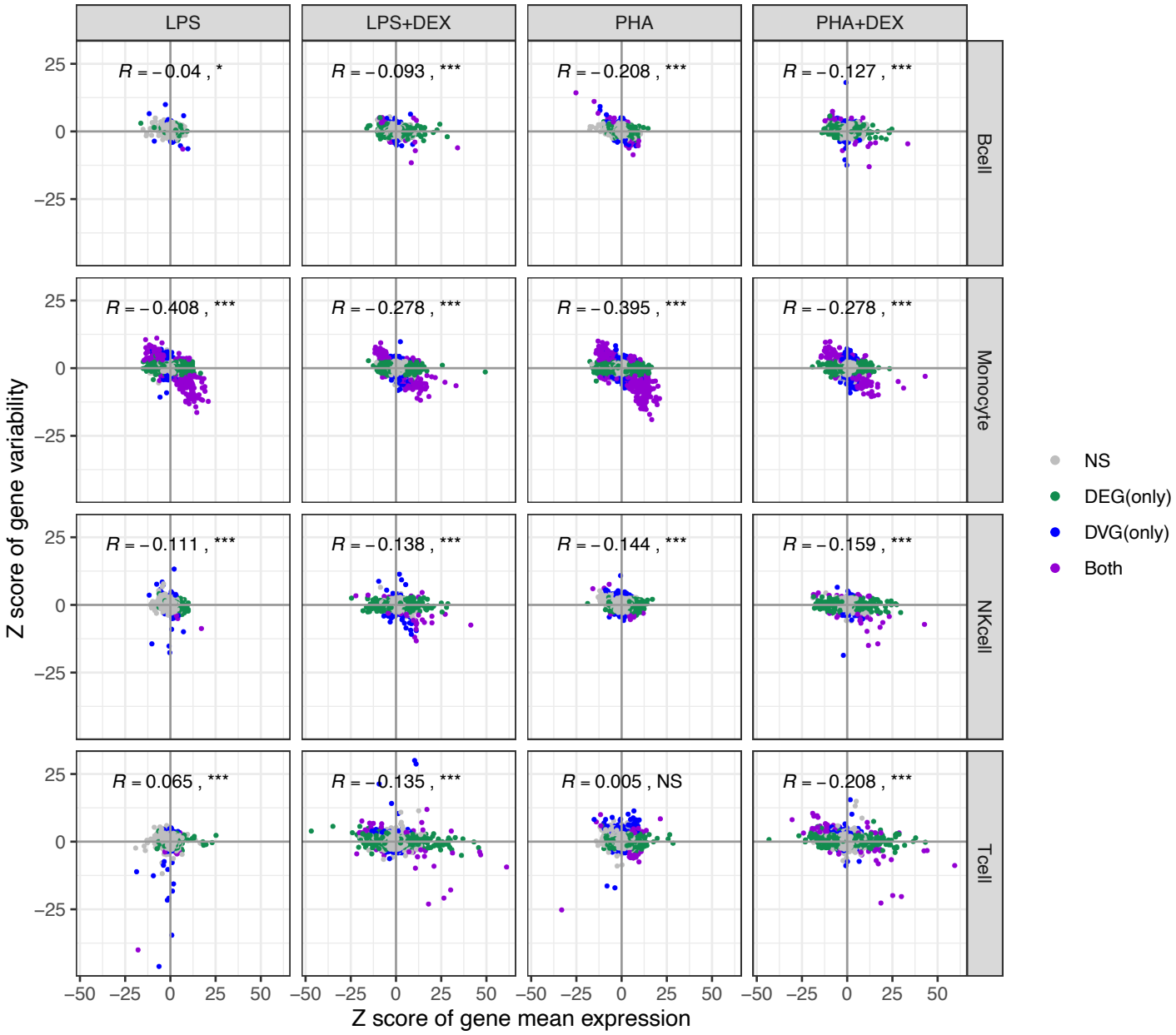


Figure S16: **The scatter plots of the z score of treatment effects on gene mean (x axis) against the z score of treatment effects on gene variability (y axis):** Color represents significant treatment effects on gene mean only (green), gene variability only (blue), both (purple) and neither (gray). The $R$ represents the correlation coefficients of the treatment effects on gene mean and gene variability, $p \geq 0.05$ (NS), $p < 0.05$ (*), $p < 0.01$ (**) and $p < 0.001$(***).

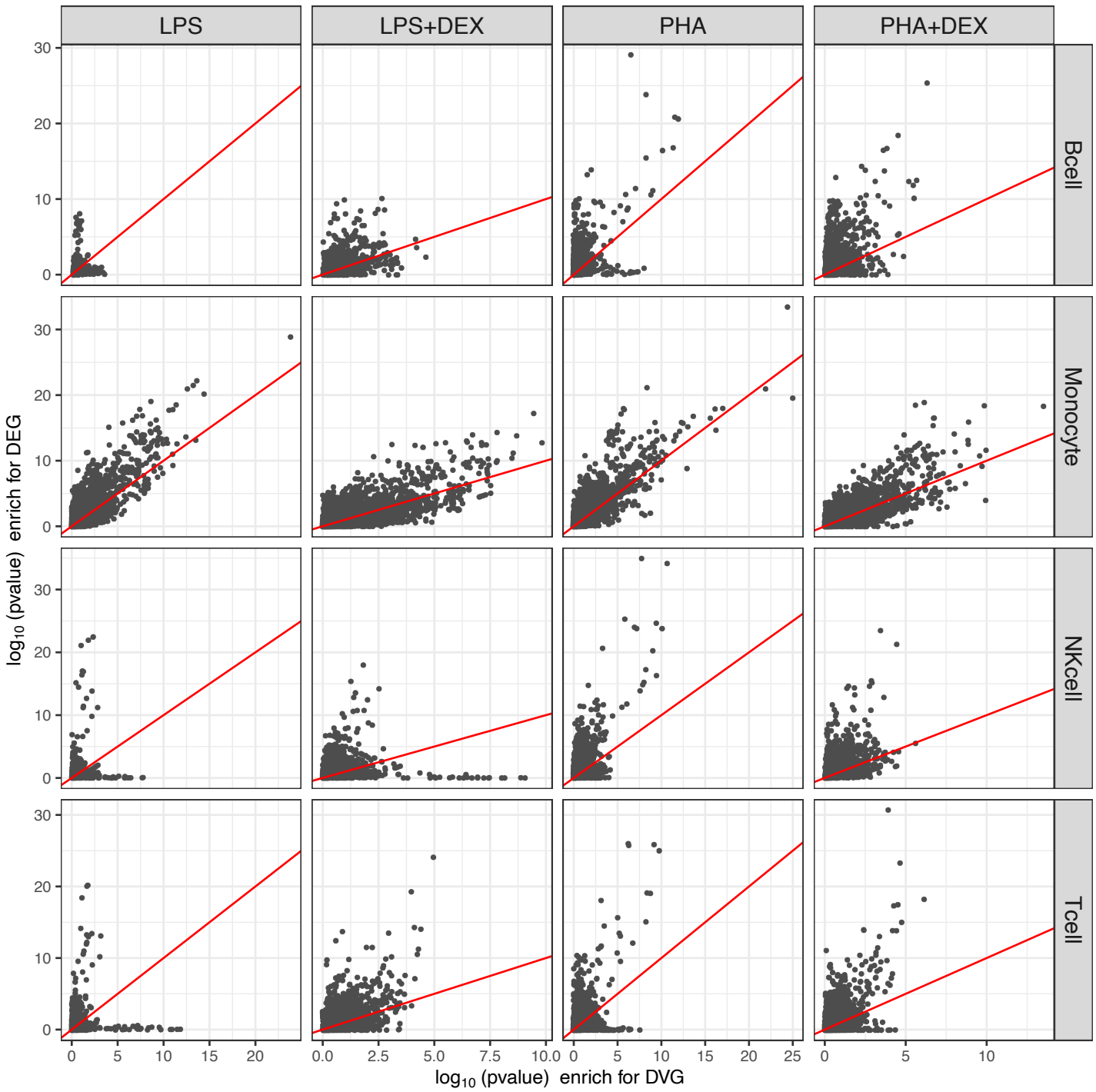


Figure S17: **Comparison of the results of GO enrichment between DEG and DVG**, x axis representing $-\log_{10}(p)$ of the GO terms that are enriched by DVG and Y axis representing $-\log_{10}(p)$ of the GO terms that are enriched by DEG.

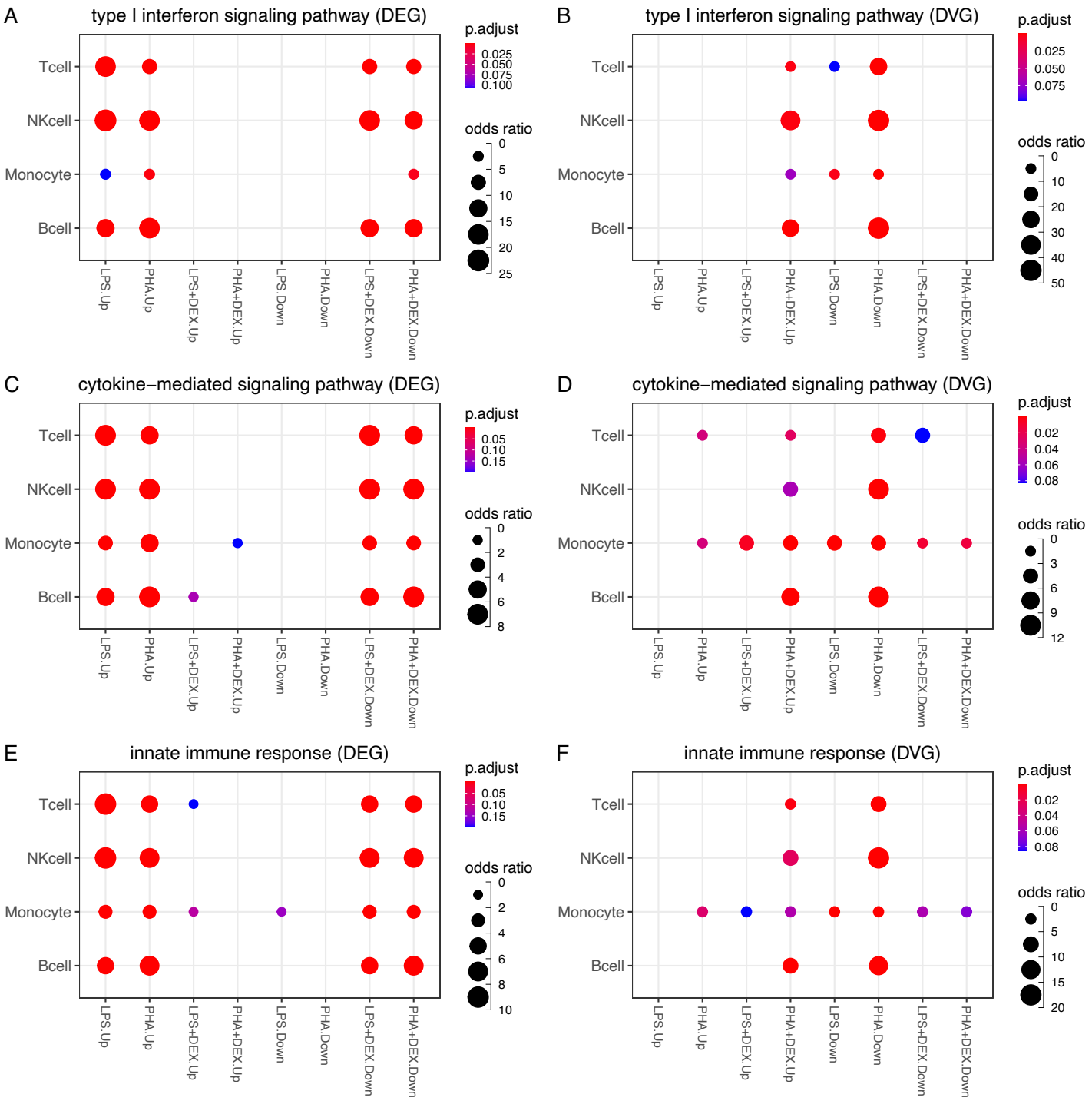


Figure S18: **Examples of shared enrichment pathways for DEG and DVG: (A and B)** represent enrichment results in the type I interferon signaling pathway for DEG and DVG, respectively, **(C and D)** represent enrichment results in the cytokine-mediated signaling pathway for DEG and DVG, respectively, and **(E and F)** represent enrichment results in innate immune response for DEG and DVG, respectively.

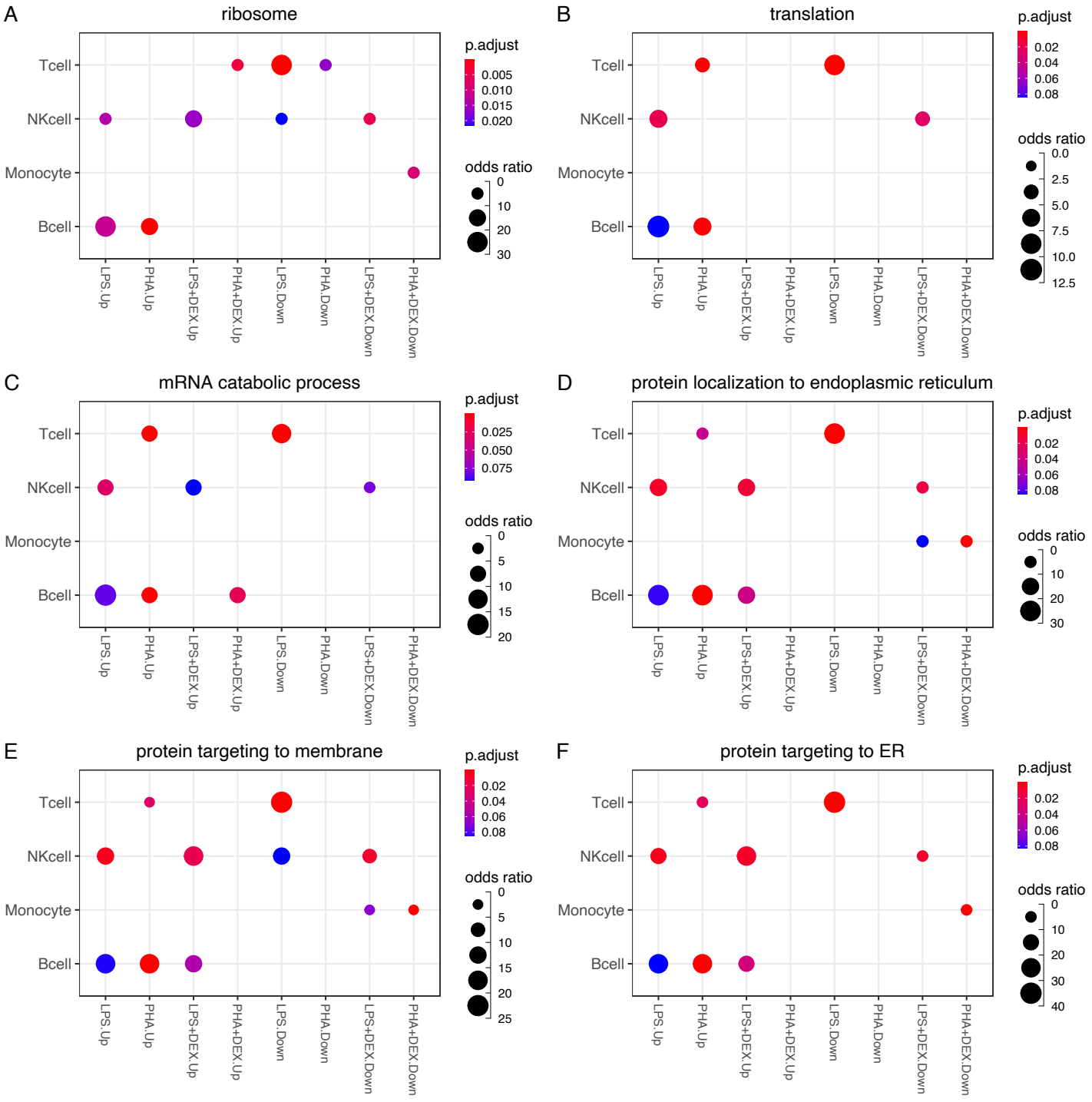


Figure S19: **Examples of the pathways that are only enriched in DVGs:** **(A-F)** represent enrichment results in ribosome, translation, mRNA catabolic process, protein localization to endoplasmic reticulum, protein targeting to membrane and protein targeting to ERrespectively.

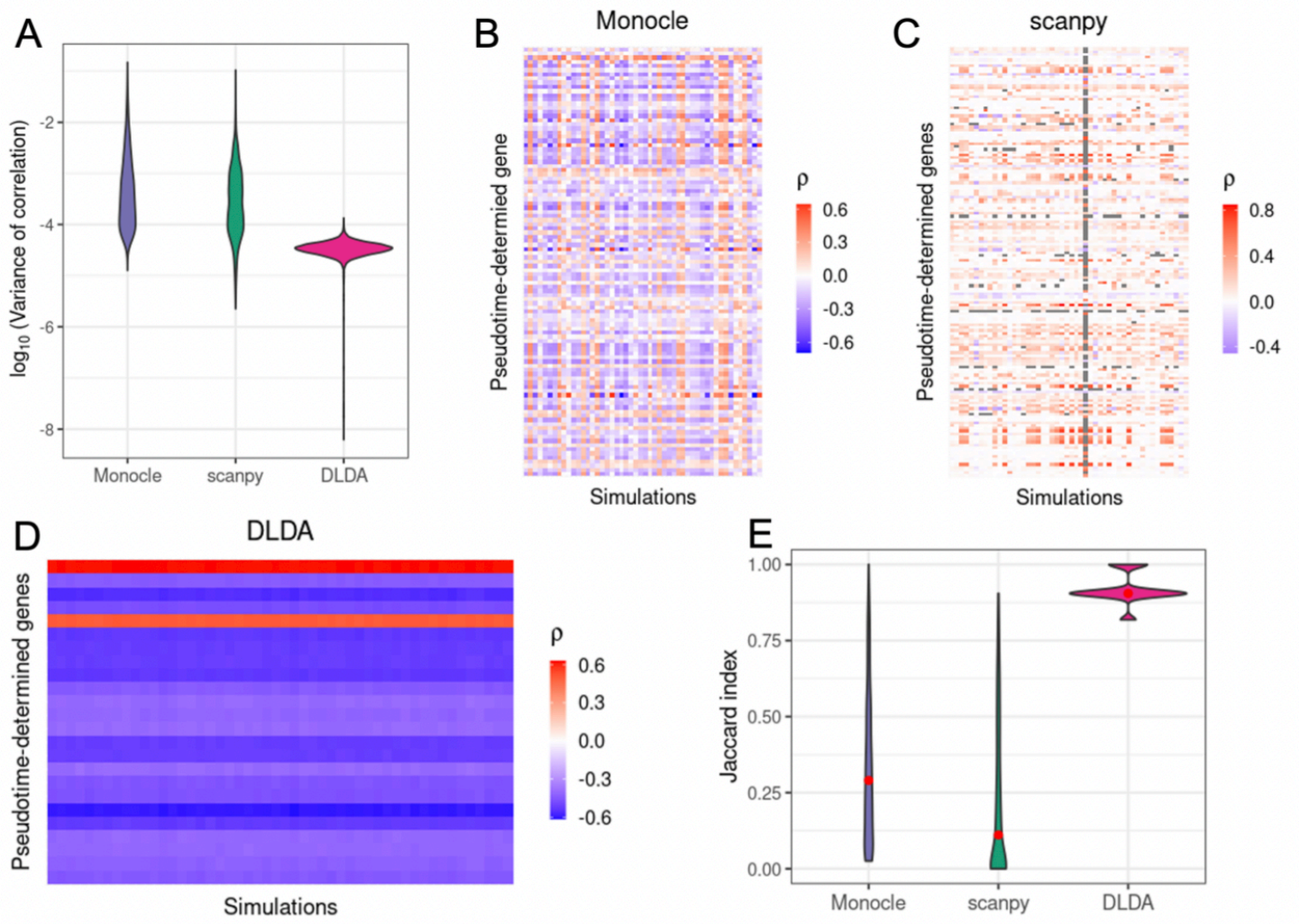


Figure S20: footnotesize **Validation of effectiveness and robustness of the treatment pseudotime trajectory using resampling (A)** Violin plot of the variance of correlation coefficients for each gene across 50 resamplings from Monocle, SCANPY and DLDA. **(B-D)** Heatmaps of the correlation coefficients of top 20 ranking pseudotime driving genes across resampling. Each row represents the same gene and each column a resampling iteration with the color representing the magnitude of the correlation between gene expression and the derived pseudo-time variable; ideally we would like to see that correlation be approximately constant. The resamplings are from **(B)** Monocle, **(C)** SCANPYand **(D)**DLDA, respectively. **(E)** Violin plot of jaccard index of the stability of the top 20 pseudotime correlated genes for each pair of resamplings across 1,225 pairwise comparisons from Monocle, SCANPY and DLDA.

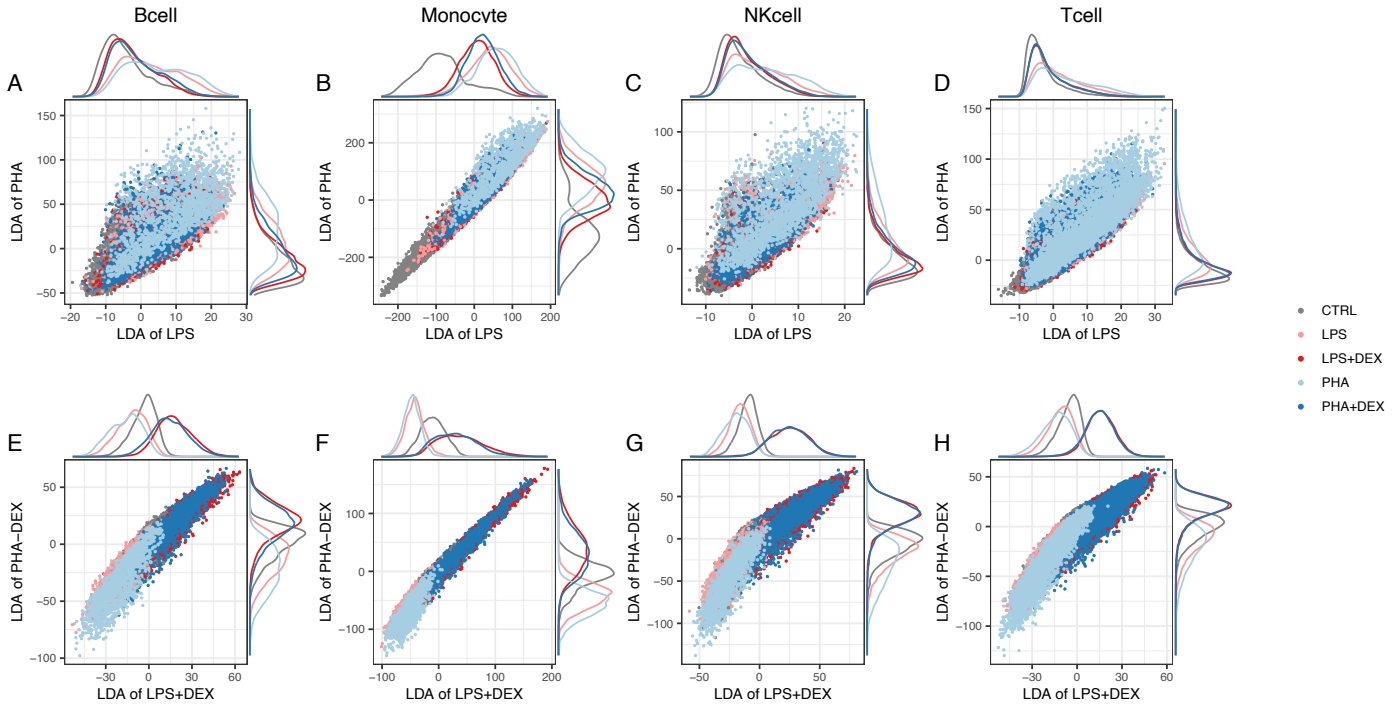


Figure S21: **Low dimensional manifold plots from DLDA across cell types: (A-D)** represent the scatter plots of the DLDA from LPS (x axis) against the DLDA from PHA (y axis) and **(E-H)** represent the scatter plots of the DLDA from LPS+DEX (x axis) against PHA+DEX (y axis).

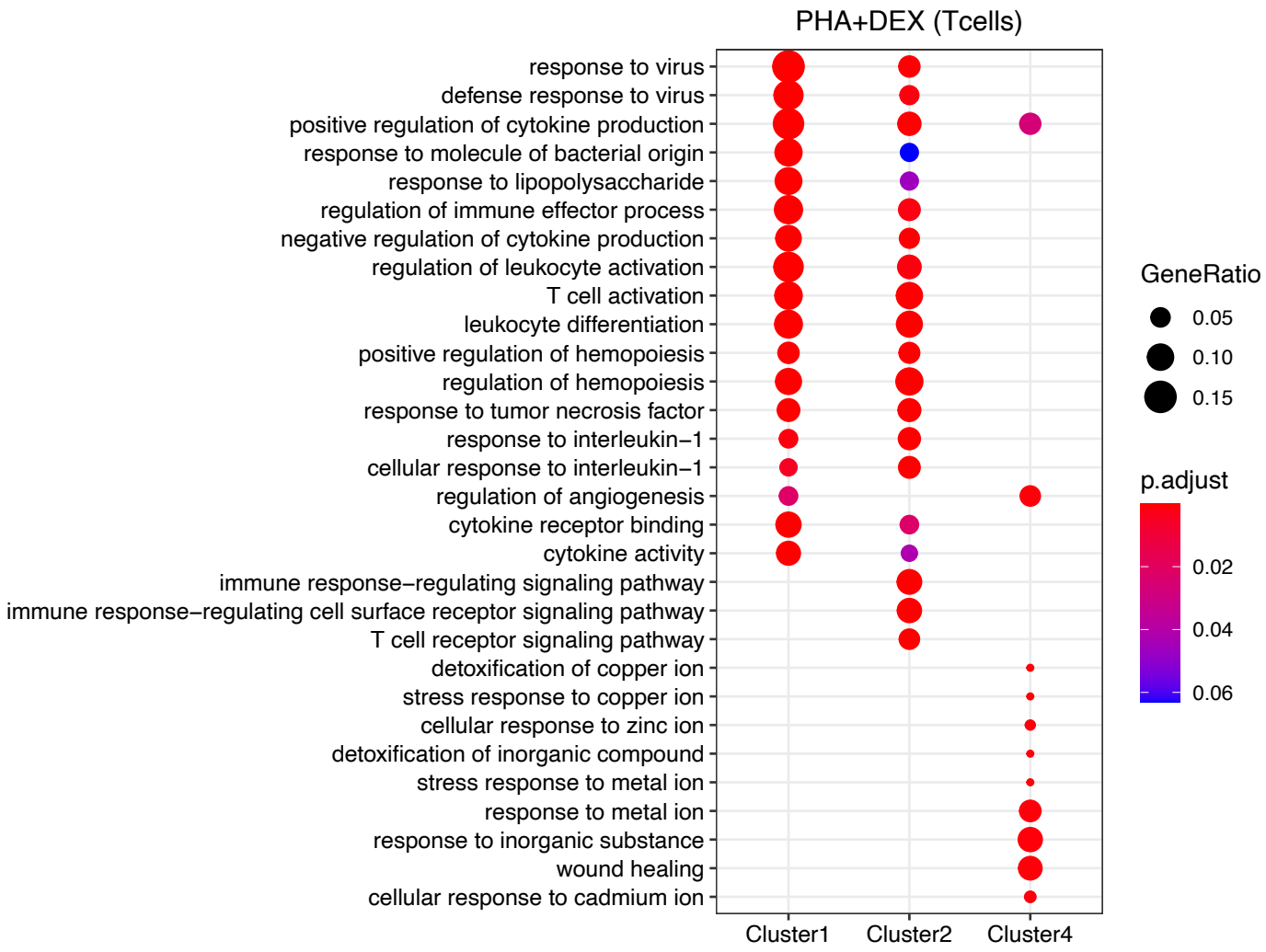


Figure S22: **Gene Ontology enrichment results for four dynamic patterns DEGs respectively**

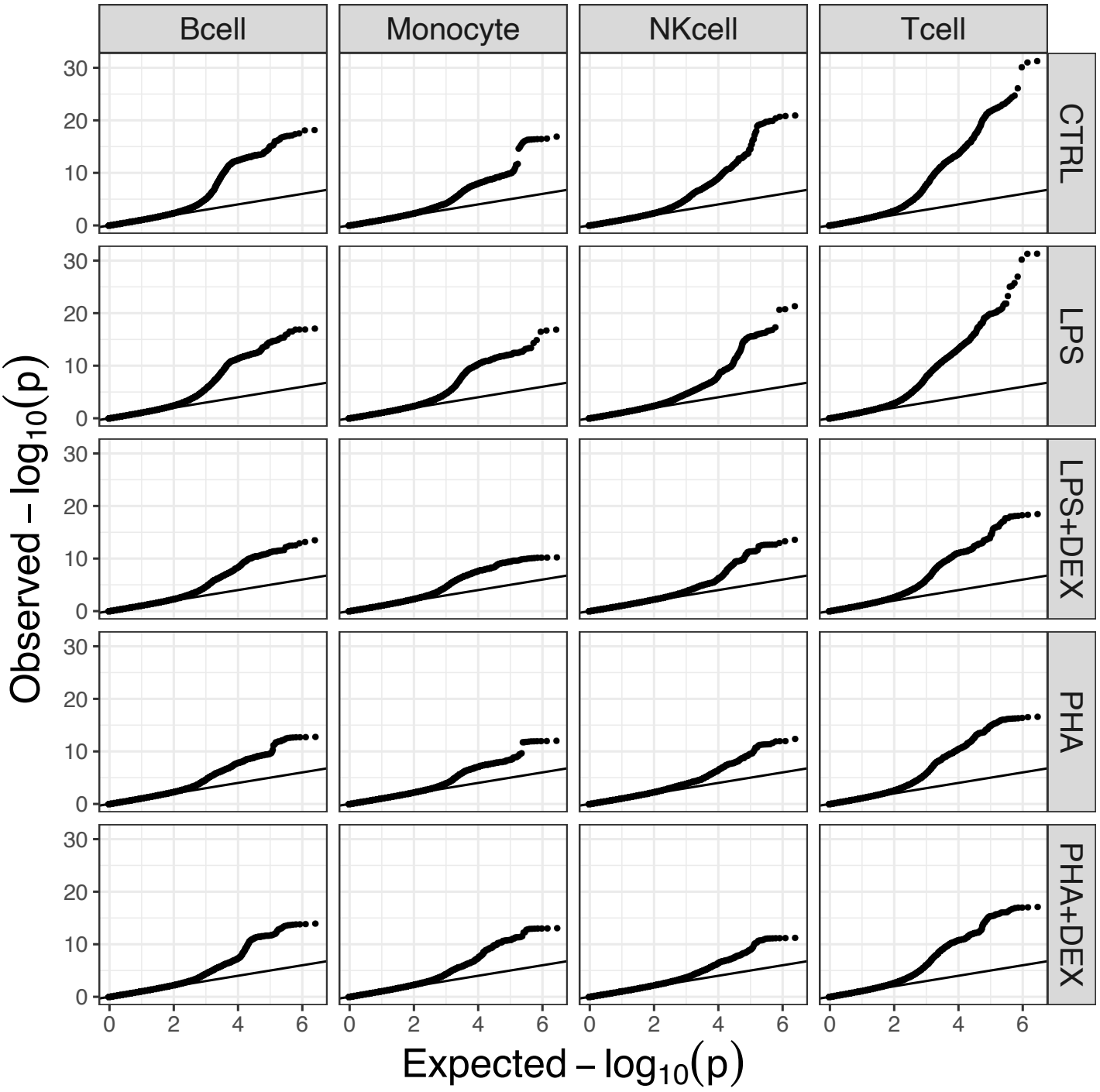


Figure S23: **QQplots of p-values from eQTL mapping with FastQTL on pseudobulk gene expression data across the 20 conditions.**

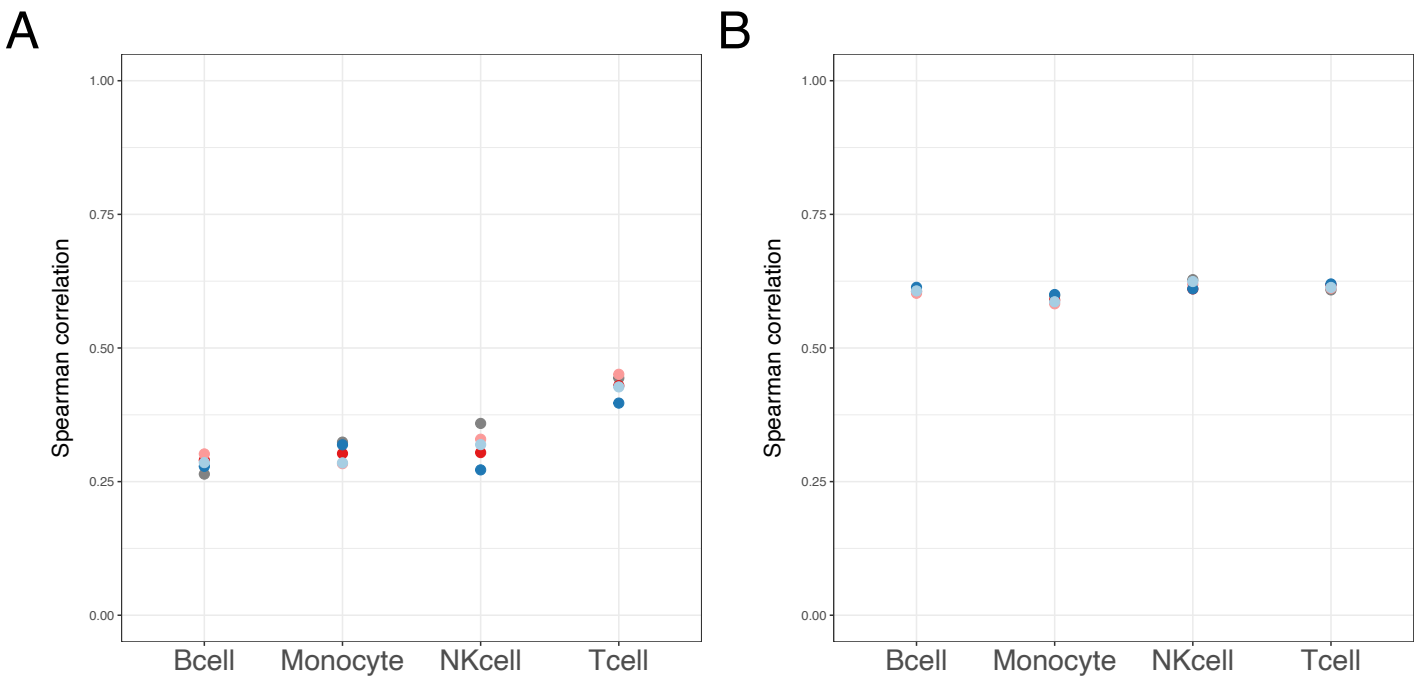


Figure S24: **Correlations between genetic effect sizes assessed in single-cell data and in bulk RNA-seq Resztak et al. (2021)A** Spearman's correlations for significant genetic effect sizes assessed by condition-by-condition analysis (FDR$< 0.1$) **B** Spearman's correlations for significant genetic effect sizes assessed by multivariate adaptive shrinkage analysis (LFSR$< 0.1$). Color denotes treatment: grey – control, light blue – PHA, dark blue – PHA+DEX, pink – LPS, red – LPS+DEX. All values are significant (p-value$< 0.05$).

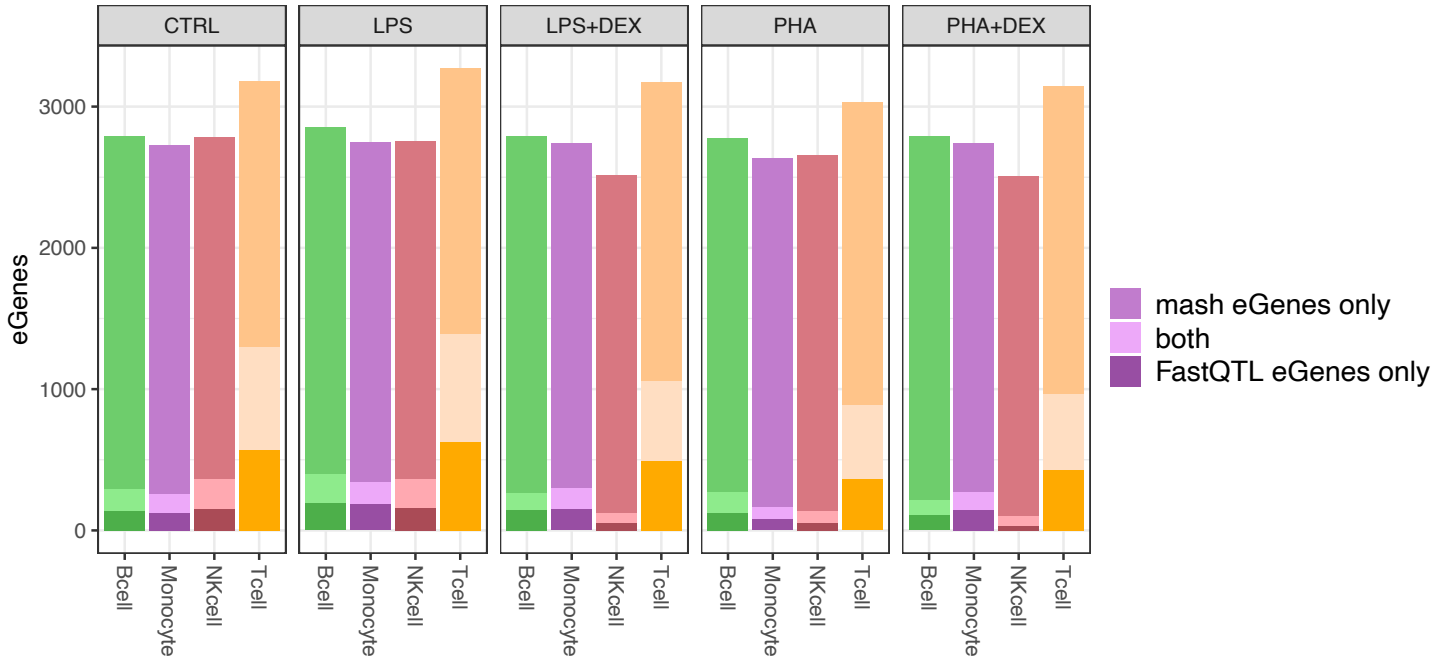


Figure S25: **eQTL mapping results.** Barplot represents the number of genes with eQTLs (eGenes) significant in only condition-by-condition analysis (FDR$<$ 0.1, dark shading), significant in multivariate adaptive shrinkage analysis only (LFSR$<$ 0.1, medium shading), and significant in both analyses (light shading).

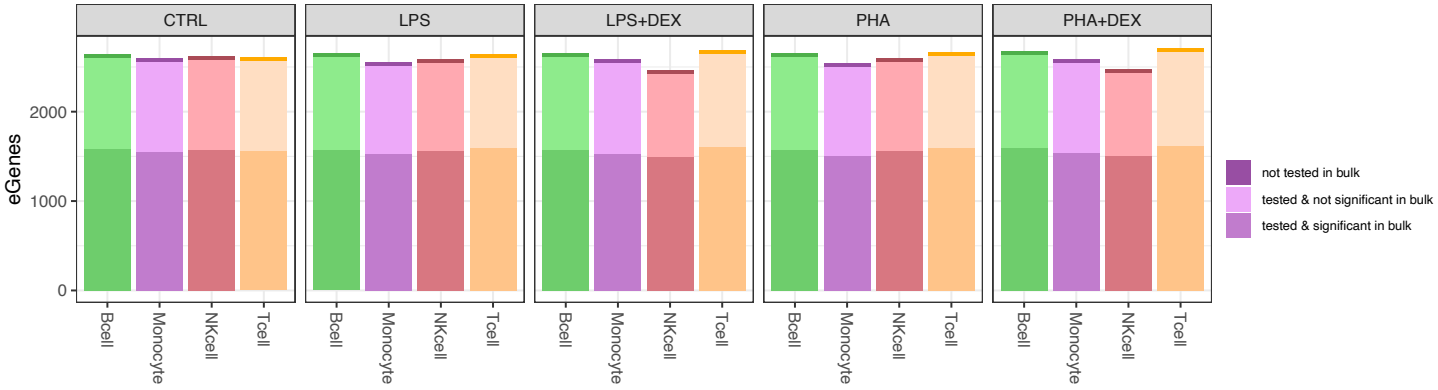


Figure S26: **Barplot represents the number of genes with significant eQTLs as assessed by multivariate adaptive shrinkage analysis (eGenes, LFSR$<$ 0.1).** Shading denotes significance in bulk dataset: significant in bulk RNA-seq data citepmid34142656 (dark shading), not tested in bulk RNA-seq data (light shading), and not significant in bulk RNA-seq data (medium shading).

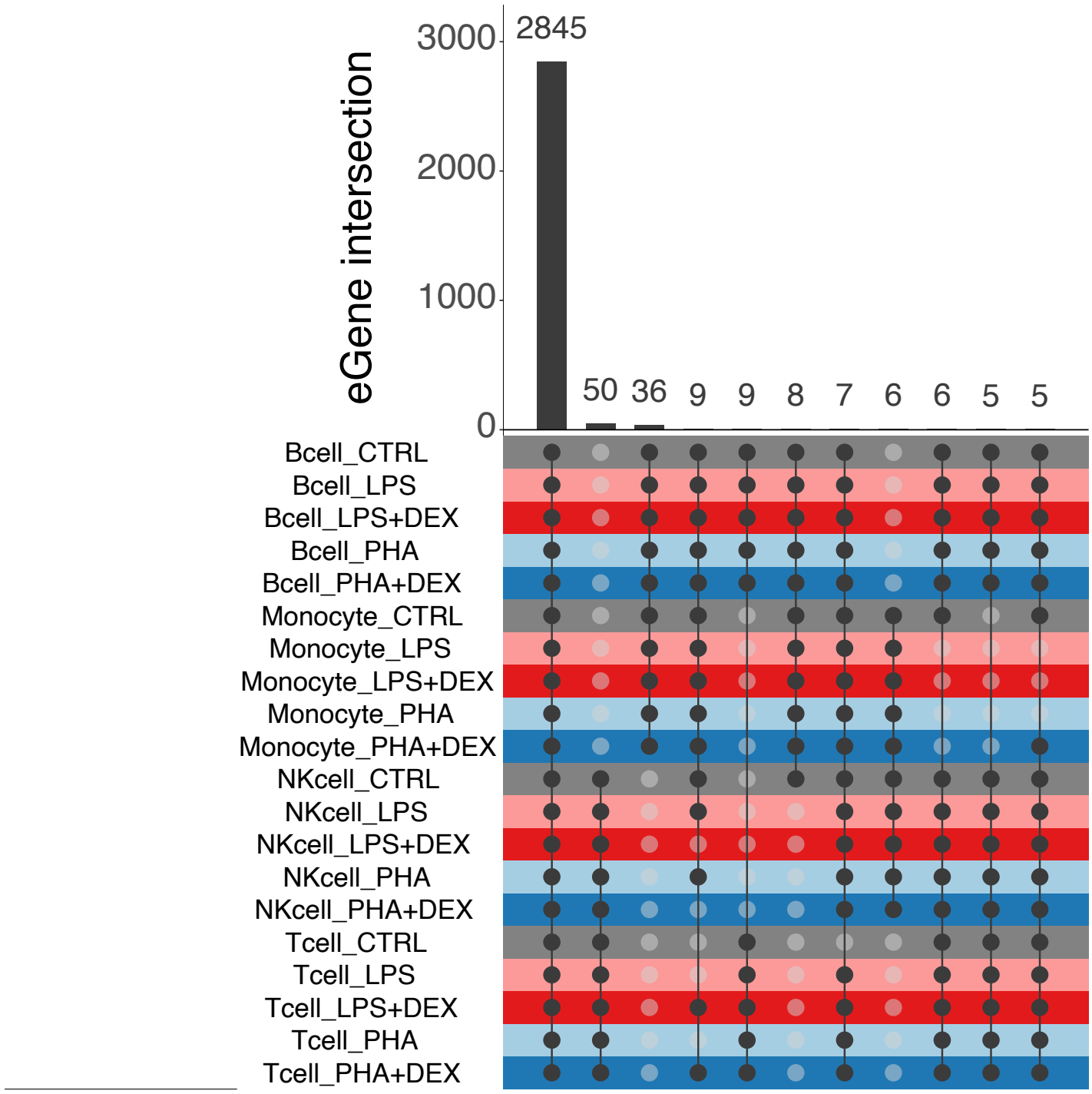


Figure S27: **eGene sharing by sign across all conditions.** Upset plot represents the number of eGenes with eQTLs shared by sign (i.e., with genetic effects in the same direction) for each unique set of conditions with intersection size of at least 5.

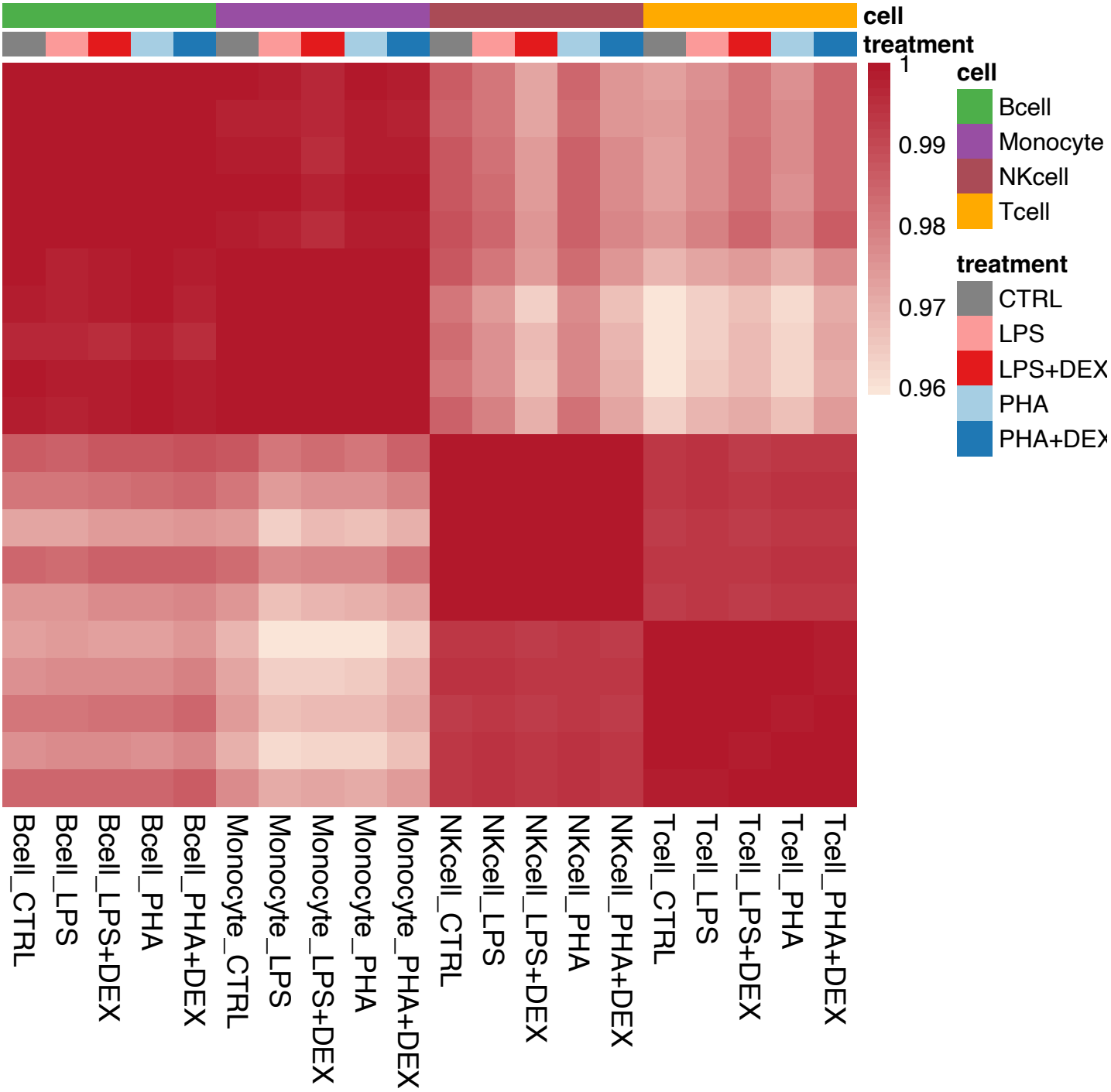


Figure S28: **eGene differences in the direction of effect across all pairs of conditions.** Heatmap represents proportion of eGenes significant in either of the two conditions which have at least one eQTL significant in either of the two conditions with opposite sign of genetic effect size estimated by multivariate adaptive shrinkage.

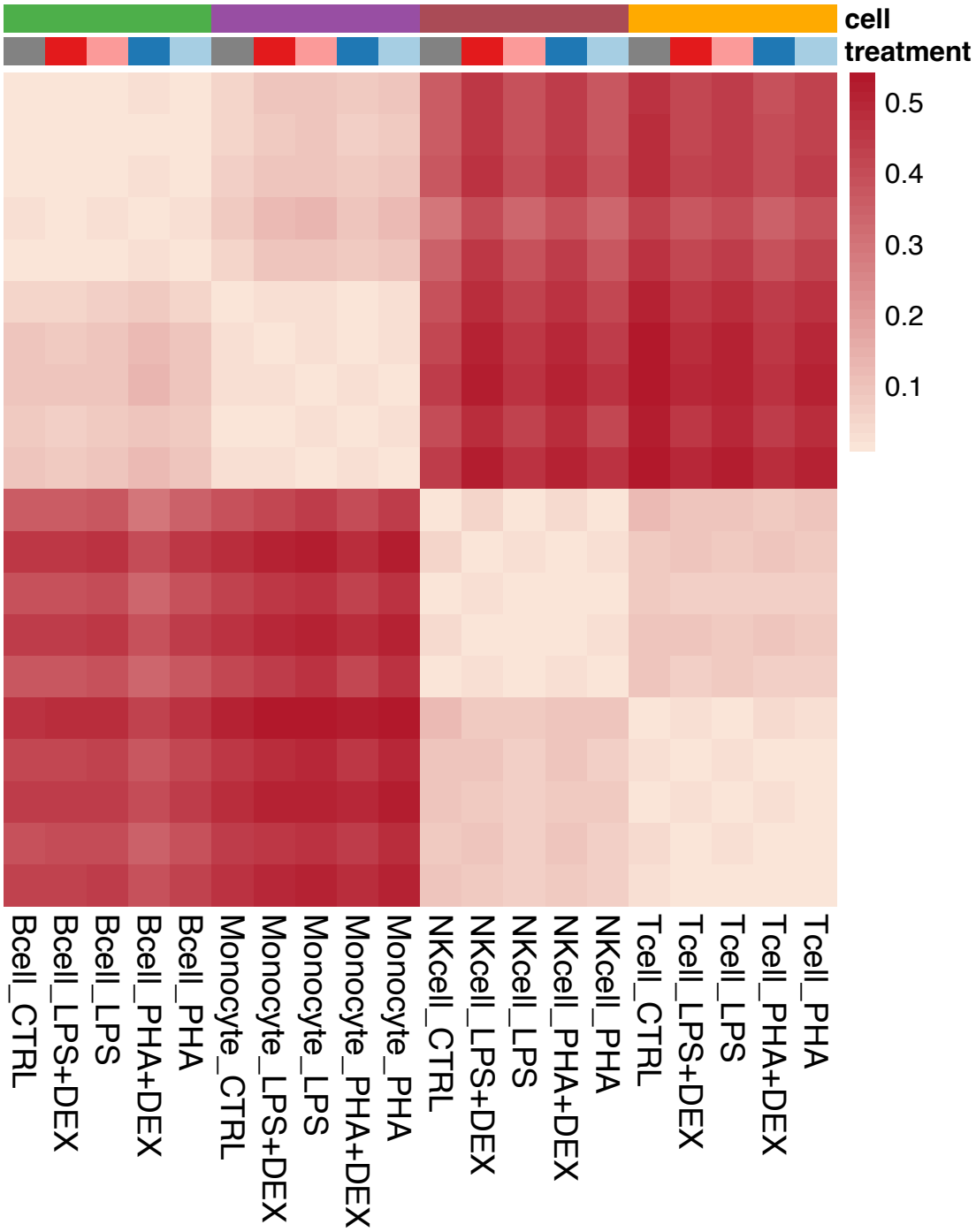


Figure S29: **eGene differences across all pairs of conditions.** Heatmap represents proportion of eGenes significant in either of the two conditions which have at least one eQTL significant in either of the two conditions with at least two-fold difference of genetic effect size estimated by multivariate adaptive shrinkage.

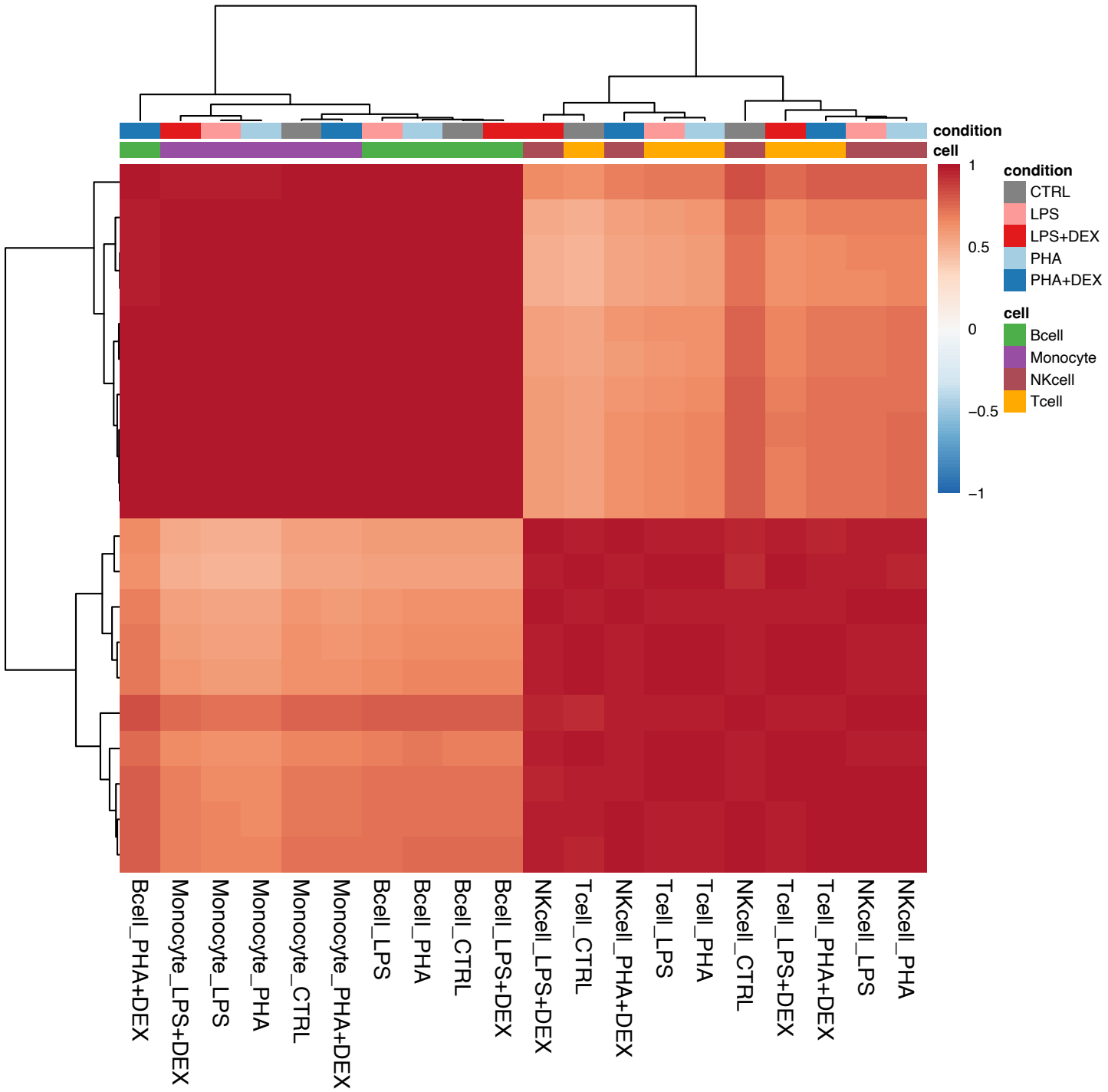


Figure S30: **Correlations between genetic effect sizes estimated with multivariate adaptive shrinkage.** Heatmap represents pairwise Pearson correlations based on union of significant eQTLs in either of the two conditions (LFSR$<0.1$). All values are significant (p-value$<0.05$).

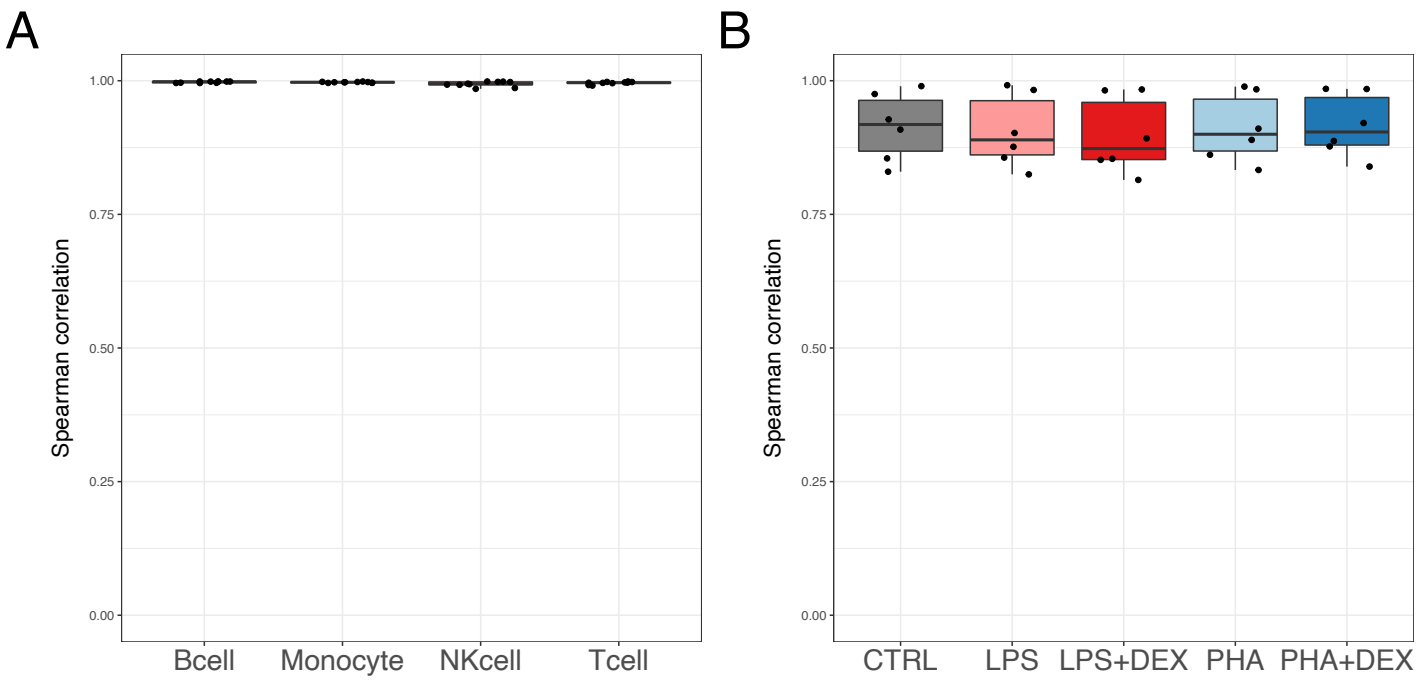


Figure S31: **Spearman's correlations between significant genetic effect sizes estimated with multivariate adaptive shrinkage (LFSR**$< 0.1$**). A** pair-wise correlations between all treatment conditions within each cell type **B** pair-wise correlations between all cell types within each treatment. All values are significant (p-value$< 0.05$).

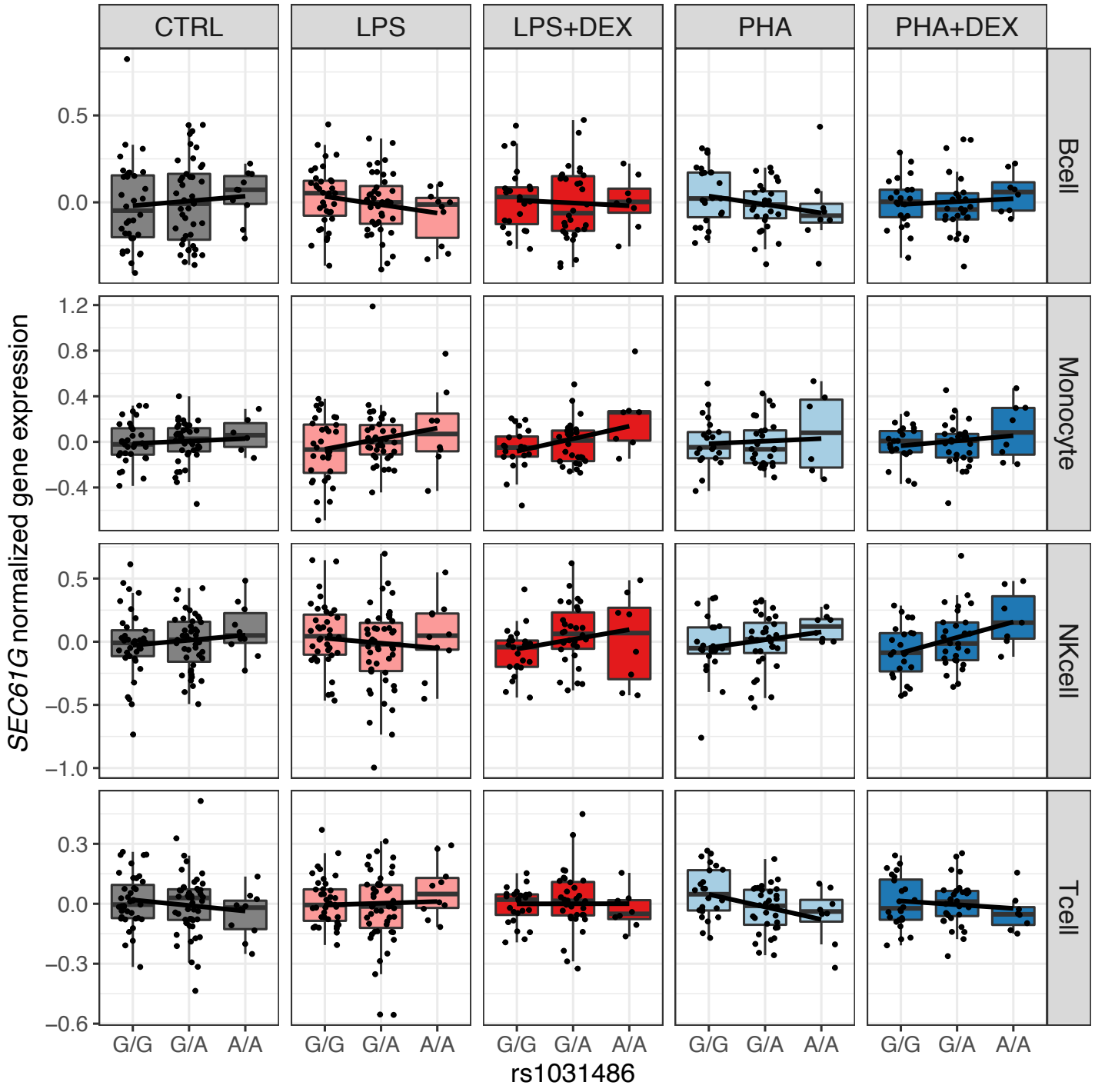


Figure S32: **Genetic effect of rs1031486 on gene expression of *SEC61G*.** Boxplots represent normalized expressions of the *SEC61G* gene (y axis) across the three genotype classes of rs1031486 (x axis) across all conditions.

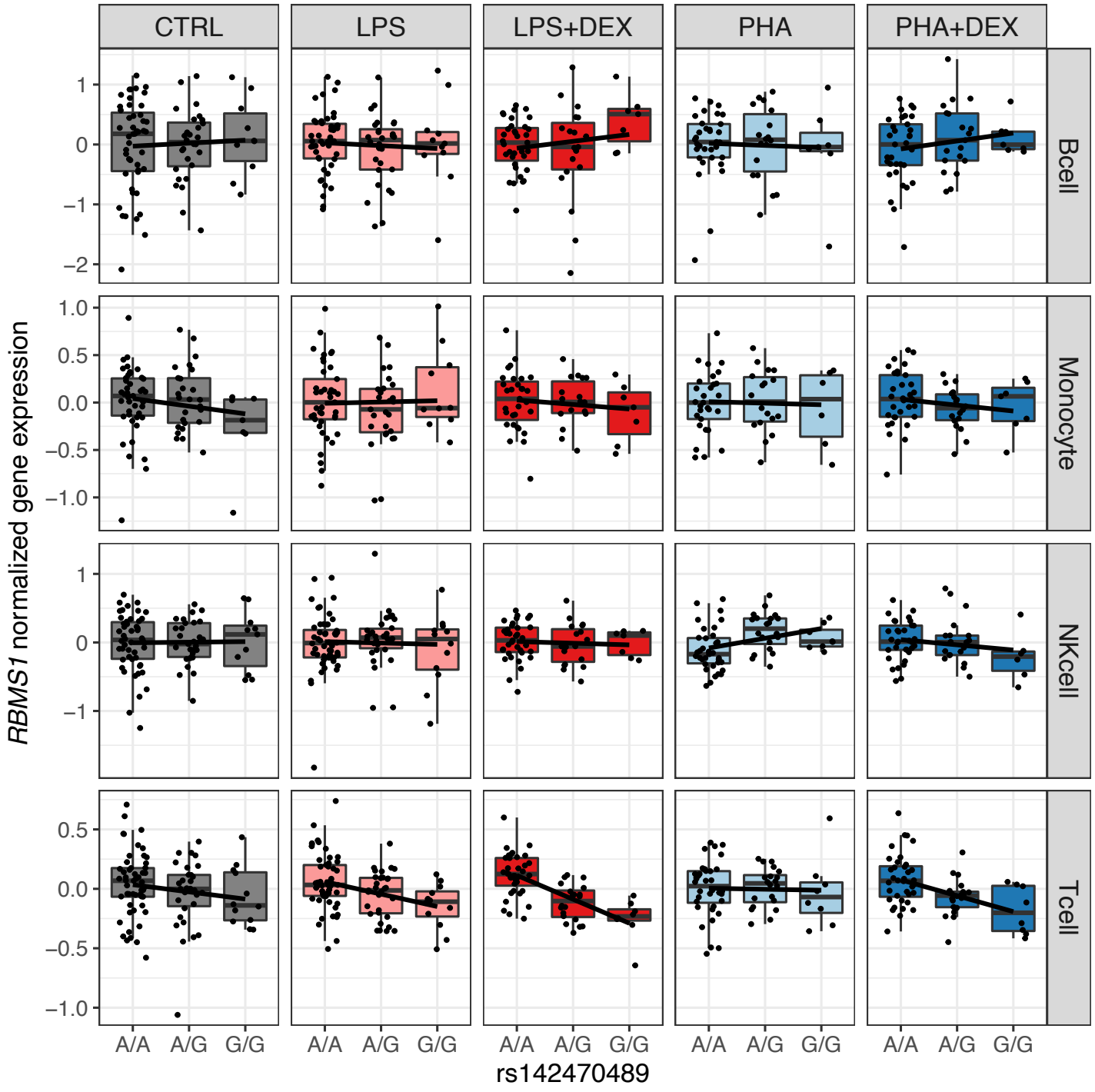


Figure S33: **Genetic effect of rs142470489 on gene expression of *RBMS1*.** Boxplots represent normalized expressions of the *RBMS1* gene (y axis) across the three genotype classes of rs142470489 (x axis) across all conditions.

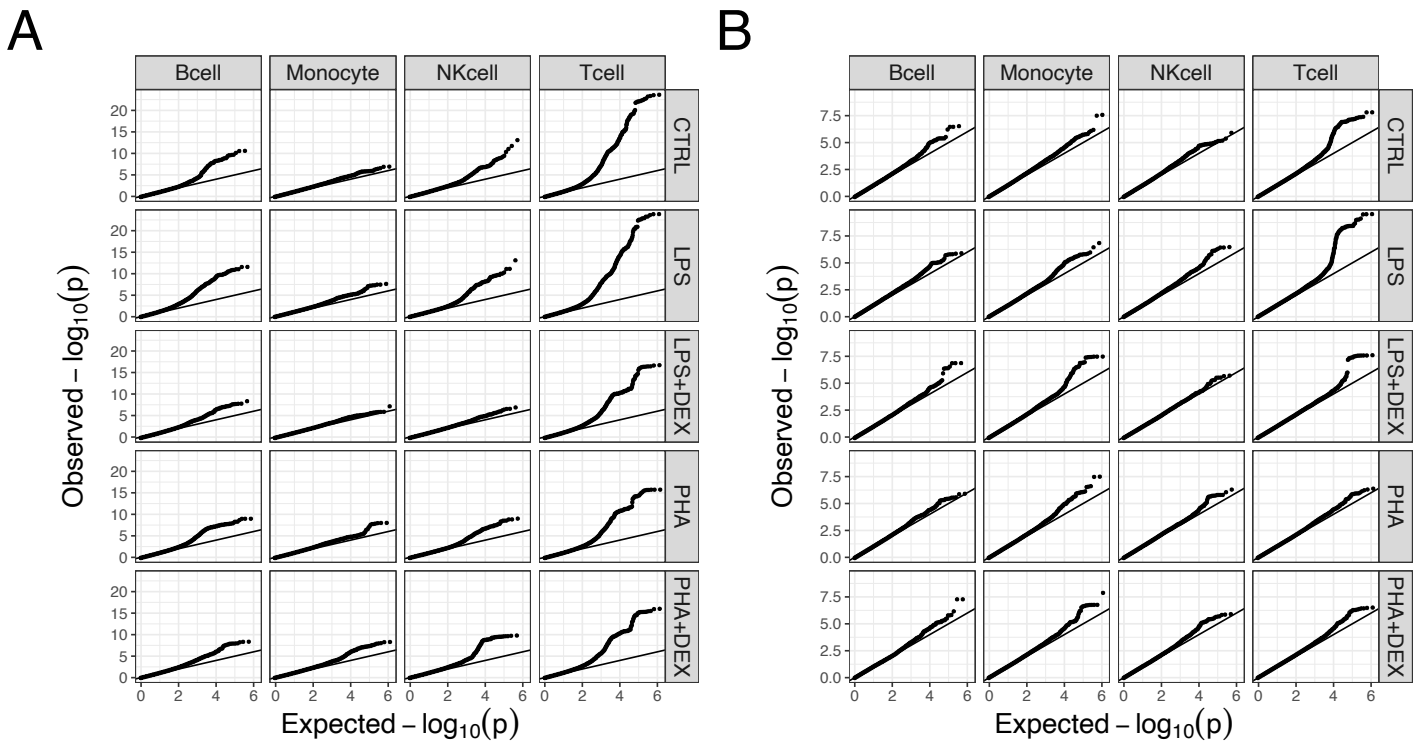


Figure S34: **QQplots for genetic analyses of mean and variability. A** p-values from mean-eQTL mapping with FastQTL **B** p-values from variability QTL mapping with FastQTL.

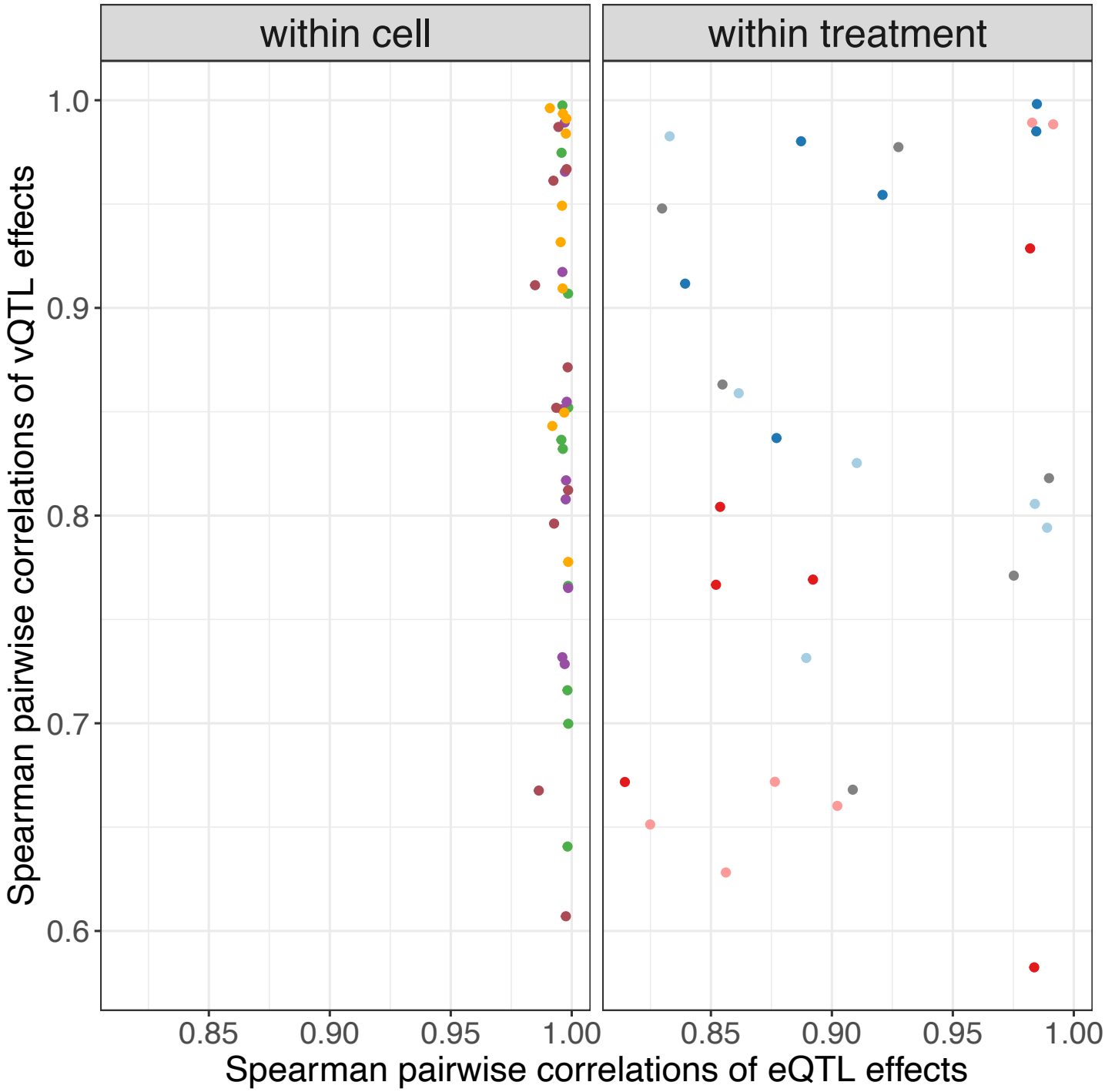


Figure S35: **Cell type- and treatment-specificity of genetic effects on gene expression and gene expression variability.** Scatterplots represent pairwise Spearman's correlations between significant genetic effects (LFSR$<$ 0.1) on gene expression (x axis), and gene expression variability (y axis) across all treatment conditions within each cell type (left panel) and across all cell types within each treatment condition (right panel).

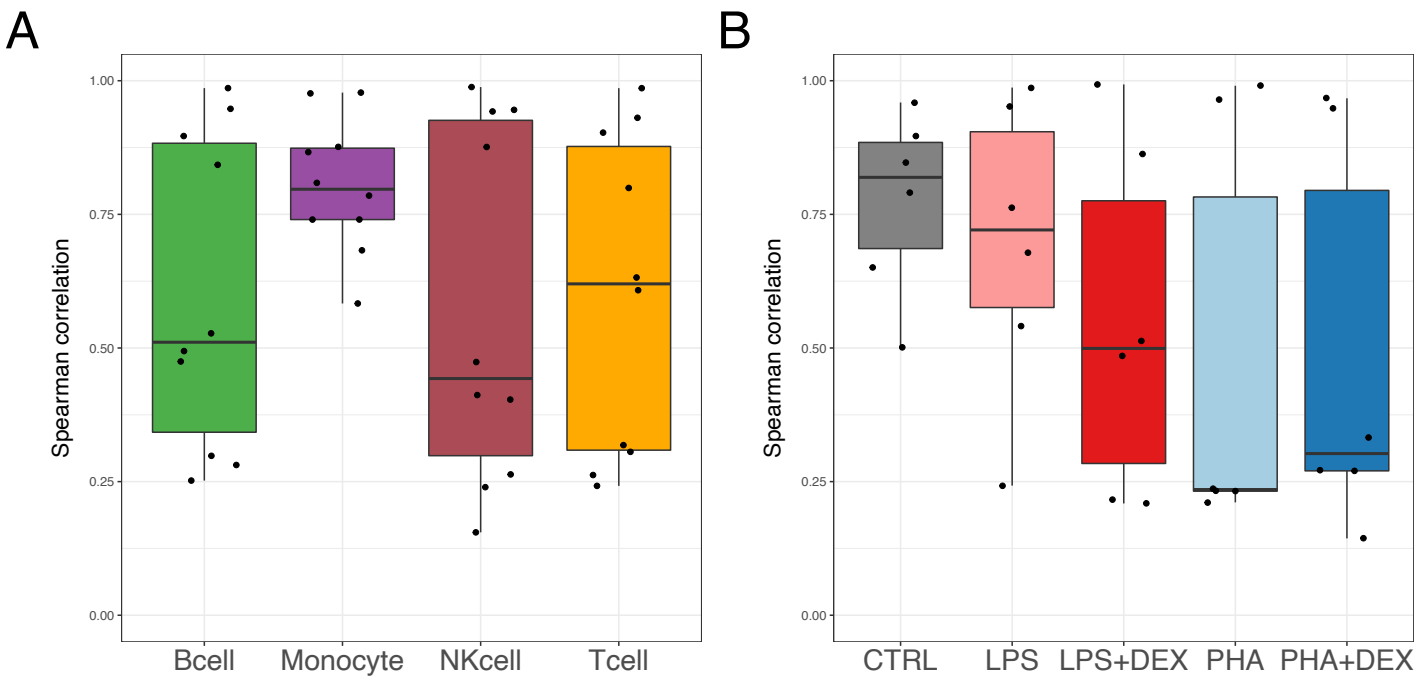


Figure S36: **Spearman's correlations between significant genetic effects on gene expression variability estimated with multivariate adaptive shrinkage (LFSR$<$ 0.1). A** – pair-wise correlations between all treatment conditions within each cell type **B** – pair-wise correlations between all cell typeswithin each treatment condition

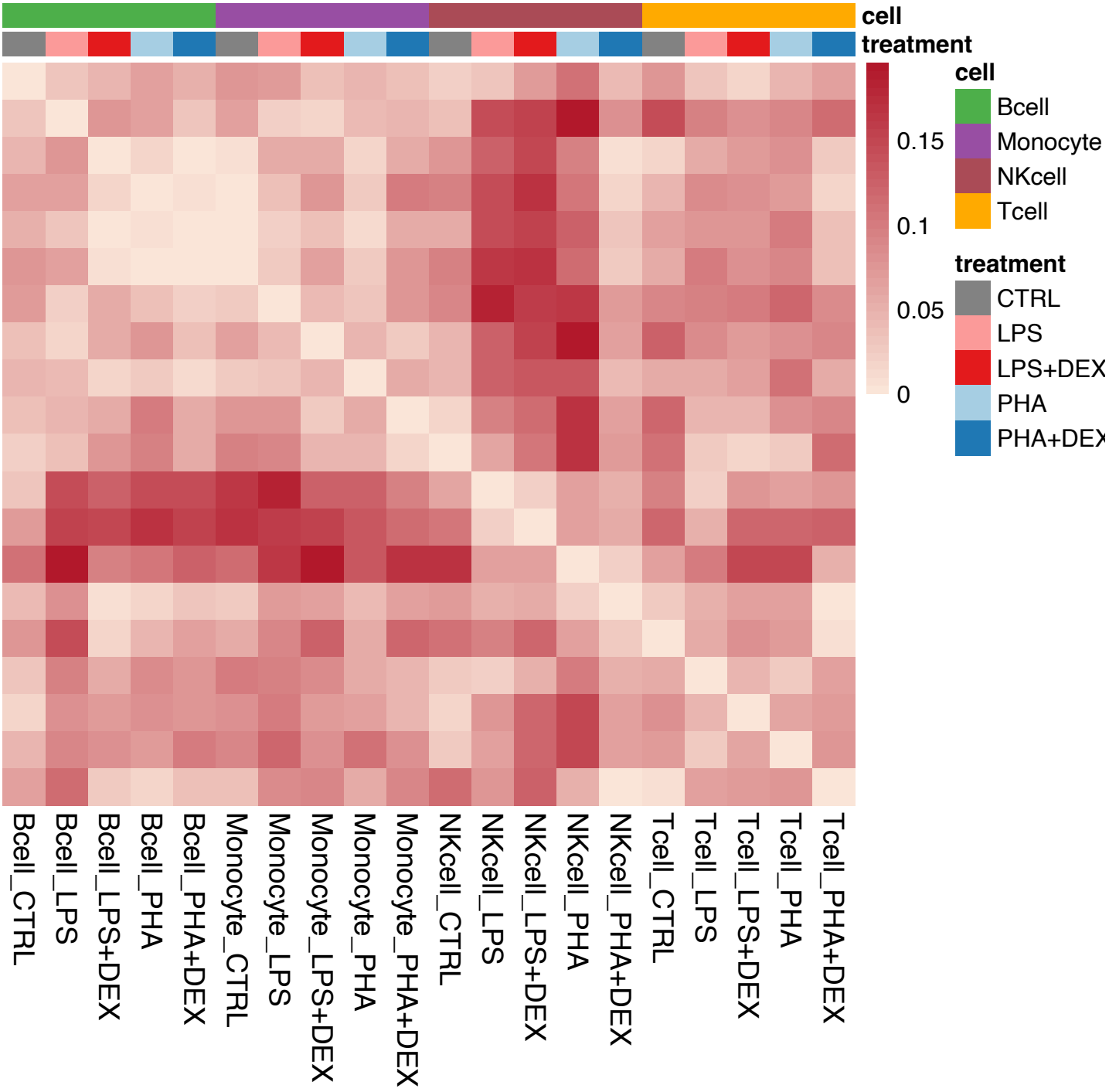


Figure S37: **vGene differences in the direction of effect across all pairs of conditions.** Heatmap represents proportion of vGenes significant in either of the two conditions which have at least one vQTL significant in either of the two conditions with opposite sign of genetic effect size estimated by multivariate adaptive shrinkage.

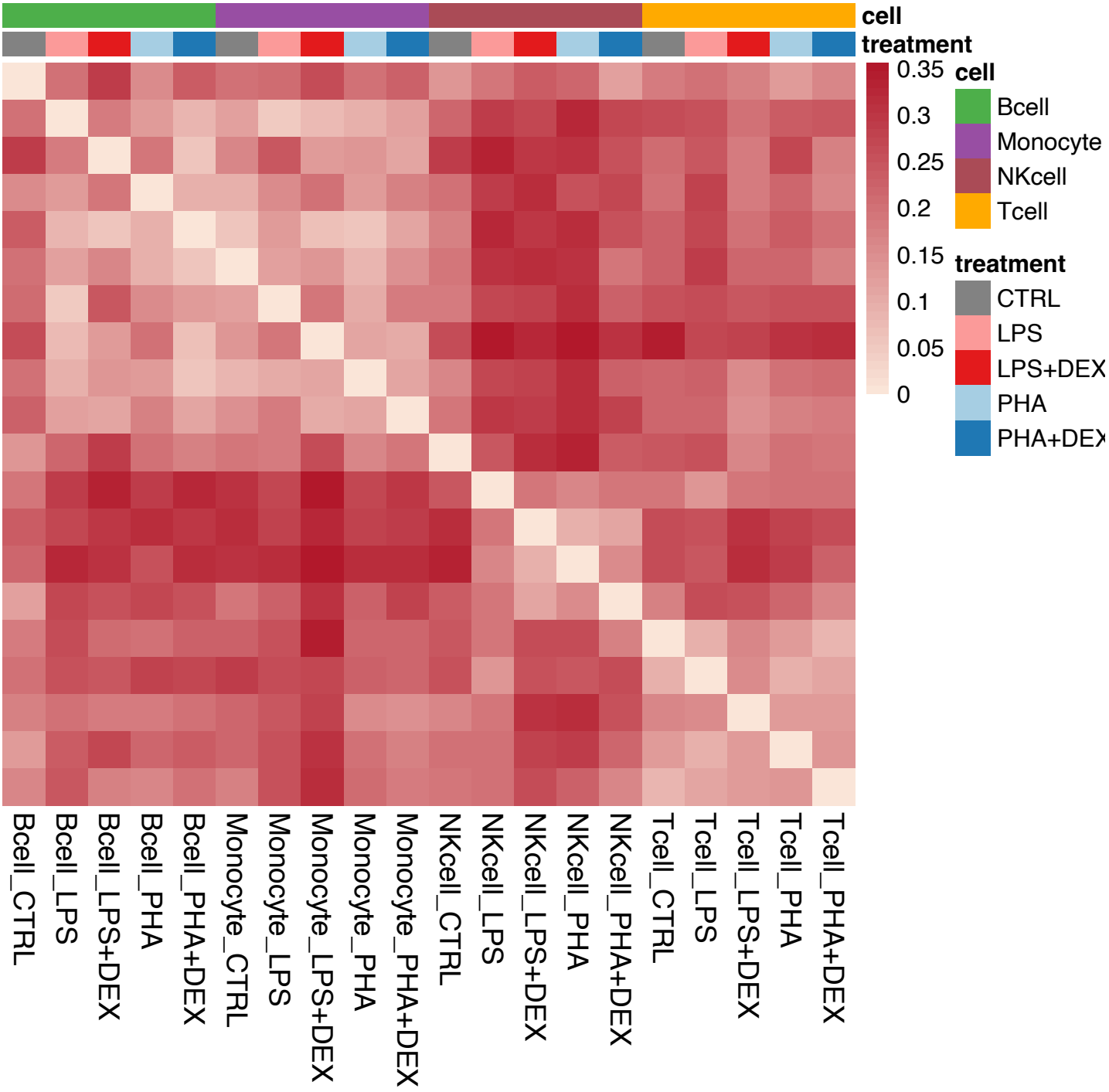


Figure S38: **vGene differences across all pairs of conditions.** Heatmap represents the proportion of vGenes not shared by magnitude (i.e., with at least 2-fold difference between genetic effects in each condition) over the union of all significant vGenes in each pair-wise comparison.

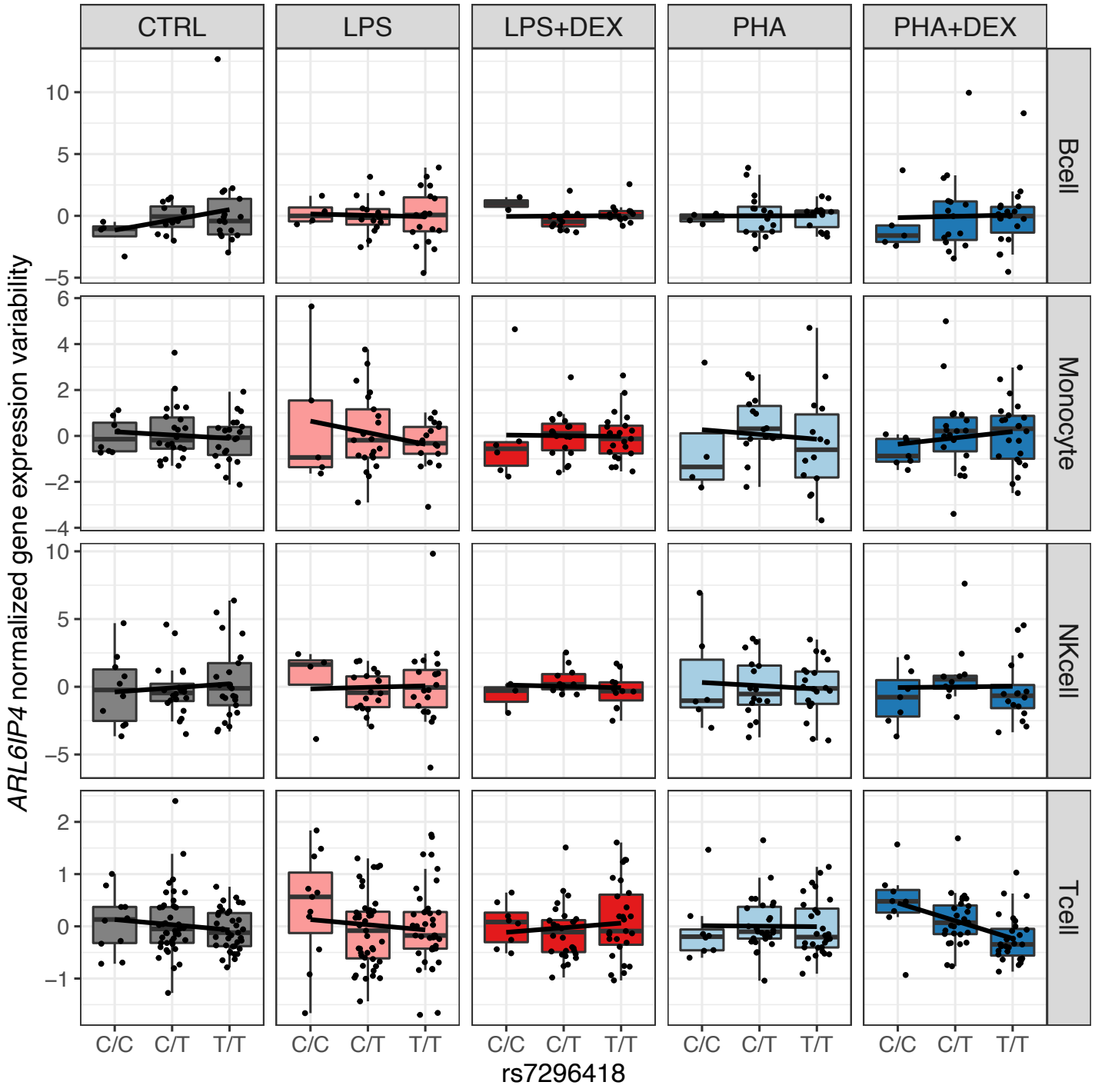


Figure S39: **Genetic effect of rs7296418 on gene expression of ARL6IP4. A** Boxplots represent normalized mean expression of the ARL6IP4 gene (y axis) across the three genotype classes of rs7296418 (x axis) across all conditions **B** Boxplots represent normalized gene expression variability of the ARL6IP4 gene (y axis) across the three genotype classes of rs7296418 (x axis) across all conditions.

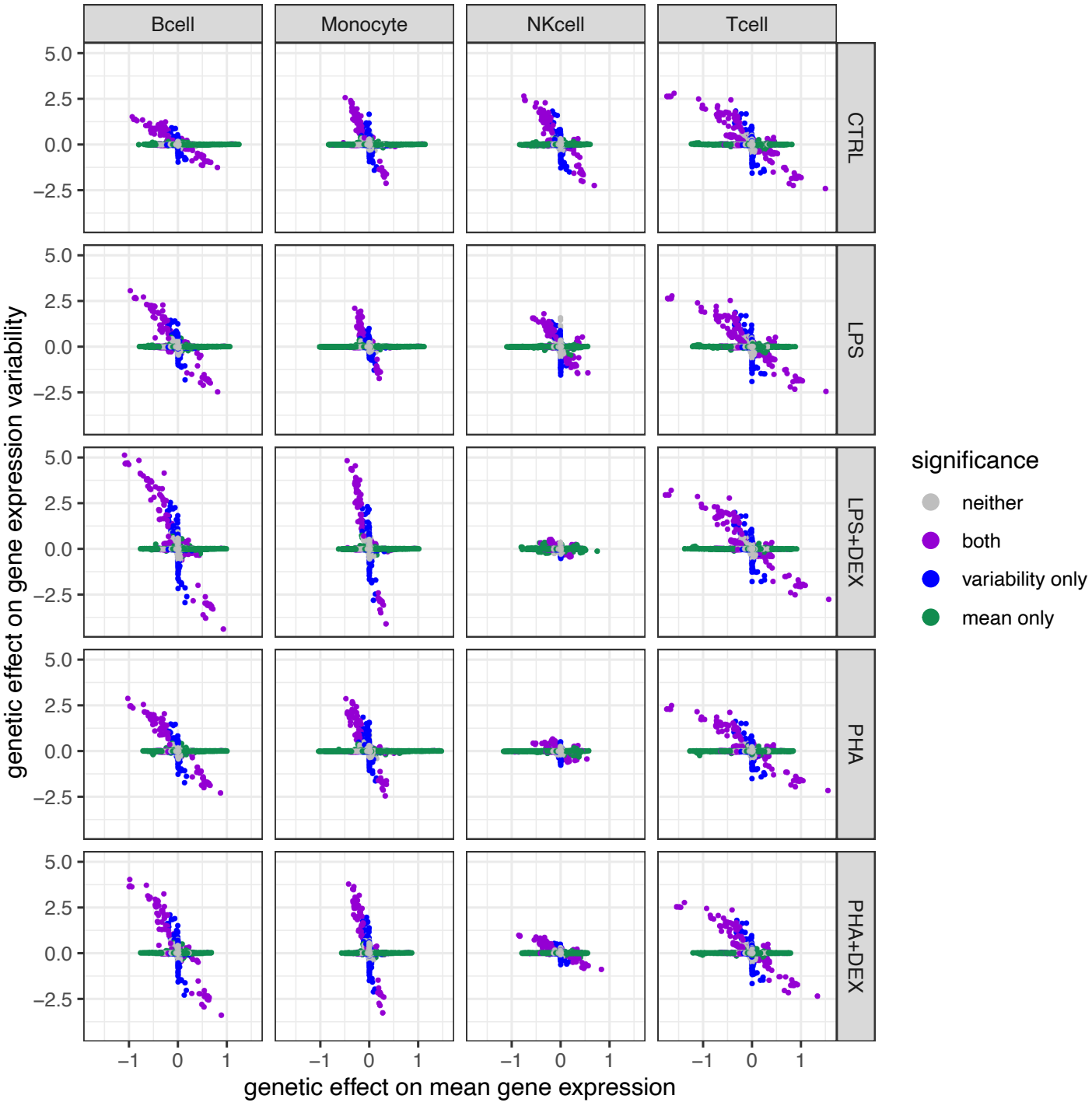


Figure S40: **Genetic effects on gene expression variability.** Scatterplots represent genetic effects on mean gene expression (x axis) versus genetic effects on gene expression variability (y axis) across all 20 conditions. Color represents genetic variants with significant effects on mean gene expression only (green), gene expression variability only (blue), both (purple), and neither (grey).

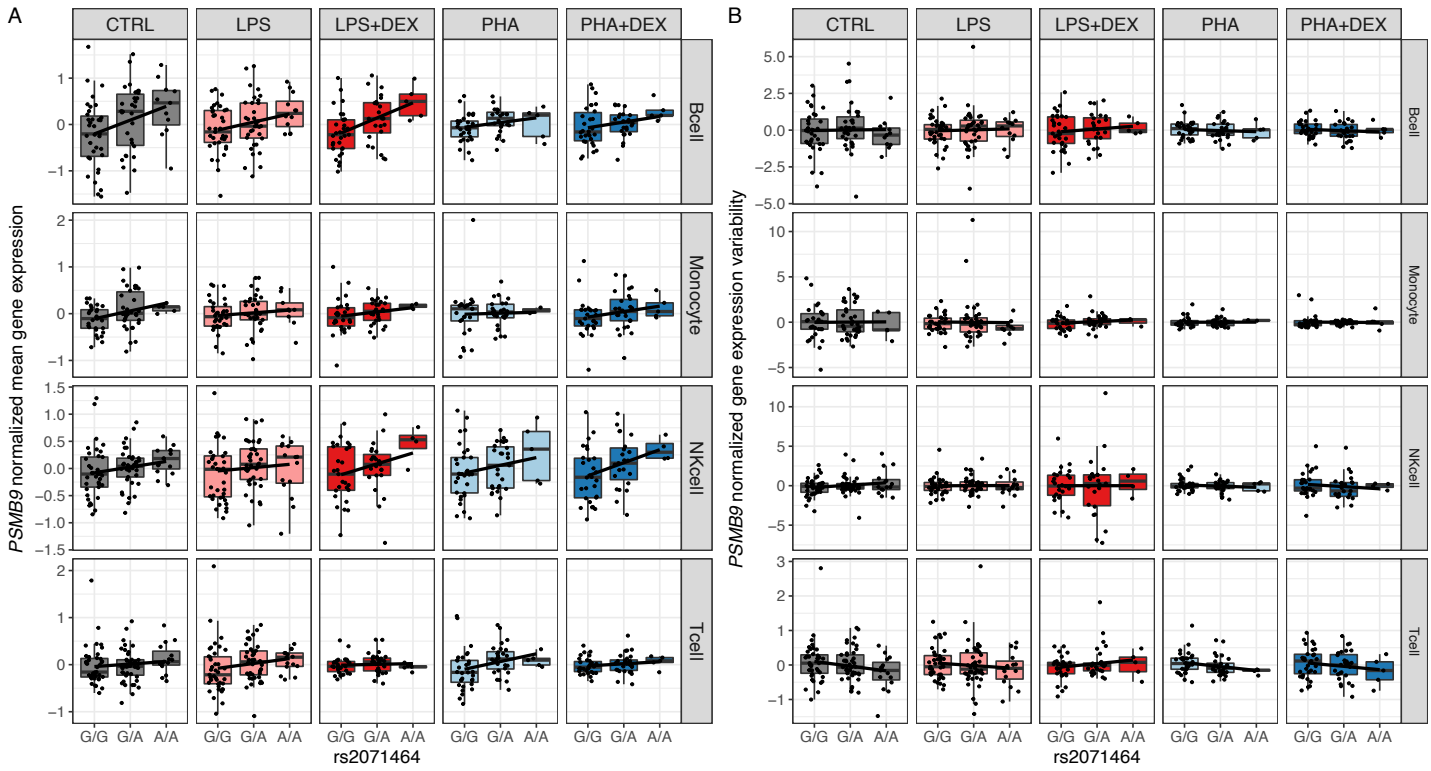


Figure S41: **Genetic effect of rs2071464 on gene expression of PSMB9. A** Boxplots represent normalized mean expression of the PSMB9 gene (y axis) across the three genotype classes of rs2071464 (x axis) across all conditions **B** Boxplots represent normalized gene expression variability of the PSMB9 gene (y axis) across the three genotype classes of rs2071464 (x axis) across all conditions.

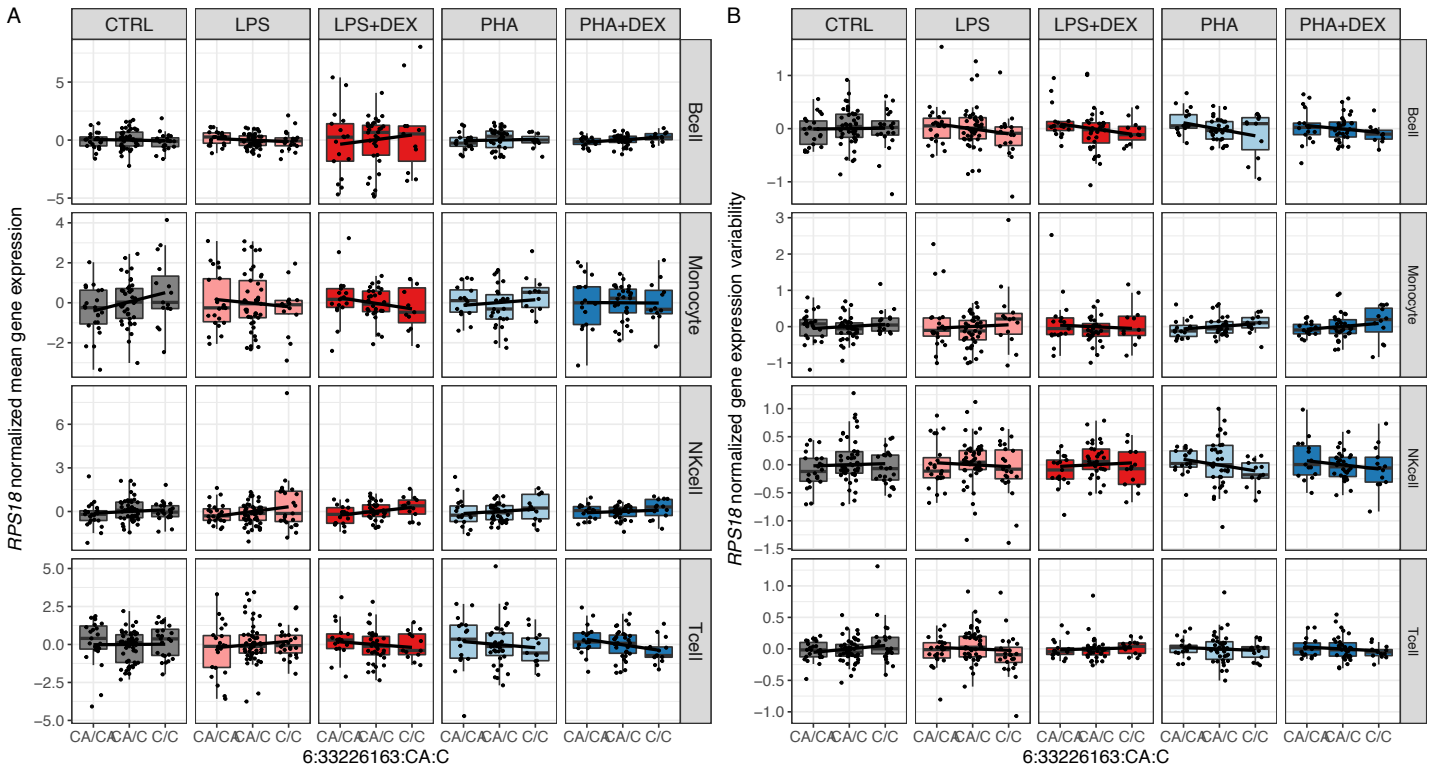


Figure S42: **Genetic effect of the SNP at 6:33226163 on gene expression of RPS18. A** Boxplots represent normalized mean expression of the RPS18 gene (y axis) across the three genotype classes of the SNP at 6:33226163 (x axis) across all conditions **B** Boxplots represent normalized gene expression variability of the RPS18 gene (y axis) across the three genotype classes of the SNP at 6:33226163 (x axis) across all conditions.

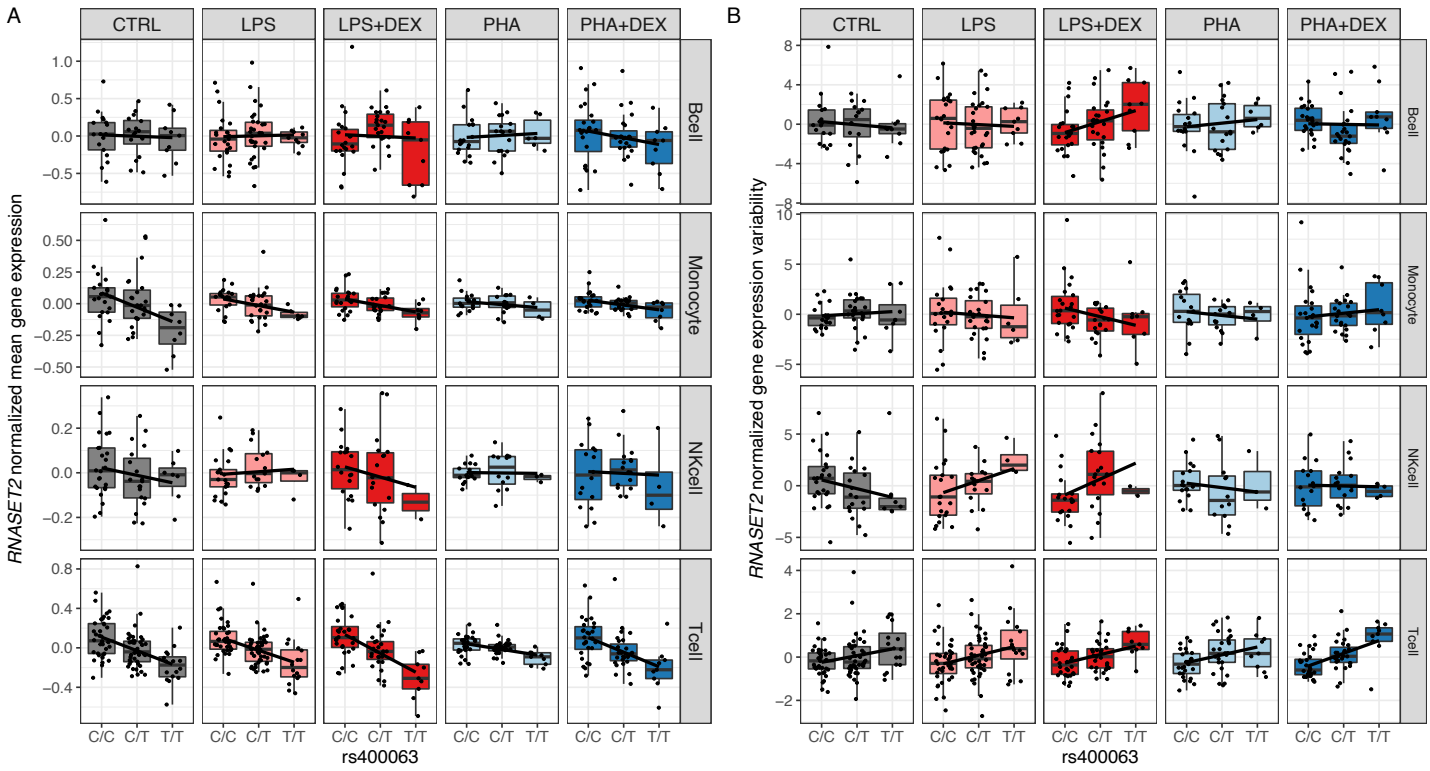


Figure S43: **Genetic effect of rs12507413 on gene expression of RNASET2. A** Boxplots represent normalized mean expression of the RNASET2 gene (y axis) across the three genotype classes of rs400063 (x axis) across all conditions **B** Boxplots represent normalized gene expression variability of the RNASET2 gene (y axis) across the three genotype classes of rsrs400063 (x axis) across all conditions.

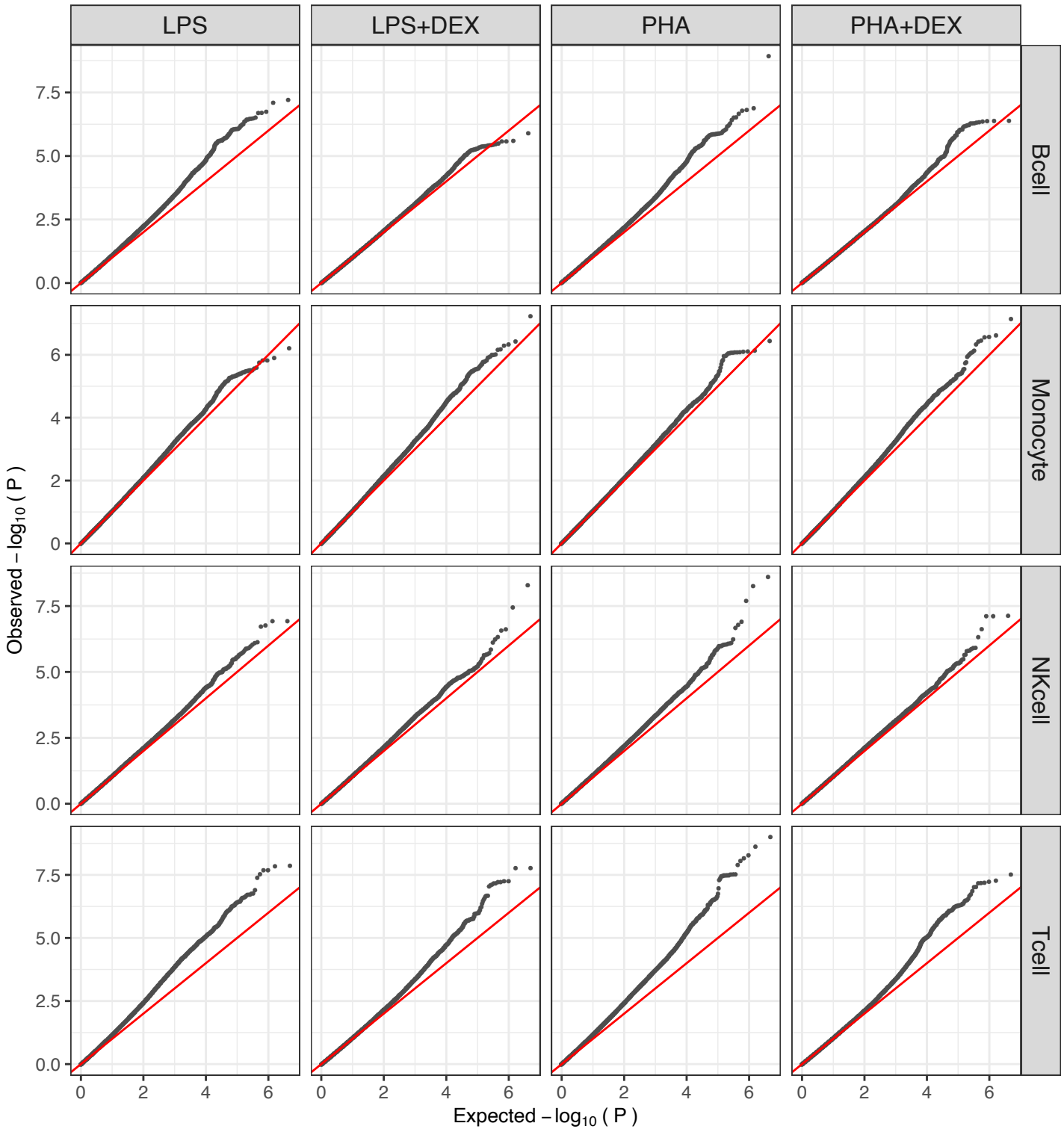


Figure S44: **QQplots of p-values from DLDA-interacting eQTL mapping across the 16 conditions.**

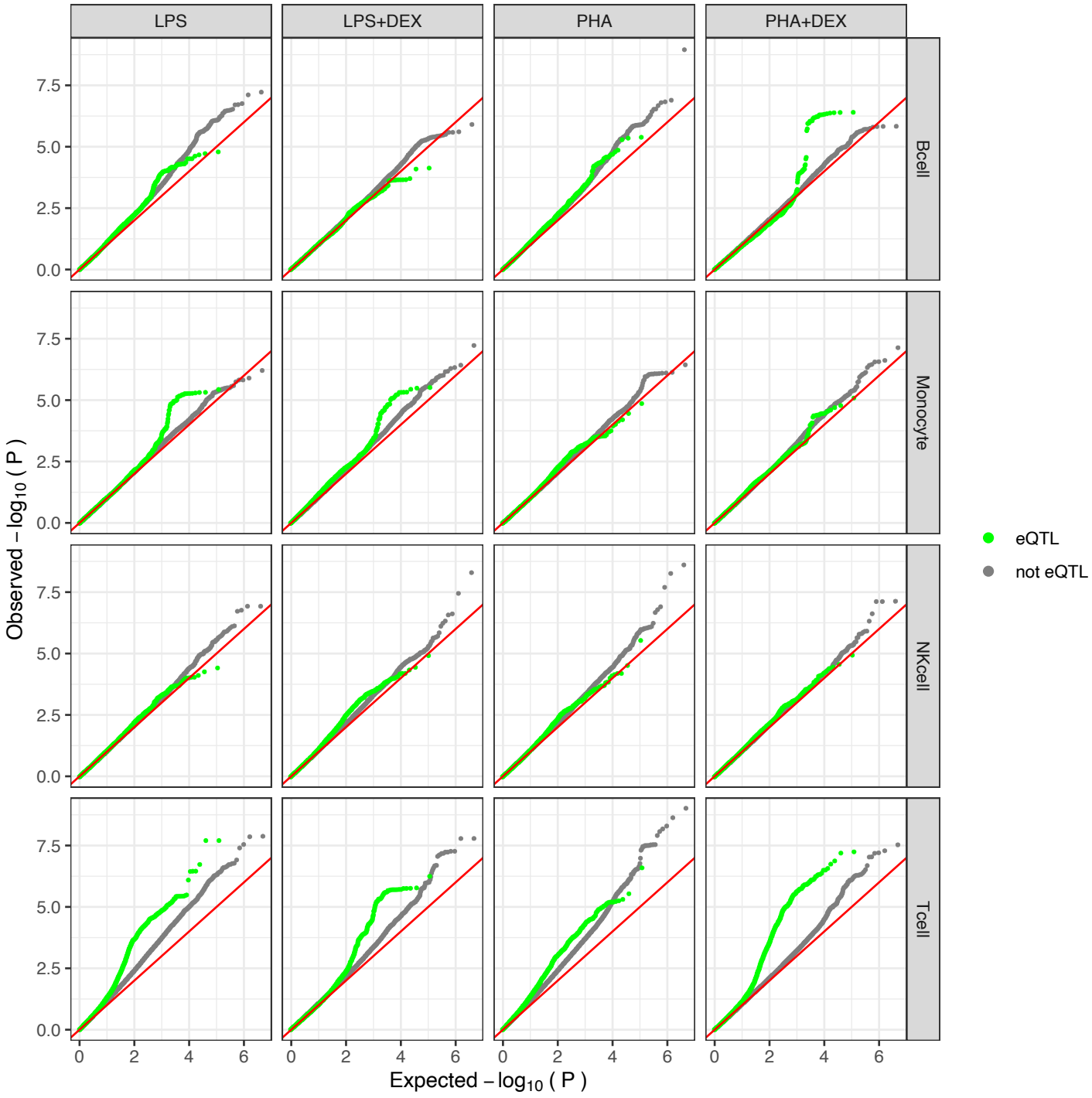


Figure S45: **Q-Qplots of p-values from DLDA-interacting eQTL mapping across the 16 conditions stratified by eQTL or not**, green colors representing the tested genetic variants are eQTLs that were detected in any condition.

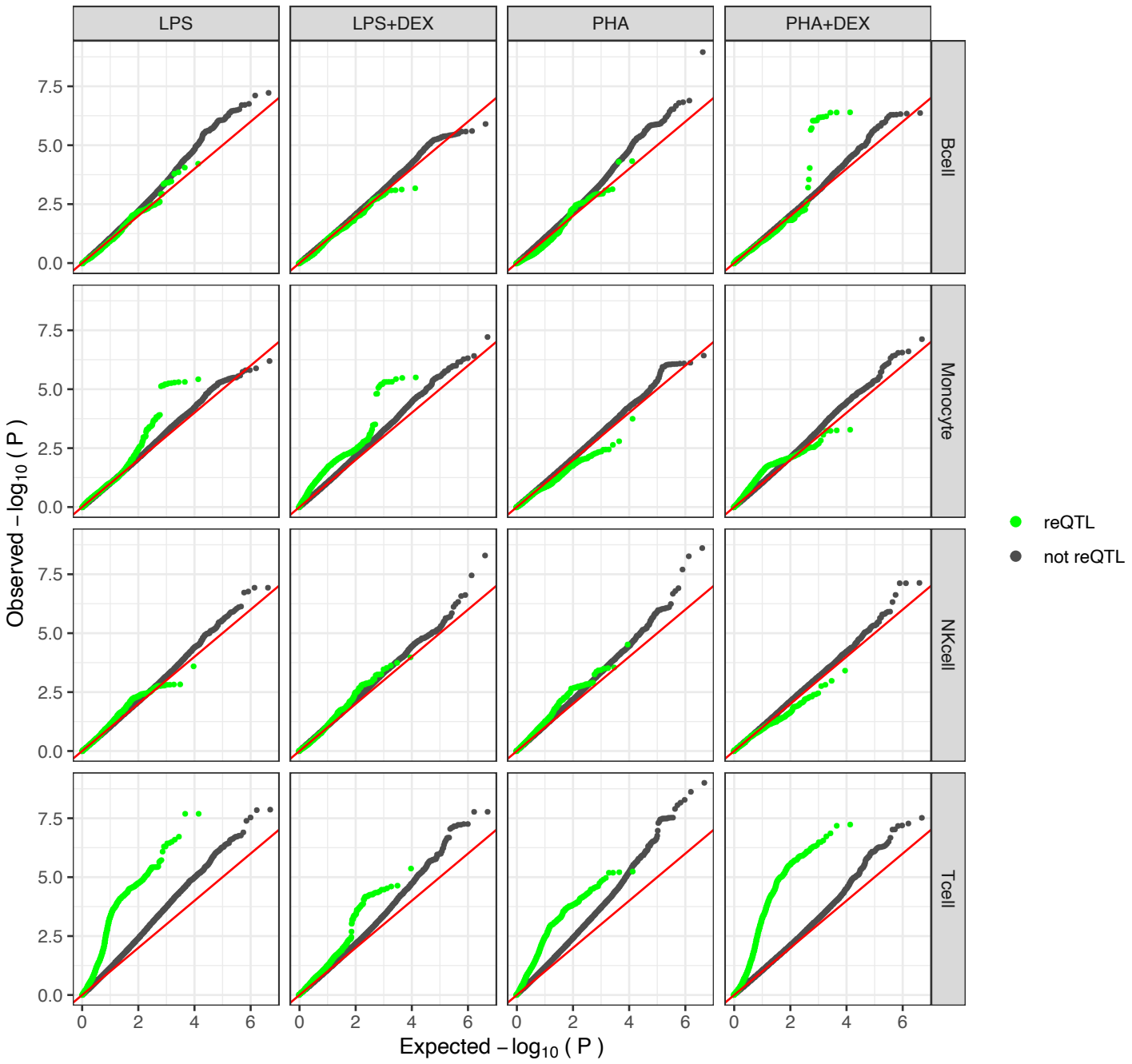


Figure S46: **Q-Qplots of p-values from DLDA-interacting eQTL mapping across the 16 conditions stratified by reQTL or not**, green colors representing the tested genetic variants are reQTLs that were detected in any condition.

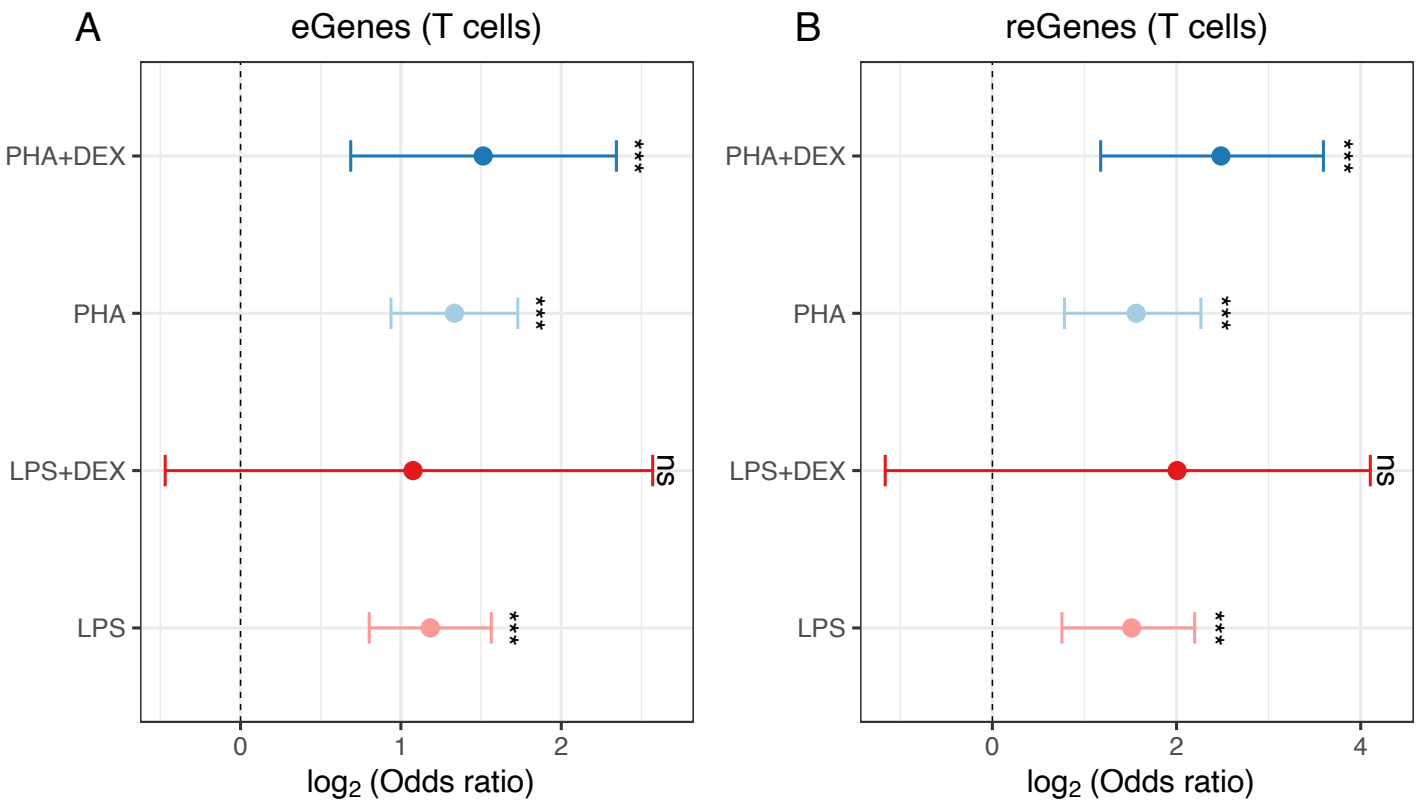


Figure S47: **Forest plots of log odds ratio across 4 conditions in the T cells**, to show if dynamic eGenes are significantly enriched in eGenes or reGenes across 4 conditions in the T cells. **(A)** test if dynamic eGenes are enriched in the eGenes discovered in the same condition, **(B)** test if dynamic eGenes are enriched in the reGenes discovered in the same condition

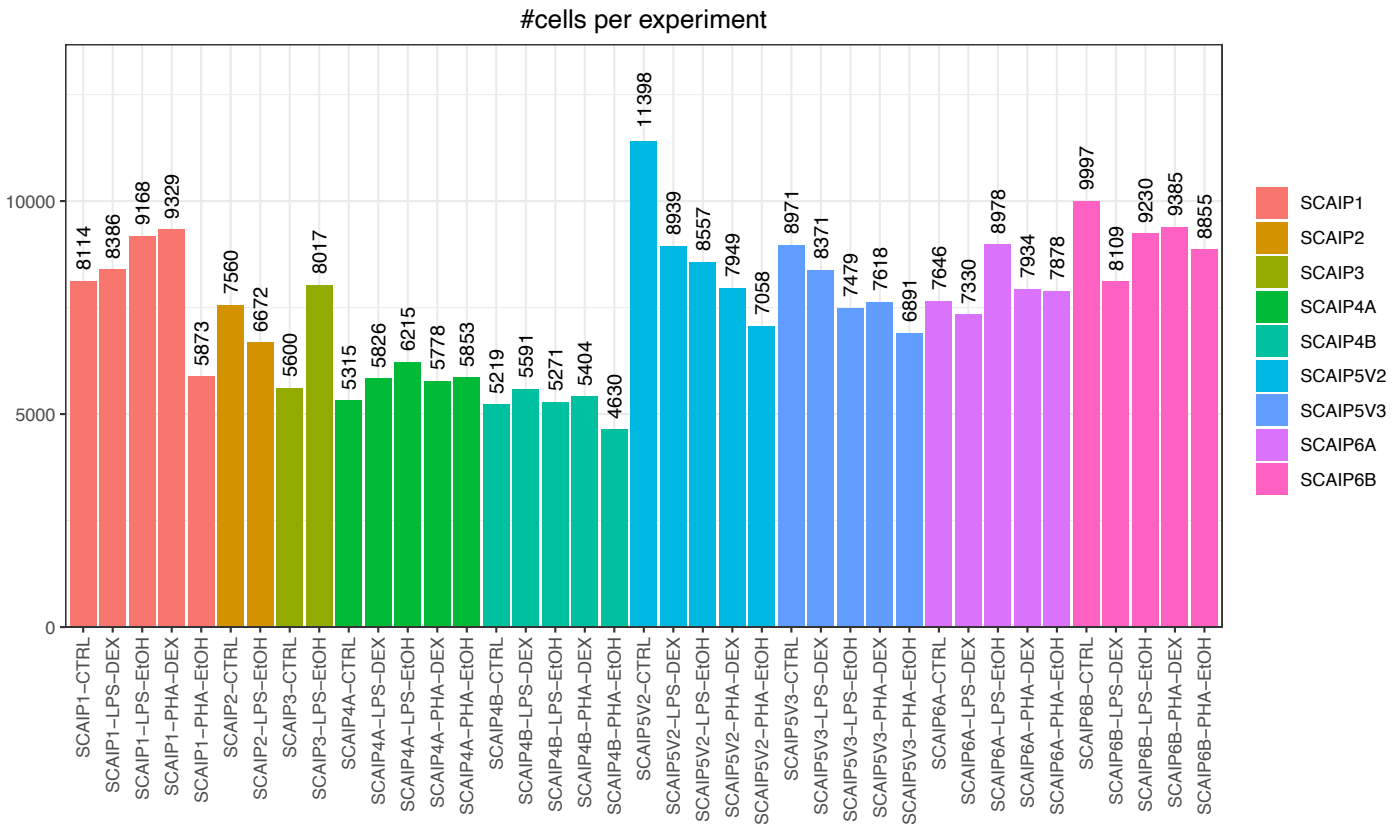


Figure S48: **Number of measured cells across 39 experiments**

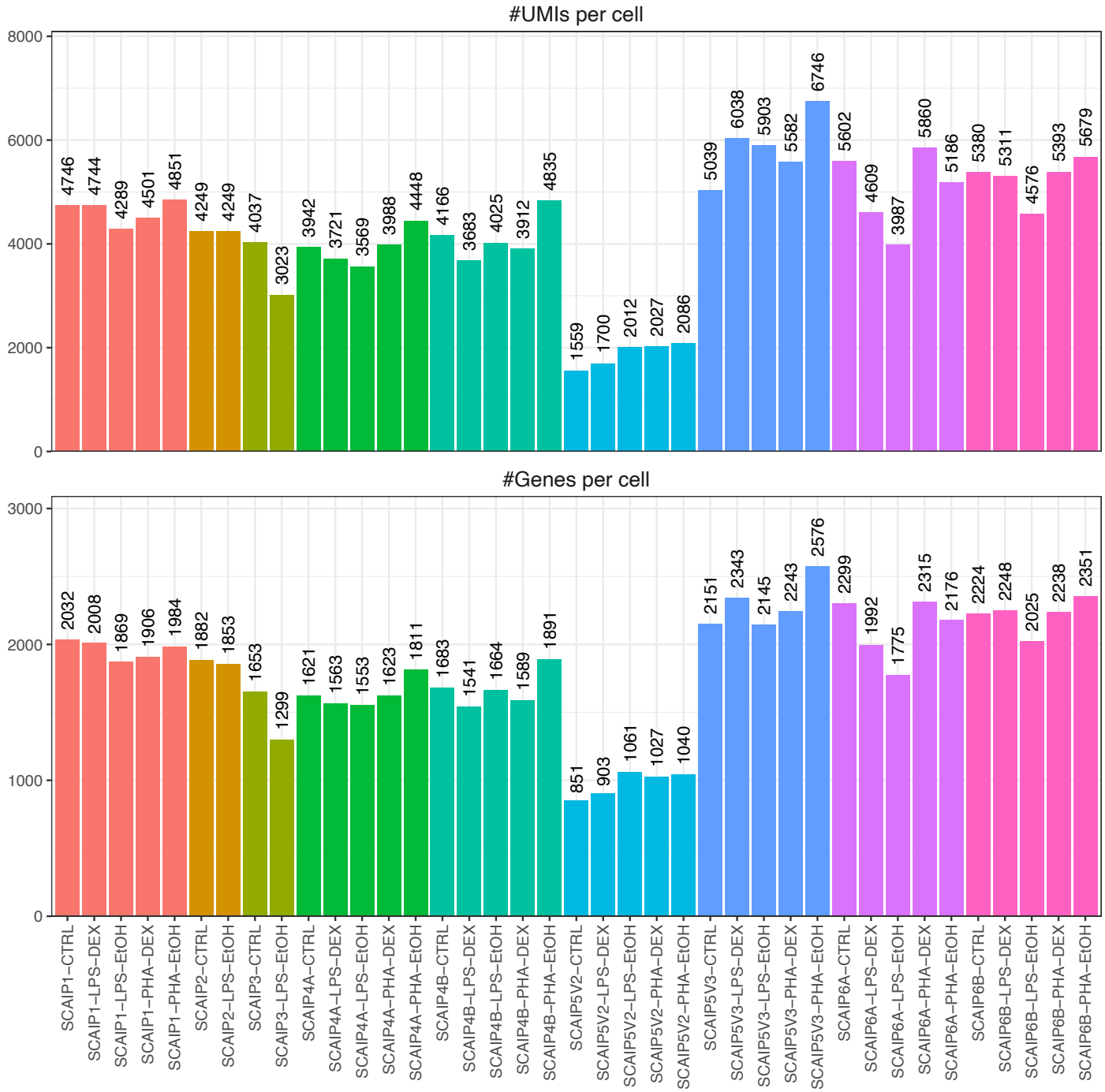


Figure S49: **Unique molecular identifiers(UMIs) and gene features per cell across 39 experiments, including spliced and unspliced reads**

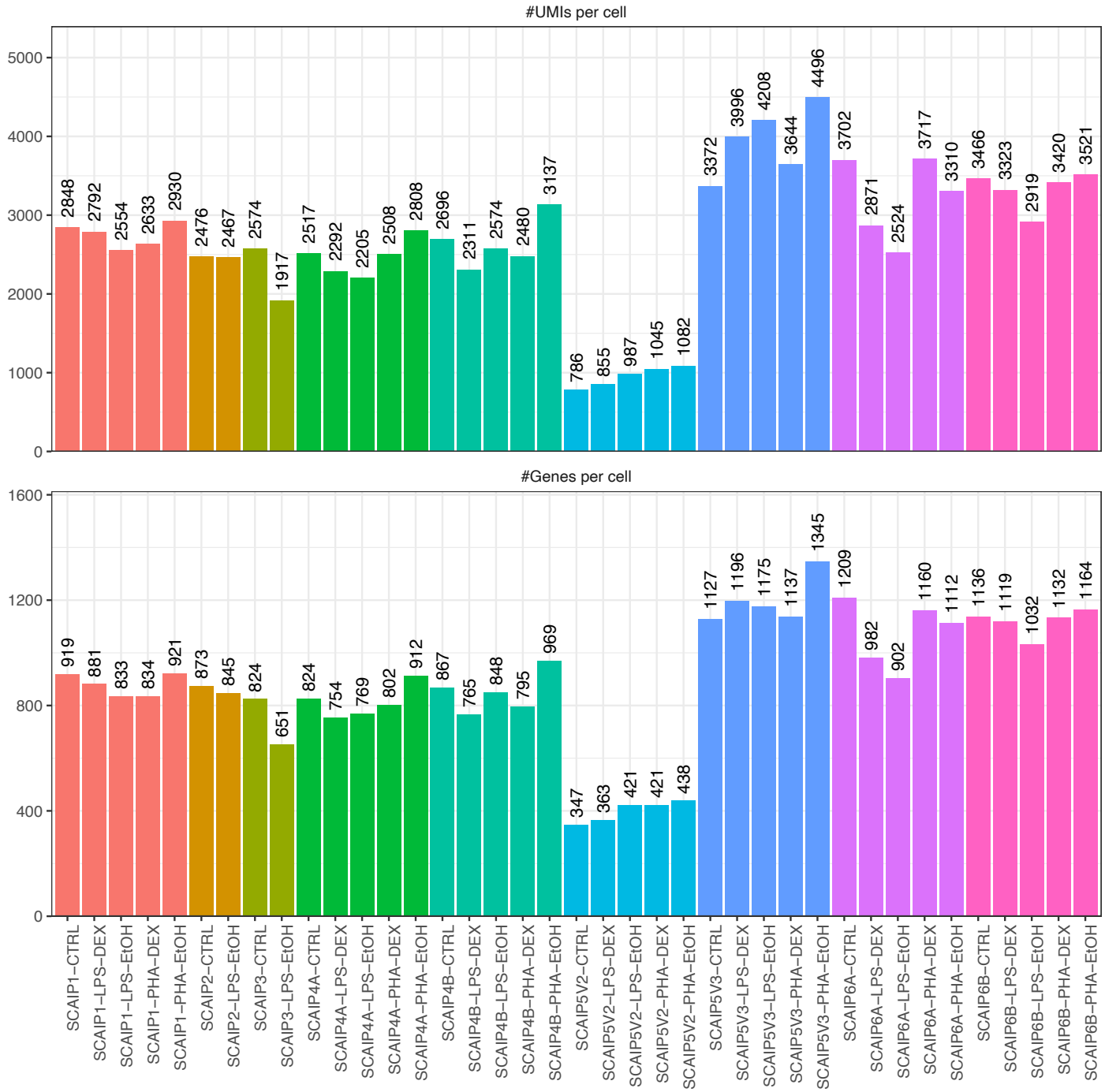


Figure S50: **Unique molecular identifiers(UMIs) and gene features per cell across 39 experiments for spliced reads**

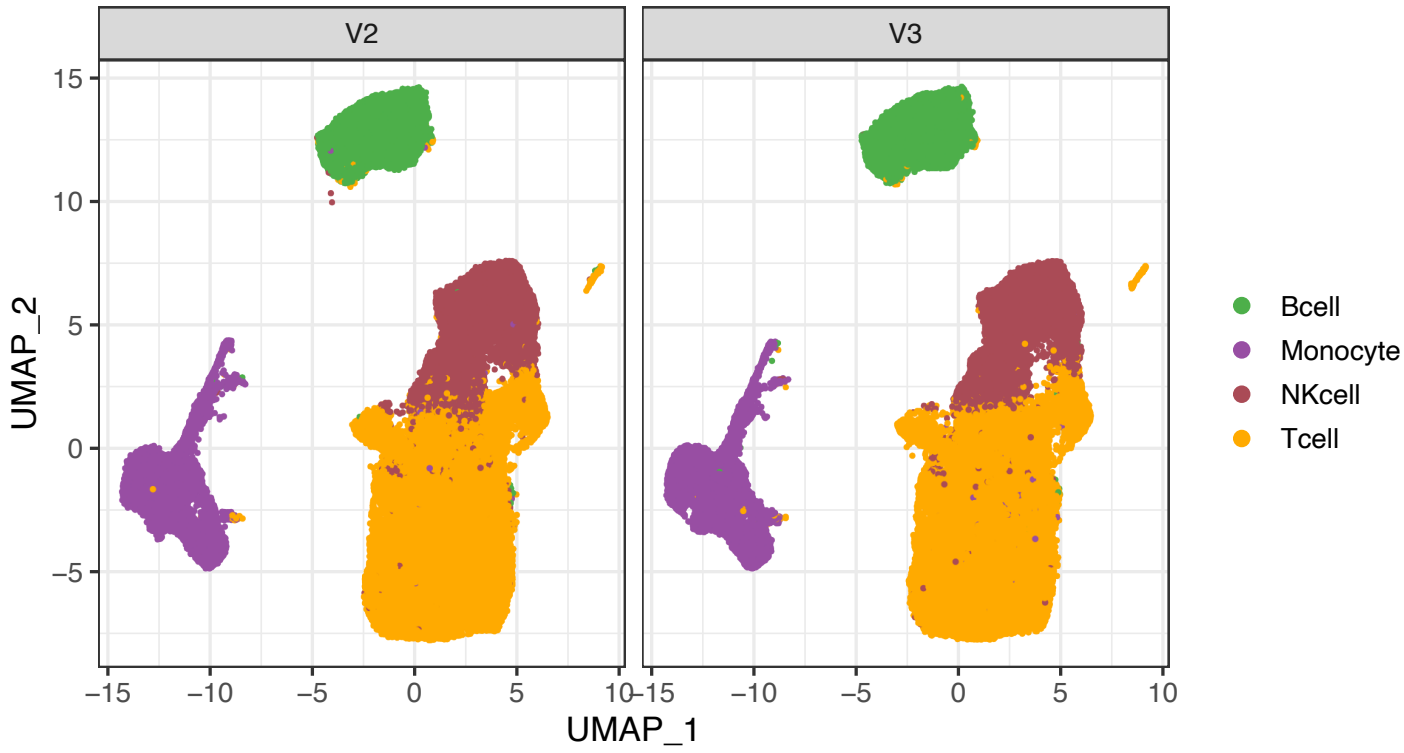


Figure S51: **UMAP of cells split by chemistry**

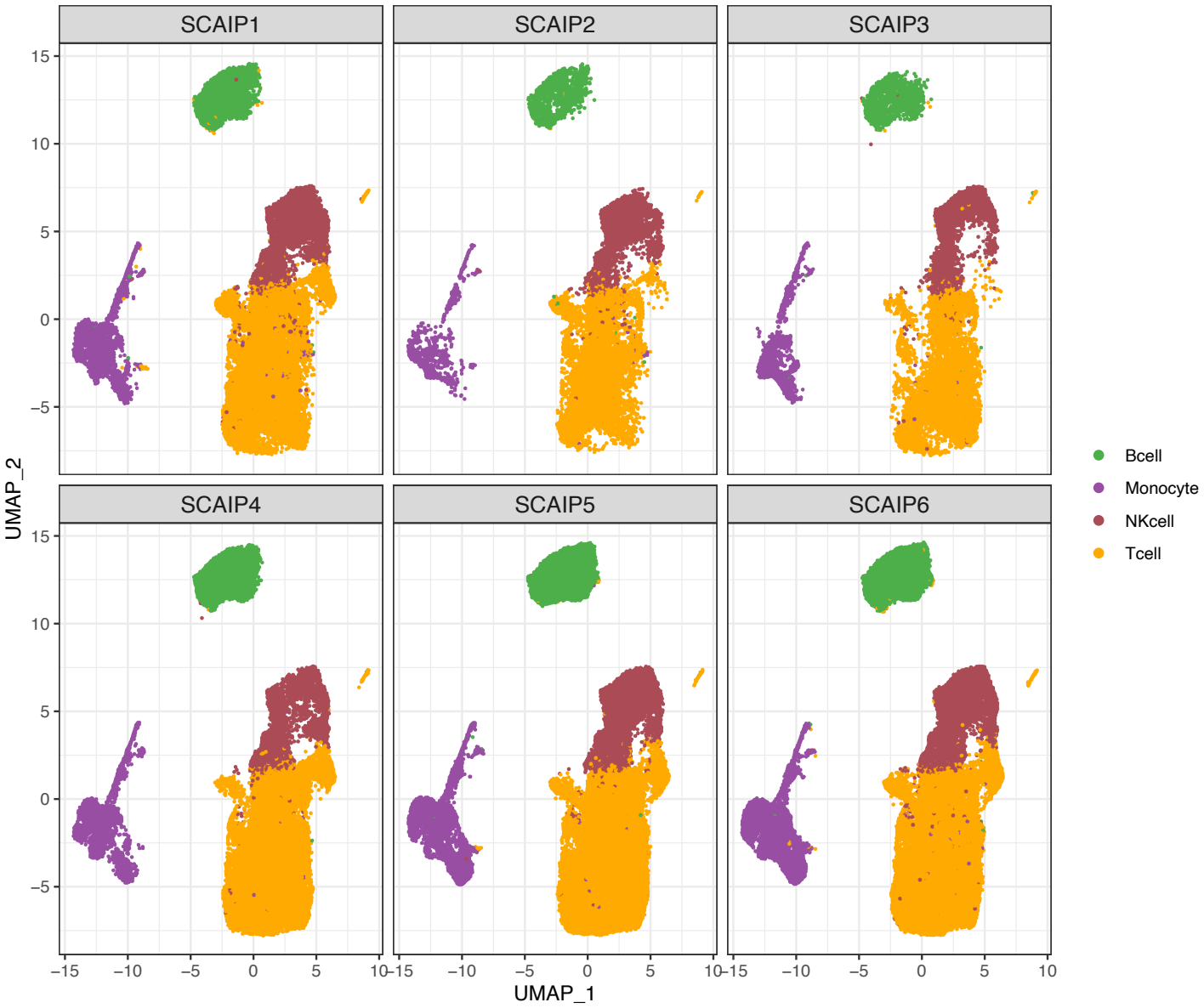


Figure S52: **UMAP of cells split by BATCH**

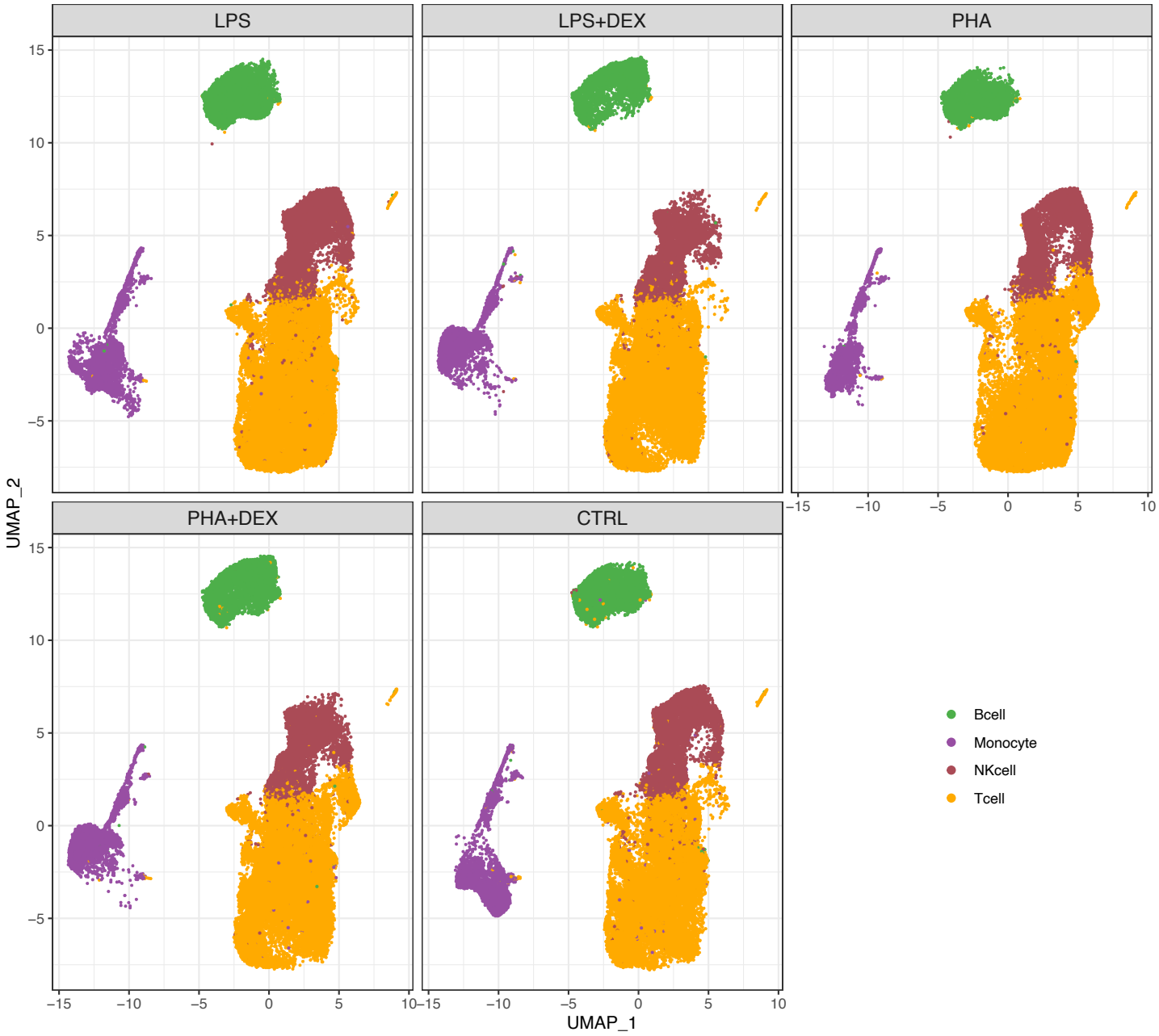


Figure S53: **UMAP of cells split by treatment**

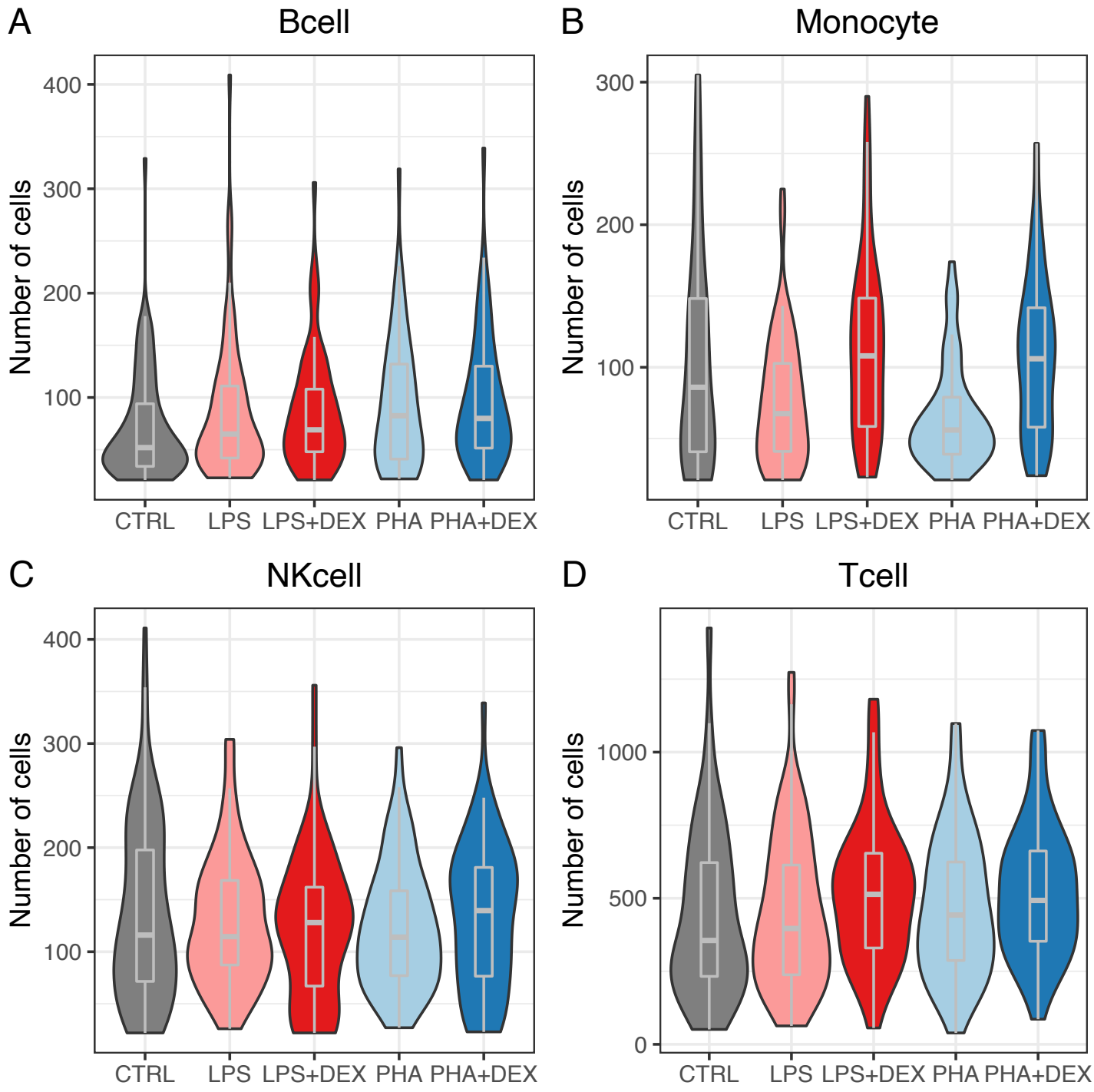


Figure S54: **Violin plots of number of cells in each combination (cell type+treatment+individual)** **A-D** represents the distribution of the number of cells in each combination across individuals in different treatments for B cells, monocytes, NK cells and T cells.

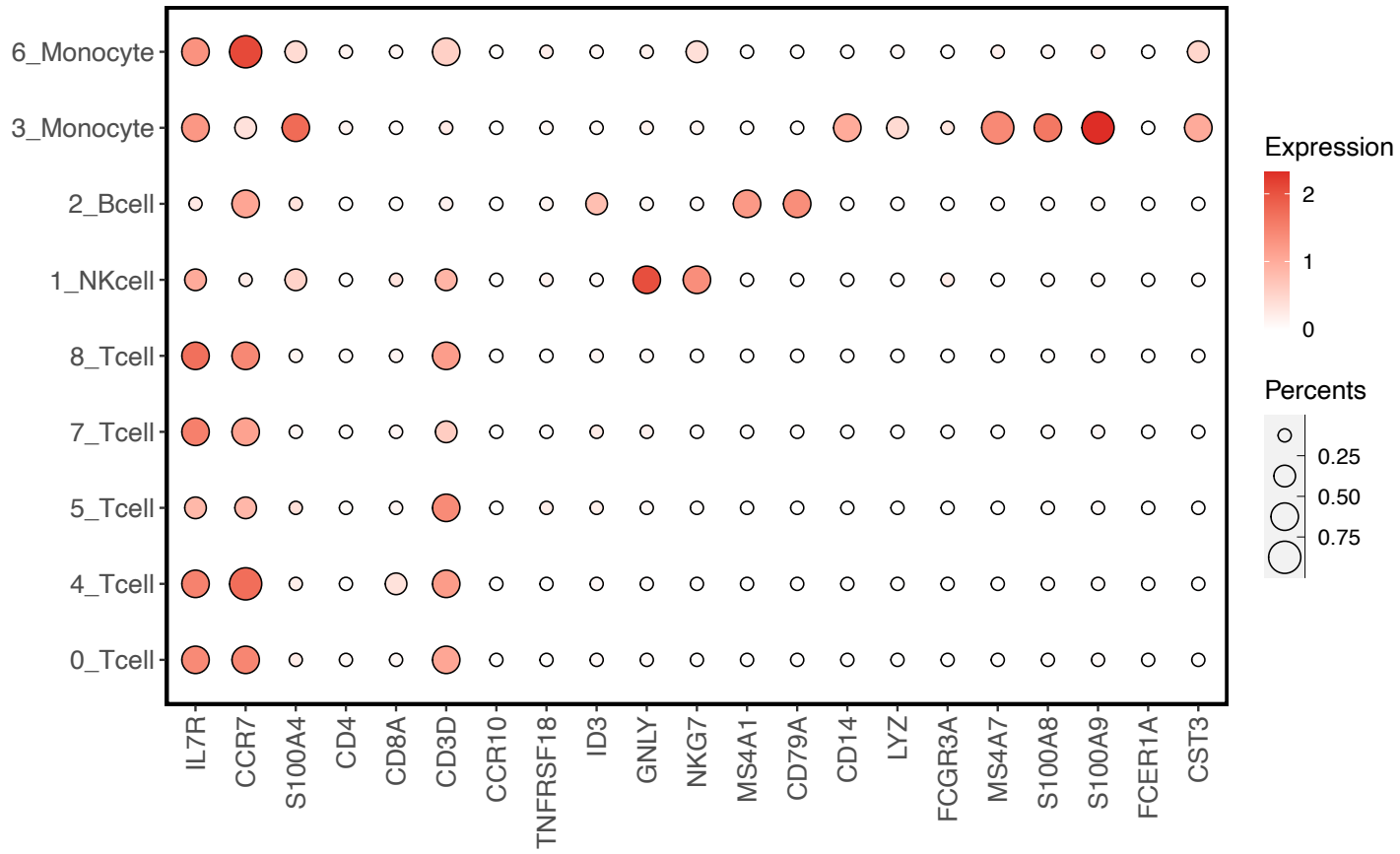


Figure S55: **Dot plots of cell type marker genes expressed in the Seurat clusters**. Red color represents high average expression values across cells in the cluster while the size of dots representing the proportion of cells expressed the marker gene in the cluster

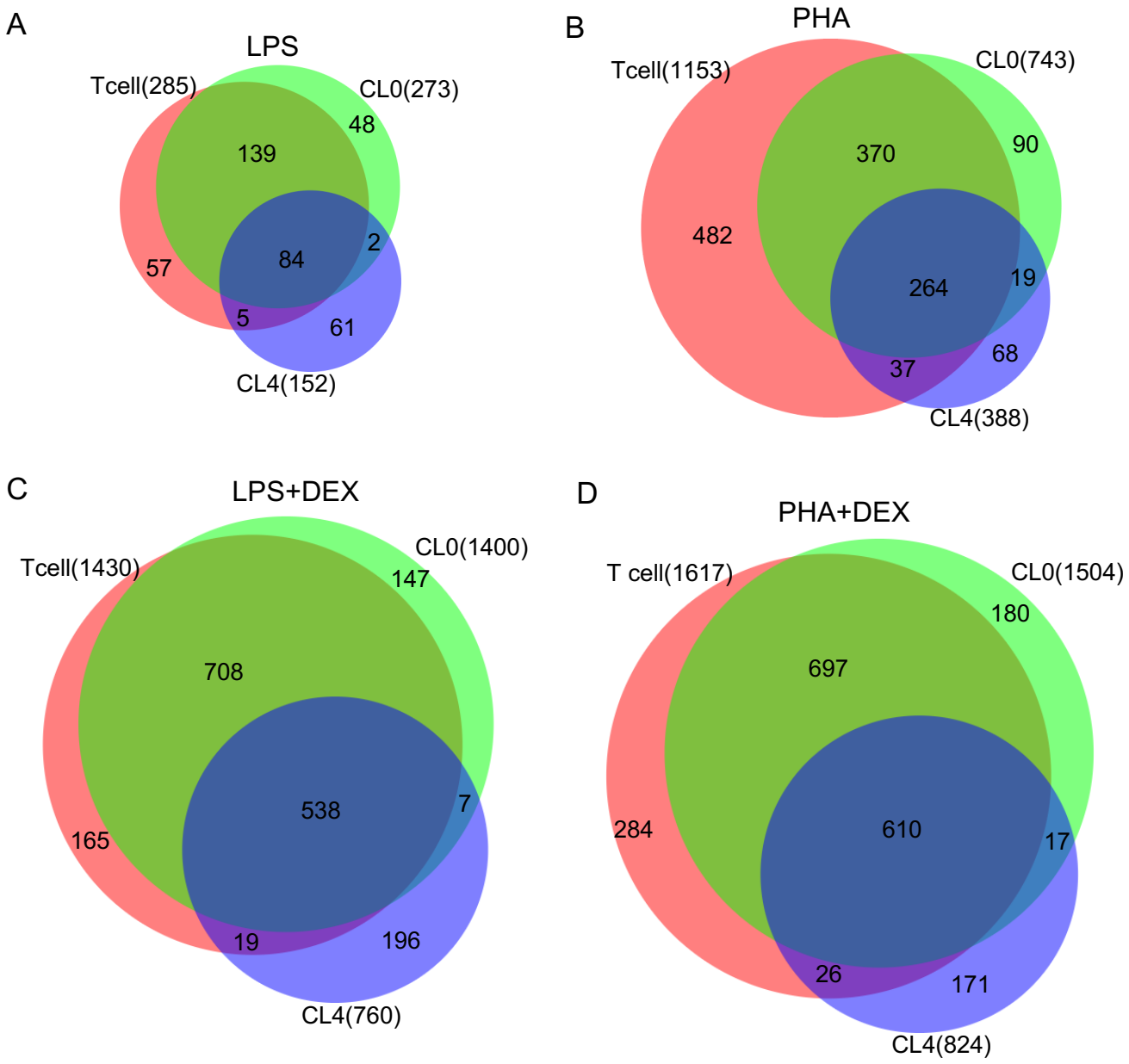


Figure S56: **Venn diagrams of overlapping DEGs in response to treatments between the overall T cells, and two major T cell sub-clusters (Cluster 0 and 4) :** A-D representing LPS, PHA, LPS+DEX and PHA+DEX respectively

## Supplementary Tables

Table S1: **Summary statistics of single-cell data for each treatment**. Column 2, number of individuals for each treatment; Column 3, median values of number of cells per individual across individuals in each treatment; Column 4, median values of average UMIs per cell from the same individual across individuals in each treatment, Column 5, median values of average detection genes per cell from the same individual across individuals in each treatment

| | #Individuals | # Cells per individual (median) | #UMIs per cell (median) | #Genes per cell (median) |
|---|---|---|---|---|
| CTRL | 96 | 586 | 2,588 | 859 |
| LPS | 96 | 658 | 2,451 | 818 |
| LPS+DEX | 64 | 821 | 2,672 | 852 |
| PHA | 64 | 714 | 2,981 | 944 |
| PHA+DEX | 64 | 858 | 2,618 | 852 |

Table S2: **Summary cell type composition of individuals for each treatment**. Column 2-5, number of cells from B-cells, Monocyte, NK-cell and T cells of the individual for each treatment (median value). The full table detailing the number of cells in each cell type/treatment/individual combination can be found in Table S24.

| | #B-cell per individual (median) | #Monocyte per individual (median) | #NK-cell per individual (median) | #T cell per individual (median) |
|---|---|---|---|---|
| CTRL | 52 | 86 | 116 | 356 |
| LPS-EtOH | 65 | 67.5 | 114 | 396 |
| LPS-DEX | 69 | 108 | 128 | 514 |
| PHA-EtOH | 82.5 | 56 | 114 | 442 |
| PHA-DEX | 80 | 106 | 140 | 492 |

Table S3: eQTL mapping results. Number of significant eQTLs and eGenes based on FastQTL results (FDR<0.1, columns 2 and 3), and multivariate adaptive shrinkage results (LFSR<0.1), columns 4 and 5.

| | FastQTL FDR<0.1 | | mash LFSR<0.1 | |
|---|---|---|---|---|
| | eQTLs | eGenes | eQTLs | eGenes |
| Bcell CTRL | 5378 | 291 | 110276 | 2649 |
| Bcell LPS+DEX | 4465 | 262 | 109921 | 2656 |
| Bcell LPS | 8135 | 396 | 109869 | 2650 |
| Bcell PHA+DEX | 3671 | 217 | 113168 | 2652 |
| Bcell PHA | 4347 | 268 | 109853 | 2678 |
| Monocyte CTRL | 4186 | 253 | 106399 | 2603 |
| Monocyte LPS+DEX | 4720 | 300 | 103217 | 2559 |
| Monocyte LPS | 5518 | 340 | 101642 | 2586 |
| Monocyte PHA+DEX | 4019 | 271 | 104661 | 2547 |
| Monocyte PHA | 2407 | 167 | 101235 | 2590 |
| NKcell CTRL | 5986 | 364 | 113162 | 2624 |
| NKcell LPS+DEX | 1566 | 122 | 103316 | 2592 |
| NKcell LPS | 5379 | 366 | 110434 | 2462 |
| NKcell PHA+DEX | 1427 | 97 | 104507 | 2602 |
| NKcell PHA | 1621 | 135 | 110859 | 2477 |
| Tcell CTRL | 20187 | 1297 | 109130 | 2605 |
| Tcell LPS+DEX | 15636 | 1052 | 114176 | 2642 |
| Tcell LPS | 22603 | 1386 | 112189 | 2684 |
| Tcell PHA+DEX | 14568 | 967 | 115410 | 2666 |
| Tcell PHA | 13279 | 884 | 112915 | 2712 |
| Total Unique | 62694 | 5190 | 129539 | 2984 |
| Total Tested | 4163269 | 13876 | 2,095,831 | 9556 |

Table S4: Overlap of eGenes with differentially expressed genes (DEGs, FDR<0.1) and differentially variable genes (DVGs, FDR<0.1). Columns represent: 1 – condition, 2 – number of eGenes which are also DEGs for the condition against its paired control, 3 – odds ratio of the overlap in column 2, 4 – p-value of the Fisher's exact test for enrichment of eGenes in DEGs, 5 - number of eGenes which are also DVGs for the condition against its paired control, 6 – odds ratio of the overlap in column 5, 7 – p-value of the Fisher's exact test for enrichment of eGenes in DVGs.

| Condition | eGenes that are DEGs | | | eGenes that are DVGs | | |
|---|---|---|---|---|---|---|
| | Overlap | OR | p-value | overlap | OR | p-value |
| Bcell LPS | 111 | 2.19 | 5.1E-09 | 8 | 1.25 | 8.0E-01 |
| Bcell LPS+DEX | 297 | 1.61 | 1.5E-09 | 33 | 1.90 | 3.2E-02 |
| Bcell PHA | 406 | 1.46 | 1.8E-08 | 52 | 3.27 | 3.2E-06 |
| Bcell PHA+DEX | 355 | 1.58 | 2.2E-10 | 41 | 1.98 | 6.3E-03 |
| Monocyte LPS | 382 | 1.15 | 3.7E-02 | 199 | 2.33 | 2.1E-13 |
| Monocyte LPS+DEX | 368 | 1.19 | 1.2E-02 | 131 | 2.63 | 3.2E-11 |
| Monocyte PHA | 660 | 1.20 | 6.4E-04 | 292 | 2.78 | 3.5E-25 |
| Monocyte PHA+DEX | 400 | 1.27 | 2.9E-04 | 178 | 2.00 | 3.4E-09 |
| NKcell LPS | 104 | 1.99 | 3.0E-07 | 27 | 1.73 | 9.4E-02 |
| NKcell LPS+DEX | 410 | 1.61 | 1.2E-12 | 54 | 2.02 | 4.0E-03 |
| NKcell PHA | 376 | 1.54 | 7.4E-10 | 49 | 3.33 | 8.1E-06 |
| NKcell PHA+DEX | 493 | 1.60 | 4.2E-14 | 36 | 2.24 | 5.5E-03 |
| Tcell LPS | 79 | 1.98 | 9.1E-06 | 57 | 3.22 | 4.4E-08 |
| Tcell LPS+DEX | 347 | 1.43 | 5.5E-07 | 66 | 2.58 | 7.9E-07 |
| Tcell PHA | 282 | 1.48 | 7.9E-07 | 89 | 3.88 | 2.2E-14 |
| Tcell PHA+DEX | 408 | 1.50 | 1.7E-09 | 100 | 2.31 | 3.8E-08 |

Table S5: Overlap of reGenes with differentially expressed genes (DEGs, FDR<0.1) and differentially variable genes (DVGs, FDR<0.1). Columns represent: 1 – condition, 2 – number of reGenes which are also DEGs for the condition against its paired control, 3 – odds ratio of the overlap in column 2, 4 – p-value of the Fisher's exact test for enrichment of reGenes in DEGs, 5 - number of reGenes which are also DVGs for the condition against its paired control, 6 – odds ratio of the overlap in column 5, 7 – p-value of the Fisher's exact test for enrichment of reGenes in DVGs.

| Condition | reGenes that are DEGs | | | reGenes that are DVGs | | |
|---|---|---|---|---|---|---|
| | Overlap | OR | p-value | overlap | OR | p-value |
| Bcell LPS | 2 | 1.95 | 2.8E-01 | 1 | 14.80 | 7.3E-02 |
| Bcell LPS+DEX | 11 | 3.12 | 2.4E-03 | 3 | 7.44 | 1.1E-02 |
| Bcell PHA+DEX | 10 | 1.76 | 1.3E-01 | 2 | 3.33 | 1.3E-01 |
| Bcell PHA | 3 | 0.72 | 7.9E-01 | 1 | 3.51 | 2.6E-01 |
| Monocyte LPS | 14 | 1.28 | 4.2E-01 | 8 | 2.21 | 5.8E-02 |
| Monocyte LPS+DEX | 5 | 0.57 | 2.7E-01 | 2 | 1.10 | 7.1E-01 |
| Monocyte PHA+DEX | 11 | 1.56 | 1.7E-01 | 7 | 3.08 | 1.4E-02 |
| Monocyte PHA | 16 | 1.01 | 1.0E+00 | 6 | 1.39 | 4.5E-01 |
| NKcell LPS | 3 | 3.56 | 6.1E-02 | 0 | NA | NA |
| NKcell LPS+DEX | 13 | 1.84 | 5.6E-02 | 1 | 0.97 | 1.0E+00 |
| NKcell PHA | 3 | 1.09 | 7.5E-01 | 0 | NA | NA |
| NKcell PHA+DEX | 12 | 1.44 | 2.7E-01 | 4 | 6.14 | 6.2E-03 |
| Tcell LPS | 0 | NA | NA | 1 | 2.07 | 3.9E-01 |
| Tcell LPS+DEX | 7 | 1.21 | 6.6E-01 | 0 | NA | NA |
| Tcell PHA+DEX | 6 | 1.09 | 8.2E-01 | 1 | 0.94 | 1.0E+00 |
| Tcell PHA | 3 | 0.61 | 6.3E-01 | 3 | 3.32 | 7.0E-02 |

Table S6: Overlap with previously known dexamethasone reGenes. Table lists dexamethasone reGenes significant in this study and in a previous study conducted in immortalized B cells Maranville et al. (2011).

| condition | reGenes shared with Maranville, 2011 |
|---|---|
| Bcell_LPS-DEX | BIRC3, RETREG1 |
| Bcell_PHA-DEX | BIRC3 |
| Monocyte_LPS-DEX | RETREG1 |
| NKcell_LPS-DEX | MS4A7 |
| Tcell_LPS-DEX | RETREG1, MS4A7 |
| Tcell_PHA-DEX | BIRC3 |

Table S7: vQTL mapping results. Number of significant vQTLs and vGenes based on FastQTL results (FDR<0.1, columns 2 and 3), and multivariate adaptive shrinkage results (LFSR<0.1), columns 4 and 5.

| | FastQTL FDR<0.1 | | mash LFSR<0.1 | |
|---|---|---|---|---|
| | vQTLs | vGenes | vQTLs | vGenes |
| Bcell CTRL | 37 | 6 | 3086 | 96 |
| Bcell LPS+DEX | 9 | 4 | 3042 | 98 |
| Bcell LPS | 0 | 0 | 2638 | 104 |
| Bcell PHA+DEX | 2 | 1 | 2728 | 100 |
| Bcell PHA | 0 | 0 | 2866 | 99 |
| Monocyte CTRL | 2 | 2 | 2816 | 101 |
| Monocyte LPS+DEX | 86 | 12 | 2827 | 96 |
| Monocyte LPS | 67 | 12 | 2573 | 100 |
| Monocyte PHA+DEX | 20 | 7 | 2937 | 100 |
| Monocyte PHA | 50 | 9 | 2856 | 103 |
| NKcell CTRL | 0 | 0 | 3211 | 99 |
| NKcell LPS+DEX | 0 | 0 | 2632 | 91 |
| NKcell LPS | 16 | 7 | 3010 | 82 |
| NKcell PHA+DEX | 0 | 0 | 2941 | 87 |
| NKcell PHA | 19 | 3 | 2819 | 90 |
| Tcell CTRL | 188 | 24 | 3052 | 106 |
| Tcell LPS+DEX | 23 | 4 | 3230 | 98 |
| Tcell LPS | 154 | 22 | 2989 | 107 |
| Tcell PHA+DEX | 17 | 3 | 3151 | 106 |
| Tcell PHA | 0 | 0 | 3089 | 101 |
| Total unique | 545 | 102 | 3563 | 123 |
| Total tested | 1549665 | 7055 | 242,494 | 1086 |

Table S8: Mean-eQTL mapping results. Number of significant mean-eQTLs and mean-eGenes based on FastQTL results (FDR<0.1, columns 2 and 3), and multivariate adaptive shrinkage results (LFSR<0.1), columns 4 and 5.

| | FastQTL FDR<0.1 | | mash LFSR<0.1 | |
|---|---|---|---|---|
| | mean-eQTLs | mean-eGenes | mean-eQTLs | mean-eGenes |
| Bcell CTRL | 604 | 50 | 9420 | 222 |
| Bcell LPS+DEX | 1068 | 73 | 10252 | 238 |
| Bcell LPS | 4075 | 225 | 10882 | 232 |
| Bcell PHA+DEX | 812 | 54 | 11098 | 228 |
| Bcell PHA | 2018 | 125 | 10313 | 249 |
| Monocyte CTRL | 56 | 12 | 8616 | 203 |
| Monocyte LPS+DEX | 1 | 1 | 7995 | 187 |
| Monocyte LPS | 401 | 39 | 7925 | 187 |
| Monocyte PHA+DEX | 410 | 59 | 8294 | 200 |
| Monocyte PHA | 15 | 1 | 8239 | 186 |
| NKcell CTRL | 783 | 71 | 10929 | 245 |
| NKcell LPS+DEX | 104 | 14 | 11250 | 214 |
| NKcell LPS | 1089 | 94 | 8635 | 254 |
| NKcell PHA+DEX | 617 | 64 | 11446 | 202 |
| NKcell PHA | 702 | 56 | 7891 | 256 |
| Tcell CTRL | 11912 | 792 | 12404 | 285 |
| Tcell LPS+DEX | 9226 | 653 | 12463 | 286 |
| Tcell LPS | 11744 | 781 | 12465 | 302 |
| Tcell PHA+DEX | 7515 | 562 | 12156 | 288 |
| Tcell PHA | 6477 | 506 | 12441 | 287 |
| Total unique | 30493 | 2430 | 13164 | 366 |
| Total tested | 1549634 | 7055 | 241568 | 1084 |

Table S9: Overlap of vGenes with differentially expressed genes (DEGs, FDR<0.1) and differentially variable genes (DVGs, FDR<0.1). Columns represent: 1 – condition, 2 – number of vGenes which are also DEGs for the condition against its paired control, 3 – odds ratio of the overlap in column 2, 4 – p-value of the Fisher's exact test for enrichment of vGenes in DEGs, 5 - number of vGenes which are also DVGs for the condition against its paired control, 6 – odds ratio of the overlap in column 5, 7 – p-value of the Fisher's exact test for enrichment of vGenes in DVGs.

| Condition | vGenes that are DEGs | | | vGenes that are DVGs | | |
|---|---|---|---|---|---|---|
| | Overlap | OR | p-value | overlap | OR | p-value |
| Bcell LPS | 7 | 6.81 | 5.5E-04 | 4 | 6.94 | 8.6E-03 |
| Bcell LPS+DEX | 10 | 2.27 | 3.1E-02 | 3 | 1.59 | 4.4E-01 |
| Bcell PHA | 18 | 2.70 | 1.1E-03 | 15 | 6.49 | 8.9E-07 |
| Bcell PHA+DEX | 12 | 1.81 | 7.5E-02 | 6 | 2.48 | 5.5E-02 |
| Monocyte LPS | 5 | 0.45 | 1.1E-01 | 7 | 0.89 | 1.0E+00 |
| Monocyte LPS+DEX | 3 | 0.45 | 2.7E-01 | 7 | 1.32 | 4.9E-01 |
| Monocyte PHA | 14 | 0.75 | 4.1E-01 | 16 | 1.28 | 4.4E-01 |
| Monocyte PHA+DEX | 9 | 1.25 | 5.5E-01 | 16 | 2.55 | 3.0E-03 |
| NKcell LPS | 5 | 2.35 | 8.8E-02 | 7 | 5.08 | 1.9E-03 |
| NKcell LPS+DEX | 9 | 1.11 | 7.0E-01 | 11 | 5.38 | 6.9E-05 |
| NKcell PHA | 8 | 1.21 | 5.4E-01 | 6 | 2.17 | 1.2E-01 |
| NKcell PHA+DEX | 13 | 1.21 | 5.1E-01 | 2 | 1.17 | 6.9E-01 |
| Tcell LPS | 6 | 4.53 | 6.3E-03 | 11 | 3.65 | 1.1E-03 |
| Tcell LPS+DEX | 13 | 1.69 | 1.3E-01 | 6 | 1.88 | 1.6E-01 |
| Tcell PHA | 16 | 3.04 | 6.2E-04 | 20 | 4.51 | 1.8E-06 |
| Tcell PHA+DEX | 18 | 2.13 | 1.3E-02 | 7 | 0.97 | 1.0E+00 |

Table S10: Summary of DLDA dynamic eQTL mapping and overlap with eGenes, and and immune diseases-associated genes identified from PTWAS

| Cell type DLDA treatment | eQTLs(FDR<0.1) | eGenes | PTWAS Genes |
|---|---|---|---|
| Bcell LPS | 139 | 32 | 2 |
| Bcel LPS+DEX | 0 | 0 | 0 |
| Bcell PHA | 114 | 40 | 7 |
| Bcell PHA+DEX | 27 | 2 | 0 |
| Monocyte LPS | 35 | 3 | 0 |
| Monocyte LPS+DEX | 37 | 3 | 1 |
| Monocyte PHA | 0 | 0 | 0 |
| Monocyte PHA+DEX | 0 | 0 | 0 |
| NKcell LPS | 4 | 3 | 0 |
| NKcell LPS+DEX | 2 | 2 | 0 |
| NKcell PHA | 6 | 4 | 1 |
| NKcell PHA+DEX | 3 | 2 | 0 |
| Tcell LPS | 2073 | 244 | 45 |
| Tcell LPS+DEX | 269 | 18 | 5 |
| Tcell PHA | 1329 | 225 | 39 |
| Tcel PHA+DEX | 1298 | 54 | 9 |
| Total unique | 3899 | 588 | 101 |

Table S11: **Results of differential expressed genes (DEGs) using DESeq2 pseudo bulk aggregated data**. Columns 1-7 are: 1) Cell type; 2) Treatment; 3) Ensembl gene ID; 4) $\log_2$ fold change of gene expression; 5) Standard error; 6) P-value; 7) FDR

`http://genome.grid.wayne.edu/SCAIP/Supp_Tables2/Supplemental_Table_S11.txt.gz`

Table S12: **Results of differential gene expression variability (DGV)**. Columns 1-7 are: 1) Cell type; 2) Treatment; 3) Ensembl gene ID; 4) $\log_2$ fold change of gene variability; 5) Standard error; 6) P-value; 7) FDR

`http://genome.grid.wayne.edu/SCAIP/Supp_Tables2/Supplemental_Table_S12.txt.gz`

Table S13: **FastQTL eQTL mapping results**. Results of eQTL mapping across the 20 conditions. Columns are: 1 - ENSEMBL gene name; 2 - genetic variant coordinates (GRCh37); major and minor alleles and dbSNP ID; 3 - genetic variant distance from the TSS of the gene; 4 - p-value of the effect of the genetic variant on expression of the gene; 5 - effect size of the genetic variant on expression of the gene; 6 - condition.

`http://genome.grid.wayne.edu/SCAIP/Supp_Tables2/Supplemental_Table_S13.txt.gz`

Table S14: **mash eQTL effect estimates**. Multivariate adaptive shrinkage estimates of genetic effects on gene expression. Columns 1-20 are the conditions; rows are the tested gene-SNP pairs.

http://genome.grid.wayne.edu/SCAIP/Supp_Tables2/Supplemental_Table_S14.txt.gz

Table S15: **mash eQTL significance**. Multivariate adaptive shrinkage significance (LFSR) of genetic effects on gene expression. Columns 1-20 are the conditions; rows are the tested gene-SNP pairs.

http://genome.grid.wayne.edu/SCAIP/Supp_Tables2/Supplemental_Table_S15.txt.gz

Table S16: **61 reGenes overlapping with immune disease genes**. Columns are: 1-ENSEMBL gene name; 2-SYMBOL gene name

http://genome.grid.wayne.edu/SCAIP/Supp_Tables2/Supplemental_Table_S16.txt.gz

Table S17: **FastQTL vQTL mapping results**. Results of vQTL mapping across the 20 conditions. Columns are: 1 - ENSEMBL gene name; 2 - genetic variant coordinates (GRCh37), major and minor alleles and dbSNP ID; 3 - genetic variant distance from the TSS of the gene; 4 - p-value of the effect of the genetic variant on gene expression variability of the gene; 5 - effect size of the genetic variant on gene expression variability of the gene; 6 - condition.

http://genome.grid.wayne.edu/SCAIP/Supp_Tables2/Supplemental_Table_S17.txt.gz

Table S18: **mash vQTL effect estimates**. Multivariate adaptive shrinkage estimates of genetic effects on gene expression variability. Columns 1-20 are the conditions, rows are the tested gene-SNP pairs.

http://genome.grid.wayne.edu/SCAIP/Supp_Tables2/Supplemental_Table_S18.txt.gz

Table S19: **mash vQTL significance**. Multivariate adaptive shrinkage significance of genetic effects on gene expression variability. Columns 1-20 are the conditions; rows are the tested gene-SNP pairs.

http://genome.grid.wayne.edu/SCAIP/Supp_Tables2/Supplemental_Table_S19.txt.gz

Table S20: **FastQTL mean-eQTL mapping results**. Results of mean-eQTL mapping across the 20 conditions. Columns are: 1 - ENSEMBL gene name; 2 - genetic variant coordinates (GRCh37), major and minor alleles and dbSNP ID; 3 - genetic variant distance from the TSS of the gene; 4 - p-value of the effect of the genetic variant on mean expression of the gene; 5 - effect size of the genetic variant on mean expression of the gene; 6 - condition.

http://genome.grid.wayne.edu/SCAIP/Supp_Tables2/Supplemental_Table_S20.txt.gz

Table S21: **mash mean-eQTL effect estimates**. Multivariate adaptive shrinkage estimates of genetic effects on gene expression mean. Columns 1-20 are the conditions, rows are the tested gene-SNP pairs.

http://genome.grid.wayne.edu/SCAIP/Supp_Tables2/Supplemental_Table_S21.txt.gz

Table S22: **mash mean-eQTL significance**. Multivariate adaptive shrinkage significance of genetic effects on gene expression mean. Columns 1-20 are the conditions, rows are the tested gene-SNP pairs.

http://genome.grid.wayne.edu/SCAIP/Supp_Tables2/Supplemental_Table_S22.txt.gz

Table S23: **Dynamic eQTL mapping results**. Results of dynamic eQTL mapping across 16 conditions, each file representing the results of dynamic eQTL mapping in one of the four cell types (B cells, Monocytes, NK cells and T cells) treated with LPS, LPS+DEX, PHA or PHA+DEX interacting with treatment response pseudotime. Columns 1-6 are: 1) Ensembl gene ID; 2) genetic variant coordinates (GRCh37); major and minor alleles and dbSNP ID; 3) genetic effect on gene expression interacting with response pseudotime; 4). Standard error of the interaction term; 5) P-value for the interaction term; 6) The stratified FDR q-value

http://genome.grid.wayne.edu/SCAIP/Supp_Tables2/Supplemental_Table_S23.txt.gz

Table S24: **table of number of cells per combination (cell type+treatment+individual** across 1,536 combinations. Columns 1-5 are: 1) combination ID; 2) number of cells per combination; 3) cell type; 4) treatments; 5) individual ID

http://genome.grid.wayne.edu/SCAIP/Supp_Tables2/Supplemental_Table_S24.txt.gz